

Functional Triblock Terpolymers for Multicompartment Micelle and Janus Particle Synthesis

DISSERTATION

zur Erlangung des akademischen Grades eines
Doktors der Naturwissenschaften (Dr. rer. nat.)
im Fach Chemie
an der Bayreuther Graduiertenschule
für Mathematik und Naturwissenschaften
der Universität Bayreuth

vorgelegt von

Andrea Gertrud Wolf

Geboren in Forchheim

Bayreuth, 2013

Die vorliegende Arbeit wurde in der Zeit von August 2008 bis April 2013 in Bayreuth am Lehrstuhl Makromolekulare Chemie II unter Betreuung von Herrn Prof. Dr. Axel H. E. Müller angefertigt.

Vollständiger Abdruck der von der Bayreuther Graduiertenschule für Mathematik und Naturwissenschaften der Universität Bayreuth genehmigten Dissertation zur Erlangung des akademischen Grades eines Doktors der Naturwissenschaften (Dr. rer. nat.).

Dissertation eingereicht am: 11.04.2013

Zugelassen am: 16.04.2013

Wissenschaftliches Kolloquium am: 07.06.2013

Amtierender Direktor: Prof. Dr. Franz X. Schmid

Prüfungsausschuss:

Prof. Dr. Axel H. E. Müller (Erstgutachter)

Prof. Dr. Alexander Böker/RWTH Aachen (Zweitgutachter)

Prof. Dr. Carlo Unverzagt

Prof. Dr. Stephan Förster (Vorsitz)

“Now, by two-headed Janus,
Nature hath framed strange fellows in her time.”

William Shakespeare, *The Merchant of Venice*

Meinen Eltern

Contents

Summary	1
Zusammenfassung.....	4
Glossary	7
1 Introduction	10
1.1 Synthesis of triblock terpolymers	10
1.2 Self-assembly of triblock terpolymers in the bulk.....	10
1.3 Self-assembly of triblock terpolymers in solution.....	13
1.3.1 Multicompartment micelles with a compartmentalized core.....	14
1.3.2 Multicompartment micelles with a compartmentalized corona.....	17
1.3.3 Multicompartment micelles by precise hierarchical self-assembly	20
1.4 Janus particles	22
1.4.1 Synthesis of Janus particles.....	22
1.4.2 Applications of Janus particles.....	26
1.5 Objective of this thesis	27
2 Experimental Part and Methods.....	28
2.1 Materials	28
2.2 Instrumentation.....	29
2.3 Methods.....	31
3 Building Blocks	37
3.1 Poly(<i>tert</i> -butoxystyrene)	37
3.1.1 Anionic and free radical polymerization.....	37
3.1.2 Hydrolysis.....	39
3.1.3 Functionalizations.....	41
3.1.4 Conclusion	46
3.2 Poly(4-(dimethylaminomethyl)styrene).....	47
3.2.1 Anionic polymerization.....	47

Contents

3.2.2	Solution properties of PDMAMS.....	50
3.2.3	Conclusion	51
4	Triblock Terpolymers: Synthesis and Bulk Morphologies	53
4.1	Poly(<i>tert</i> -butoxystyrene)- <i>block</i> -polybutadiene- <i>block</i> -poly(<i>tert</i> -butyl methacrylate) (tSBT)	53
4.2	Poly(<i>tert</i> -butoxystyrene)- <i>block</i> -polybutadiene- <i>block</i> -poly(2-(dimethylamino)ethyl methacrylate) (tSBD)	56
4.3	Poly(4-(dimethylaminomethyl)styrene)- <i>block</i> -poly(allyl methacrylate)- <i>block</i> -poly(<i>tert</i> -butyl methacrylate) (DSAT)	59
4.4	Conclusion.....	60
5	Janus Particles from tSBT Bulk Structures.....	62
5.1	Preparation of Janus particles.....	62
5.2	Hydrolysis and solution structure of Janus cylinders	72
5.3	Conclusion.....	76
6	Solution Structures of tSBD and tSBT.....	78
6.1	Stimuli-responsive micelles from tSBD.....	78
6.2	Multicompartment micelles from tSBD	81
6.3	Multicompartment micelles from tSBT.....	85
6.4	Janus spheres from tSBT multicompartment micelles	85
6.5	Conclusion.....	89
7	References.....	91
	List of Publications.....	99
	Danksagung.....	101

Summary

This thesis describes the synthesis of ABC triblock terpolymers with functional moieties via living anionic polymerization, followed by Janus particle (JP) and multicompartment micelle (MCM) synthesis from the as prepared triblock terpolymers.

JPs, bicompartmentalized, non-centrosymmetric colloids, are an important issue in today's materials science. The manifold ways to synthesize them and their exceptional properties have become an intensively investigated field of research during recent years. A synthesis method that can accomplish the tasks of the preparation of spherical as well as non-spherical JPs that are well-defined and in the nanometer size range is based on converting self-assembled triblock terpolymer bulk structures via selective cross-linking of the middle block. Until now such soft JPs were prepared mainly from polystyrene-*block*-polybutadiene-*block*-poly(methyl methacrylate) and polystyrene-*block*-polybutadiene-*block*-poly(*tert*-butyl methacrylate). However, these polymers do not offer many possibilities of chemical alterations and stimuli-responsive elements.

Therefore, potential new functional monomers for the use in JP synthesis from triblock terpolymer bulk structures were identified and their anionic polymerization examined, *p*-*tert*-butoxystyrene (tS) and 4-(dimethylaminomethyl)styrene (DMAMS). Polymers with low polydispersity indices could be prepared from both monomers in tetrahydrofuran (THF) with *sec*-butyllithium (*sec*-BuLi) as initiator. In the course of this research the first successful living anionic polymerization of DMAMS with a narrow molecular weight distribution in a *sec*-BuLi/THF system was conducted. This illustrates the importance of the treatment of the THF with *sec*-BuLi before the actual polymerization to eliminate residual impurities and form lithium alkoxides. The latter hinder the coordination of tertiary amino groups to the Li⁺ counterions which would disturb the addition of monomer and a controlled polymerization.

Poly(*p*-*tert*-butoxystyrene) (PtS) was hydrolyzed to poly(*p*-hydroxystyrene) (PHS) which is water-soluble at high pH values, opening the possibility to prepare water-soluble JPs. Both, treatment with hydrochloric acid and with trimethylsilyl iodide, were employed. Further, the inherent possibility of polymer functionalization due to the hydroxyl group of PHS was demonstrated by the successful reaction with 1,3-propanesultone and 4-pentynoic acid to introduce sulfonate and alkyne groups, respectively. The pH-responsive behavior of poly(4-(dimethylaminomethyl)styrene) could be confirmed and for the first time an LCST behavior was documented with cloudpoints of 59.3 °C at pH 7 and 28.5 °C at pH 8.

PtS was then used in the preparation of two triblock terpolymers, poly(*tert*-butoxystyrene)-*block*-polybutadiene-*block*-poly(*tert*-butyl methacrylate) (tSBT) and poly(*tert*-butoxystyrene)-*block*-polybutadiene-*block*-poly(2-(dimethylamino)ethyl methacrylate) (tSBD). tSBT exhibited a lamella-cylinder (lc) bulk morphology with polybutadiene (PB) spheres surrounded by alternating lamellae of PtS and poly(*tert*-butyl methacrylate) (PtBMA). However, the bulk structure of tSBD consisted of a symmetrical lamella-lamella pattern that is not suitable for JP synthesis. Further, DMAMS was used to synthesize poly(4-(dimethylaminomethyl)styrene)-*block*-poly(allyl methacrylate)-*block*-poly(*tert*-butyl methacrylate) (DSAT). Poly(allyl methacrylate) was chosen here as cross-linkable middle block instead of PB as the polymerization of PDMAMS-PB could not be conducted successfully. However, DSAT did not exhibit a bulk morphology suitable for JPs.

From tSBT bulk material, three different types of non-spherical JPs could be obtained. Photo-cross-linking of the lamella-cylinder (lc)-morphology by co-casting a radical photo-initiator and UV exposure resulted in the expected Janus cylinders. When the bulk material was first swollen in acetonitrile and cross-linked by cold vulcanization, Janus sheets were obtained. Swelling in acetonitrile/decane emulsion led to a new type of JPs, Janus ribbons. In both cases a phase transition had occurred; in case of the Janus sheets a thin PB layer had formed between the original PB cylinders, resulting in an undulated-lamella morphology. For the formation of Janus ribbons a connecting PB phase had formed in every second interspace along the major axis of the cylinders. Casting a tSBT film from *tert*-butanol, a non-solvent for PB, also enabled the synthesis of spherical JPs. This way, the importance and versatile application of swelling agents and cross-linking methods for the preparation of JPs from bulk structures was demonstrated. The obtained Janus cylinders were hydrolyzed to have one PHS and one poly(methacrylic acid) (PMAA) hemicylinder, resulting in water-soluble particles.

Further, solution structures of tSBD and tSBT triblock terpolymers were investigated. In water, tSBD formed core-corona micelles that exhibited pH-responsive and LCST behavior due to the responsive poly(2-(dimethylamino)ethyl methacrylate) corona. Employing the novel method of directed hierarchical self-assembly, "football" MCMs were obtained from tSBD whereas tSBT formed "clover" structures. Cross-linking of the B block in such MCMs and their subsequent dissolution in a solvent for all three blocks can be used to prepare spherical JPs. However, as tSBD MCMs existed in water, no sufficient cross-linking method could be found to cross-link the organic PB phase within the aqueous solution. For tSBT MCMs in ethanol the standard approach of adding a photo-initiator to the MCM solution followed by UV exposure was successfully employed and spherical JPs were obtained. These

were again hydrolyzed to acquire water-soluble JPs. Apart from some isolated single Janus spheres, cryogenic transmission electron microscopy mainly revealed the formation of “clover” and “hamburger” oligomers possibly due to the slightly better solubility of PMAA. Here, the applicability of the concept of directed hierarchical self-assembly to create MCMs was demonstrated for two different triblock terpolymers and the corresponding method of solution-based JP synthesis was successfully conducted for tSBT.

Zusammenfassung

Die vorliegende Arbeit beschreibt die Synthese von ABC Triblock-Terpolymeren mit funktionellen Einheiten mittels lebender anionischer Polymerisation, gefolgt von der Synthese von Janus-Partikeln (JP) und Multikompartiment-Micellen (MCM) aus den hergestellten Triblock-Terpolymeren.

JPs, zweigeteilte, nicht-zentrosymmetrische Kolloide, sind ein wichtiges Thema in den heutigen Materialwissenschaften. Die mannigfaltigen Möglichkeiten ihrer Synthese und ihre außergewöhnlichen Eigenschaften sind während der letzten Jahre zu einem intensiv bearbeiteten Forschungsgebiet geworden. Eine Synthese-Methode, die die Herstellung von sowohl sphärischen als auch nicht-sphärischen, wohl-definierten JPs im Größenbereich von Nanometern ermöglicht, basiert auf der Umwandlung von selbstangeordneten Triblock-Terpolymer-Bulkstrukturen über die selektive Vernetzung des Mittelblocks. Bis zum jetzigen Zeitpunkt wurden derartige weiche JPs hauptsächlich aus Polystyrol-*block*-polybutadien-*block*-polymethylmethacrylat und Polystyrol-*block*-polybutadien-*block*-poly(*tert*-butylmethacrylat) hergestellt. Diese Polymere verfügen jedoch nicht über viele Möglichkeiten für chemische Umsetzungen und stimuli-responsive Elemente.

Deshalb wurden potentielle neue funktionale Monomere für die Anwendung in der JP-Synthese aus Triblock-Terpolymer-Bulkstrukturen ermittelt sowie deren anionische Polymerisation untersucht, *p-tert*-Butoxystyrol (tS) und 4-(Dimethylaminomethyl)styrol (DMAMS). Aus beiden Monomeren konnten in Tetrahydrofuran (THF) mit *sec*-Butyllithium (*sec*-BuLi) als Initiator Polymere mit niedrigen Polydispersitätsindizes hergestellt werden. Im Zuge dieser Untersuchung wurde die erste erfolgreiche lebende anionische Polymerisation von DMAMS mit einer engen Molekulargewichtsverteilung in einem THF/*sec*-BuLi-System durchgeführt. Dies verdeutlicht, wie wichtig es ist, das THF vor der eigentlichen Polymerisation mit *sec*-BuLi zu behandeln um restliche Unreinheiten zu beseitigen und Lithium-Alkoxide zu bilden. Letztere verhindern die Koordination von tertiären Amino-Gruppen an die Li⁺-Gegenionen was die Anlagerung von Monomeren und damit eine kontrollierte Polymerisation stören würde.

Poly(*p-tert*-butoxystyrol) (PtS) wurde zu Poly(*p*-hydroxystyrol) (PHS) hydrolysiert, das bei hohen pH-Werten wasserlöslich ist und damit die Möglichkeit der Synthese von wasserlöslichen JPs eröffnet. Sowohl die Behandlung mit Salzsäure als auch mit Trimethylsilyliodid wurde dafür eingesetzt. Zusätzlich wurde die aufgrund der Hydroxyl-Gruppe inhärente Möglichkeit der Polymer-Funktionalisierung anhand der erfolgreichen Umsetzung mit 1,3-

Propansulton und 4-Pentinsäure zur Einführung von Sulfonat- bzw. Alkin-Gruppen demonstriert. Das pH-responsive Verhalten von Poly(4-(dimethylaminomethyl)styrol) konnte bestätigt werden und zum ersten Mal wurde ein LCST-Verhalten mit Trübungstemperaturen von 59,3 °C bei pH 7 und 28,5 °C bei pH 8 dokumentiert.

Anschließend wurde PtS bei der Herstellung von zwei Triblock-Terpolymeren, Poly(*tert*-butoxystyrol)-*block*-polybutadien-*block*-poly(*tert*-butylmethacrylat) (tSBT) und Poly(*tert*-butoxystyrol)-*block*-polybutadien-*block*-poly(2-(dimethylamino)ethylmethacrylat) (tSBD), eingesetzt. tSBT wies eine Lamellen-Zylinder-Bulkstruktur mit Polybutadien (PB)-Kugeln umgeben von alternierenden PtS- und Poly(*tert*-butylmethacrylat) (PtBMA)-Lamellen auf. Die Bulkstruktur von tSBD bestand jedoch aus einem symmetrischen lamellaren Muster, das nicht für die Synthese von JPs geeignet ist. Weiterhin wurde DMAMS benutzt um Poly(4-(dimethylaminomethyl)styrol)-*block*-polyallylacrylat-*block*-poly(*tert*-butylmethacrylat) (DSAT) zu synthetisieren. Als vernetzbarer Mittelblock wurde an dieser Stelle anstatt PB Polyallylacrylat gewählt, da die Polymerisation von PDMAMS-PB nicht erfolgreich durchgeführt werden konnte. DSAT zeigte allerdings keine für die Synthese von JPs geeignete Bulk-morphologie.

Aus tSBT-Bulkmaterial konnten drei verschiedene Arten von JPs gewonnen werden. Die Photo-Vernetzung der Lamelle-Zylinder (lc)-Morphologie durch den Einsatz eines radikalischen Photoinitiators und UV-Bestrahlung ergab die erwarteten Janus-Zylinder. Wurde das Bulkmaterial erst in Acetonitril gequollen und dann durch kalte Vulkanisation vernetzt, waren Janus-Plättchen das Ergebnis. Quellen in einer Acetonitril/Dekan-Emulsion führte zu einer neuen Art von JPs, Janus-Bändern. In beiden Fällen fand ein Phasenübergang statt. Im Fall der Janus-Plättchen hatte sich eine dünne PB-Schicht zwischen den ursprünglich vorhandenen Zylindern gebildet, mit dem Ergebnis einer ondulierten Lamellen-Morphologie. Für die Bildung von Janus-Bändern hatte sich eine verbindende PB-Phase lediglich in jedem zweiten Zwischenraum entlang der Hauptachse der Zylinder gebildet. Das Filmgießen von tSBT aus *tert*-Butanol, einem Nicht-Lösungsmittel für PB, ermöglichte auch die Synthese von sphärischen JPs. Auf diese Weise wurde die Wichtigkeit und vielseitige Anwendung von unterschiedlichen Quell-Reagenzien und Vernetzungsmethoden bei der Herstellung von JPs aus Bulkstrukturen demonstriert. Die Janus-Zylinder wurden hydrolysiert um einen PHS- und einen Polymethacrylsäure (PMAA)-Halbzylinder und somit wasserlösliche Partikel zu erhalten.

Weiterhin wurden die Lösungs-Strukturen von tSBD und tSBT Triblock-Terpolymeren untersucht. In Wasser bildete tSBD Micellen mit einer Kern-Korona-Struktur, die aufgrund der

responsiven Poly(2-dimethylamino)ethylmethacrylat)-Korona pH-responsives und LCST-Verhalten zeigten. Durch die Anwendung der neuartigen Methode der gerichteten hierarchischen Selbstanordnung wurden aus tSBD „Fußball“-MCMs erhalten während tSBT „Kleeblatt“-Strukturen formte. Das Vernetzen des B-Blocks in derartigen MCMs und ihre anschließende Auflösung in einem Lösungsmittel für alle drei Polymer-Blöcke kann für die Herstellung von sphärischen JPs genutzt werden. Da tSBD in Wasser vorlag konnte jedoch keine ausreichende Vernetzungs-Methode gefunden werden, um die organische PB-Phase innerhalb dieser wässrigen Lösung zu vernetzen. Bei den tSBT-MCMs in Ethanol wurde erfolgreich die Standard-Vorgehensweise der Beimischung eines Photo-Initiators zur MCM-Lösung gefolgt von UV-Bestrahlung benutzt und sphärische JPs wurden erhalten. Diese wurden wiederum hydrolysiert um wasserlösliche JPs zu erlangen. Neben einigen isolierten einzelnen Janus-Kugeln zeigte die Untersuchung mittels cryo-Transmissions-elektronenmikroskopie hauptsächlich die Bildung von „Kleeblatt“- und „Hamburger“-Oligomeren, wahrscheinlich aufgrund der geringfügig besseren Löslichkeit vom PMAA. Die Anwendbarkeit des Konzepts der gerichteten hierarchischen Selbstanordnung zur Herstellung von MCMs wurde hier für zwei verschiedene Triblock-Terpolymere demonstriert und die darauf beruhende Methode der lösungs-basierten JP-Synthese erfolgreich für tSBT durchgeführt.

Glossary

χ	Flory-Huggins interaction parameter
λ	wavelength
μm	micrometer
Å	Ångström
a.i.	arbitrary intensity
AIBN	2,2'-azobis(isobutyronitrile)
AMA	allyl methacrylate
ATR	attenuated total reflection
a.u.	arbitrary units
bp	boiling point
BuLi	butyllithium
ca.	circa
cm	centimeter
cryo-TEM	cryogenic transmission electron microscopy
d	distance
DCC	dicyclohexylcarbodiimide
DLS	dynamic light scattering
DMAc	dimethylacetamide
DMAEMA	2-(dimethylamino)ethyl methacrylate
DMAMS	4-(dimethylaminomethyl)styrene
DMAP	4-(dimethylamino)pyridine
DMF	dimethylformamide
DMSO	dimethyl sulfoxide
DPE	diphenylethylene
DSAT	poly(4-(dimethylaminomethyl)styrene)- <i>block</i> -poly(allyl methacrylate)- <i>block</i> -poly(<i>tert</i> -butyl methacrylate)
et al.	et alii
EtOH	ethanol
FRP	free radical polymerization
FT	fourier-transform
g	gram
h	hour(s)
HPLC	high-performance liquid chromatography
HSBT	polyhydroxystyrene- <i>block</i> -polybutadiene- <i>block</i> -poly(<i>tert</i> -butyl

	methacrylate)
$[I]_0$	initial initiator concentration
IR	infrared spectroscopy
JP	Janus particle
K	Kelvin
kV	kilovolt
k_{app}	apparent first-order rate constant
k_p	propagation rate constant
L	liter
lc	lamella-cylinder
LCST	lower critical solution temperature
ll	lamella-lamella
ls	lamella-sphere
m	mass
M	molar
$[M]_0$	initial monomer concentration
MALS	multi angle light scattering
mbar	millibar
MCM	multicompartment micelle
mg	milligram
MHz	megahertz
min	minute
mL	milliliter
mM	millimolar
mmol	millimol
M_n	number average molecular weight
$M_{n,th}$	theoretical number average molecular weight
MWCO	molecular weight cut-off
MWD	molecular weight distribution
N	degree of polymerization
NIR	near-infrared
nm	nanometer
NMR	nuclear magnetic resonance
PAMA	poly(allyl methacrylate)
PB	polybutadiene
PDEAEMA	poly(2-(diethylamino)ethyl methacrylate)
PDI	polydispersity index

PDMAEMA	poly(2-(dimethylamino)ethyl methacrylate)
PDMAMS	poly(4-(dimethylaminomethyl)styrene)
pH _{cr}	critical pH value
PHS	poly(<i>para</i> -hydroxystyrene)
pK _{a,app}	apparent pK _a
PMAA	poly(methacrylic acid)
PMMA	poly(methyl methacrylate)
ppm	parts per million
PS	polystyrene
PtBA	poly(<i>tert</i> -butyl acrylate)
PtBMA	poly(<i>tert</i> -butyl methacrylate)
PtS	poly(<i>para-tert</i> -butoxystyrene)
PTFE	polytetrafluoroethylene
RI	refractive index
rpm	revolutions per minute
RT	room temperature
SAXS	small-angle x-ray scattering
SBM	polystyrene- <i>block</i> -polybutadiene- <i>block</i> -poly(methyl methacrylate)
SBT	polystyrene- <i>block</i> -polybutadiene- <i>block</i> -poly(<i>tert</i> -butyl methacrylate)
sec	seconds
SEC	size exclusion chromatography
SEM	scanning electron microscopy
SFM	scanning force microscopy
TBAB	tetrabutylammonium bromide
tBMA	<i>tert</i> -butyl methacrylate
T _{cl}	cloudpoint
TEM	transmission electron microscopy
THF	tetrahydrofuran
TMSI	trimethylsilyl iodide
TPO	2,4,6-trimethylbenzoyldiphenylphosphine oxide
tSBD	poly(<i>tert</i> -butoxystyrene)- <i>block</i> -polybutadiene- <i>block</i> -poly(2-(dimethylamino)ethyl methacrylate)
tSBT	poly(<i>tert</i> -butoxystyrene)- <i>block</i> -polybutadiene- <i>block</i> -poly(<i>tert</i> -butyl methacrylate)
ul	undulated-lamellar
UV	ultraviolet
wt	weight

1 Introduction

1.1 Synthesis of triblock terpolymers

In modern materials science and nanotechnology a key issue is the preparation of highly ordered, defect-free structures of nano- or micro-size which are mostly prepared by bottom-up approaches such as self-assembly. This calls for building blocks with a precisely defined size and shape to ensure specific and predictable interactions and assembly products.^{1,2} In the field of polymer science AB and ABA di- and triblock copolymers and ABC triblock terpolymers are perfect materials for this purpose as they offer control over length scale, morphology and domain functionality.³ For the synthesis of linear triblock terpolymers, living anionic polymerization by sequential monomer addition stays a common synthetic approach.³ When its inherent problems like suitable addition order of the monomers or tolerance against functional groups can be overcome, it leads to the well-defined polymeric materials we desire for controlled self-assembly. However, by the development and improvement of other “living”/controlled polymerization methods, the synthesis of tailor-made triblock terpolymers with specific chemical composition and functionality and low molecular polydispersity and heterogeneity is also possible by group transfer polymerization (GTP), cationic polymerization, atom transfer radical polymerization (ATRP), reversible addition-fragmentation chain-transfer (RAFT) polymerization and sometimes a combination of these methods.⁴

1.2 Self-assembly of triblock terpolymers in the bulk

While the investigation of morphologies of AB block copolymers and ABA block terpolymers as well as $(AB)_n$ starblock copolymers dates back to the seventies and early eighties of the last century, the exploration of morphologies of ABC triblock terpolymers came into view only in the nineties.⁵ The phase behavior of diblock copolymers is driven by an unfavorable mixing enthalpy and a small mixing entropy, while the covalent bond connecting the blocks prevents macroscopic phase separation. The latter depends on the Flory-Huggins interaction parameter χ_{AB} , a measure of the incompatibility between the two blocks, the volume fractions of the blocks, f_A ($f_B = 1 - f_A$), as well as the total degree of polymerization N . The degree of microphase separation is determined by the segregation product χN . Three different regimes are distinguished: the weak-segregation limit (WSL) for $\chi N \leq 10$, the intermediate segregation region (ISR) for $10 < \chi N \leq 50$ and the strong segregation limit (SSL) for $\chi N \rightarrow \infty$.⁶ As a function of composition, AB block copolymers in general adopt four different

morphologies, spheres, cylinders, double gyroid and lamellae (Figure 1-1).⁷ Additionally, the existence of a perforated lamellar phase was discussed.^{8,9}

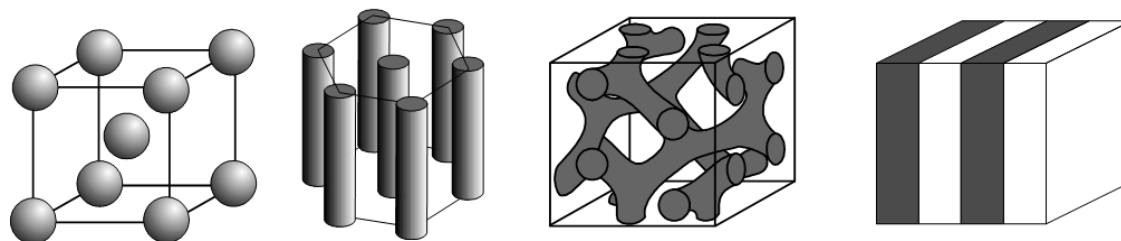


Figure 1-1. Schemes of the different stable morphologies in binary block copolymers (from left to right: spheres, cylinders, double gyroid, lamellae). Reprinted with permission from Ref [7].

While the physical concepts to describe the phase behavior stay the same, naturally, triblock terpolymers have a higher number of experimental parameters than diblock copolymers. For a given triblock terpolymer system, there are three different Flory-Huggins interaction parameters χ_{AB} , χ_{BC} and χ_{AC} . Further, for each particular polymer there are three additional independent parameters: the volume fraction of blocks A and B, f_A and f_B , and the degree of polymerization, N . Altogether, there are six parameters that determine the equilibrium structure of a given triblock terpolymer. Therefore, the number of possible morphologies, compared to the four for AB diblock copolymers, increases dramatically. Figure 1-2 shows possible morphologies of a linear ABC triblock terpolymer. They are also influenced by the block order in the triblock terpolymer and change for other terpolymer architectures. Here, especially miktoarm stars are an evolving field of investigation,¹⁰⁻¹² however not a topic of this thesis.

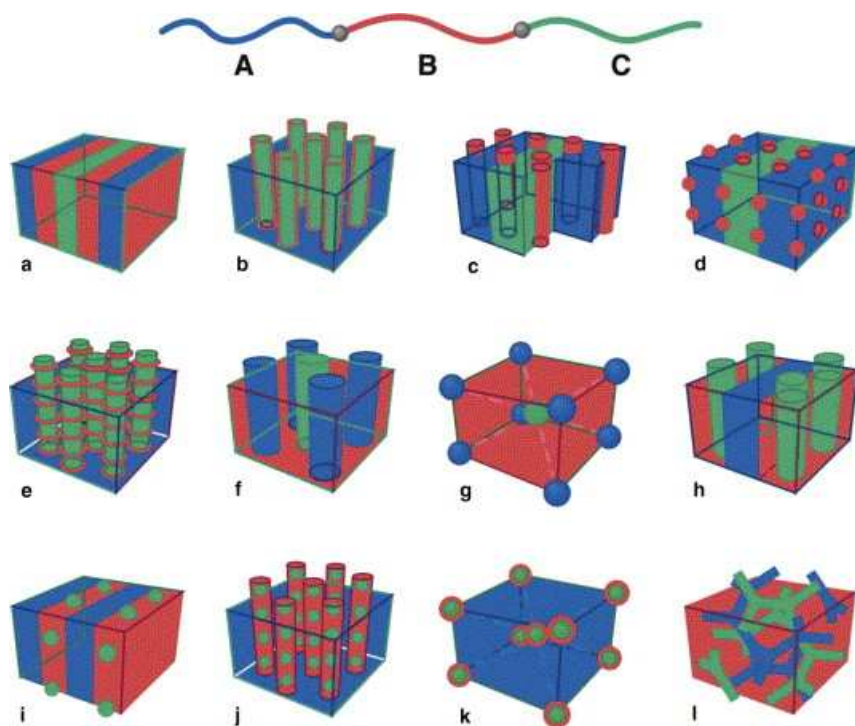


Figure 1-2. Overall schematic of the most predominant morphologies observed in ABC linear terpolymers. Reprinted with permission from Ref [3].

The exploration of triblock terpolymer bulk morphologies takes place through the combination and interplay of theoretical^{3,13-15} and experimental studies. An extremely significant contribution to the latter was made by Stadler and collaborators.³ They did a lot of work on the morphological behaviour of especially polystyrene-*block*-polybutadiene-*block*-poly(methyl methacrylate) (SBM) triblock terpolymers.^{5,7,16-21} Figure 1-3 shows a ternary phase diagram of SBM at room temperature with some of the discovered morphologies.

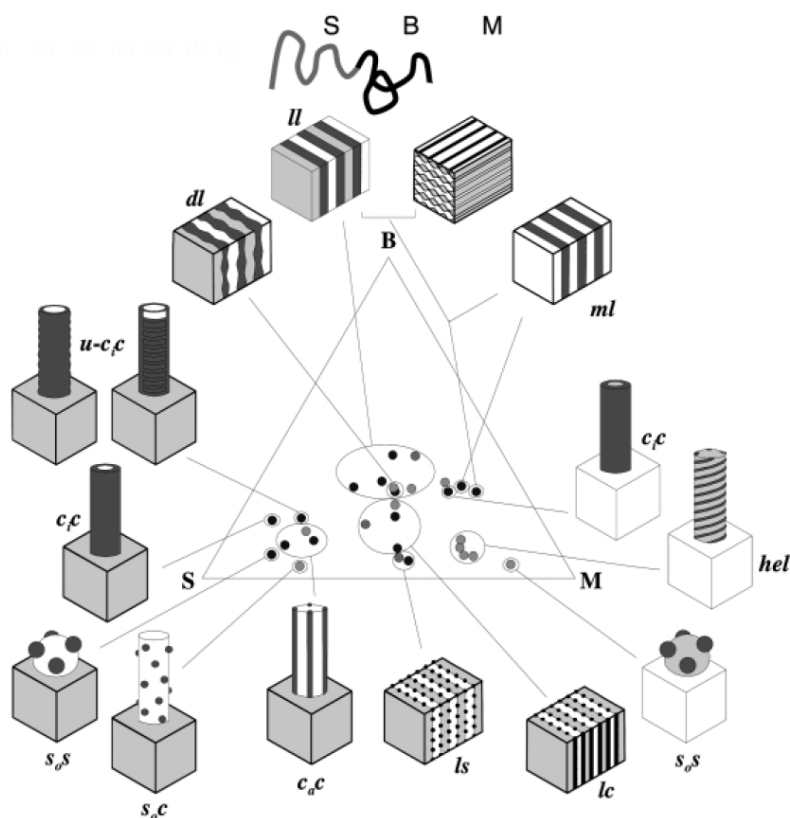


Figure 1-3. Scheme of the different morphologies known from SBM triblock copolymers. Reprinted from Ref [7].

1.3 Self-assembly of triblock terpolymers in solution

In analogy to their bulk behavior, diblock copolymers and triblock terpolymers also self-assemble in block-selective solvents.⁶ Like in the case of bulk structures, the number of possible structures in solution is considerably enhanced for triblock terpolymers in comparison to diblock copolymers. Triblock terpolymers in which two incompatible blocks are insoluble in the respective solvent form micelles with a compartmentalized core and a homogenous corona; if only one block is insoluble, it will form the homogenous core while the other two build the corona. Within the latter, if the middle block is the insoluble one, either no chain segregation (mixed corona) or lateral chain segregation (Janus micelle) can take place; if one of the outer blocks is the insoluble one, the corona will consist of AB diblock copolymer arms (radially segregated corona). Moreover, triblock terpolymers may form vesicles in solution.²² Figure 1-4 shows the schemes of all mentioned structures.

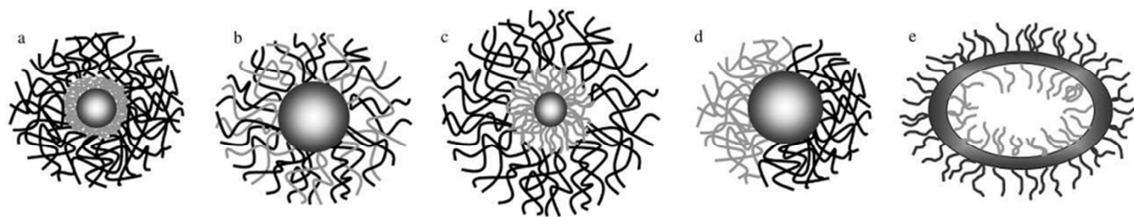


Figure 1-4. Schematic representation of different types of micelles formed by ABC triblock terpolymers. Core-shell-corona micelles with a compartmentalized core (a), micelles with a mixed corona (no chain segregation) (b), core-shell-corona micelles with a compartmentalized corona (radial chain segregation) (c), Janus micelles with an asymmetric corona (lateral chain segregation) (d), and vesicles (e). Adapted with permission from Ref [22].

A recent review by Wyman and Liu²³ offers a detailed insight into micellar structures of triblock terpolymers. In the following the main types and selected examples are presented.

1.3.1 Multicompartment micelles with a compartmentalized core

Micelles with a compartmentalized core were the first investigated examples of micelles from triblock terpolymers. They are characterized by the so-called “core-shell-corona” structure (sometimes called “onion” or “three-layers” structure) with a core of the insoluble block A, surrounded by the also collapsed, insoluble block B and a corona formed by the soluble block C (Figure 1-4a).²⁴ Early examples were reported by Kriz,²⁵ Eisenberg²⁶ and Ishizone.²⁷ In most cases, micellization is induced in an aqueous phase for triblock terpolymers with hydrophobic blocks A and B and a hydrophilic outer block C. An example in organic solvent is the work of Liu and Liu.²⁸ Here, a poly(glyceryl methacrylate)-*block*-poly(2-cinnamoyloxyethyl methacrylate)-*block*-poly(allyl methacrylate) (PGMA-PCEMA-PAMA) polymer formed core-shell-corona structures in methanol/tetrahydrofuran (THF) and toluene/methanol solvent mixtures. While PCEMA formed the shell in both cases, depending on the solvent mixture either PAMA or PGMA built the core, the respective other block the corona. In pure methanol, the polymer formed branched cylindrical micelles. Manners et al. used a poly(ferrocenylphenylphosphine)-*block*-poly(ferrocenyldimethyl-silane)-*block*-poly(dimethylsiloxane) (PFP-PFS-PDMS) triblock terpolymer to produce micelles with an organometallic core.²⁹ In hexane, a selective solvent for PDMS, spherical micelles were formed for polymers with a sufficiently long PFP block that prevented crystallization of PFS. For shorter PFP blocks ($DP \leq 6$) PFS crystallized during micelle formation and resulted in

cylindrical micelles. However, the exact location of the incompatible PFP and PFS domains in the spherical micelles could not be revealed.

While all the given examples exhibit the classical core-shell-corona structure, also morphologies with a non-continuous shell exist. A prominent example is the sphere-on-sphere or “raspberry” morphology Laschewsky et al. showed for a poly(4-methyl-4-(4-vinylbenzyl)morpholin-4-ium chloride)-*block*-polystyrene-*block*-poly(pentafluorophenyl-4-vinylbenzyl ether) (PVBM-PS-PVBFP) triblock terpolymer in water.³⁰ The hydrophobic PS block formed a core decorated with spherical domains of PVBFP, surrounded by the hydrophilic PVBM-corona (Figure 1-5a,b,c). In a follow-up work the group presented another triblock terpolymer with a lipophilic-hydrophilic-fluorophilic block order that also resulted in a sphere-on-sphere morphology at a first glance, but consisted of fluorocarbon-rich domains that were not exclusively located on the surface of the hydrophobic core domain, but interpenetrated the same as shown by cryo-electron tomography.³¹ Further, the group of Laschewsky demonstrated the importance of block order when the same type of triblock terpolymer was changed to a hydrophilic-lipophilic-fluorophilic block order and then resulted in a core-shell-corona structure.³²

Apart from materials with fluorocarbon-rich or other extraordinary block materials, formation of multicompartment core micelles with a non-continuous shell can also be observed for triblock terpolymers consisting of simple, common monomers, like polybutadiene-*block*-poly(2-vinylpyridine)-*block*-poly(*tert*-butyl methacrylate) (PB-P2VP-PtBMA).³³ Schacher et al. reported, when the polymer was dissolved in acetone, a non-solvent for polybutadiene, the formation of micelles with a PB core and a corona consisting of P2VP and PtBMA was expected. However, the procedure resulted in rather well-defined micelles with a sphere-on-sphere multicompartment core and a PtBMA corona (Figure 1-5d,e). The polymer was further examined after hydrolysis of the last block to PMAA.³⁴ At high pH, PB-P2VP-PMAA formed core-shell-corona micelles with a continuous shell of P2VP. However, at pH 4 partial intramicellar interpolyelectrolyte complex (*im*-IPEC) formation between P2VP and PMAA resulted in a patchy, collapsed shell. This was even more pronounced for the quaternized analog, PB-P2VPq-PMAA, which forms aggregates also exhibiting a non-continuous, patchy shell. Similar multicompartment micelles with a patchy shell due to *im*-IPEC formation were also reported for polybutadiene-*block*-poly(*tert*-butyl methacrylate)-*block*-poly(2-(dimethylamino)ethyl methacrylate)³⁵ and polybutadiene-*block*-poly(1-methyl-2-vinyl pyridinium)-*block*-poly(sodium methacrylate)³⁶ by Schacher and coworkers.

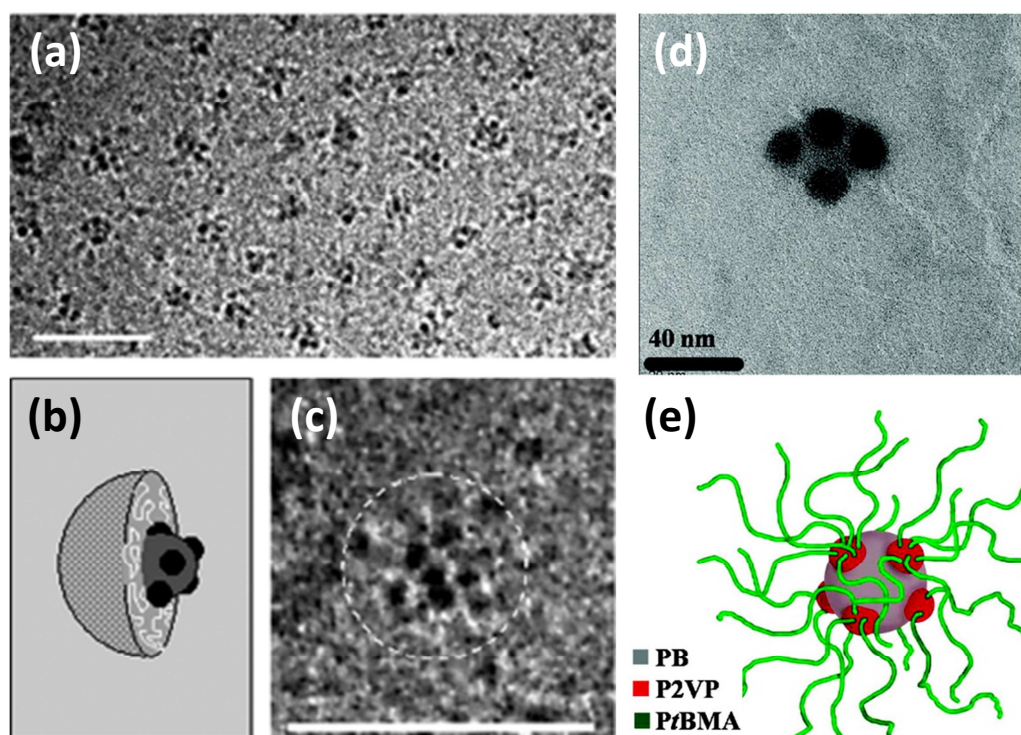


Figure 1-5. Cryo-TEM images (a,c) and a schematic representation (b) of the structure of multi-compartment micelles obtained by self-assembly of the triblock copolymer PVBM-PS-PVBFP in aqueous medium. The corona of the micelles is not visible. The scale bars correspond to 50 nm. Adapted with permission from Ref [30]. TEM image of a single MCM of PB-P2VP-PtBMA (d) and proposed solution structure of the micelle (e). Adapted with permission from Ref [33]. Copyright 2009 American Chemical Society.

For some applications, it is desirable to preserve the micelle structure by cross-linking of one of its compartments.²⁴ This way, their dynamic structure can be fixated to facilitate the transfer of such aggregates into non-selective solvents or to stabilize them even below the critical micellar concentration.^{33,37} Cross-linking can be achieved through a variety of strategies, cold vulcanization or radical cross-linking of PB-domains,³³ UV-induced cross-linking of cinnamoyl methacrylates,^{28,38,39} amidation of PAA⁴⁰ or the use of a bifunctional alkyl iodide to cross-link amino-methacrylate groups.⁴¹ Recent approaches include the employment of Click-chemistry⁴² and a temperature-responsive polymeric NHS-PNIPAM-NHS (NHS = *N*-hydroxysuccinimidyl ester, PNIPAM = poly(*N*-isopropylacrylamide)) cross-linking agent.⁴³

Indeed, stimuli-responsive multicompartment micelles are another important issue in the field. They can be used as sensors, for the stimuli-controlled release of drugs or stabilization of pigments, etc.²² Typical stimuli-responsive blocks are pH-sensitive such as PAA, P2VP and P4VP and thermoresponsive like PNIPAM.²³ The group of McCormick synthesized pH-

responsive α -methoxypoly(ethylene oxide)-*block*-poly[*N*-(3-aminopropyl)methacrylamide]-*block*-poly[2-(diisopropylamino)ethyl methacrylate] (mPEO-PAPMA-PDPAEMA) triblock terpolymers that self-assembled into micelles consisting of PDPAEMA cores, PAPMA shells, and mPEO coronas above pH 6.0. After cross-linking of the PAPMA shells, the size of the shell-cross-linked micelles (SCLMs) increased with decreasing solution pH due to the swelling of the PDPAEMA block.⁴³ Other examples of pH-responsive SCLMs from triblock terpolymers were shown by the group of Liu.^{39,42} One possible application for them is controlled drug-release. This is also possible with non-cross-linked micelles that release the drug upon dissociation at a certain pH value as shown for monomethoxy-capped poly(ethylene glycol)-*block*-poly(2-(dimethylamino)ethyl methacrylate)-*block*-poly(2-(diethylamino)ethyl methacrylate) polymer.⁴⁴ Triblock terpolymers that show intramicellar IPEC formation do so at a certain pH value or in a certain pH range during which the IPEC forming blocks carry the relevant charges.^{34,35,45} However, under different pH or salinity conditions they can also form different morphologies, like core-shell-corona or flower-like micelles.³⁵ Tsitsilianis et al. could prepare a whole plethora of nanostructured particles and hydrogels from poly(2-vinylpyridine)-*block*-poly(acrylic acid)-*block*-poly(*n*-butyl methacrylate) (P2VP-PAA-PnBMA) block terpolymer in aqueous solutions.⁴⁶ The multiresponsive molecule demonstrated a unique diversity of structural organizations caused by the combination of the P2VP and PAA building blocks and the deriving variety of interactions (either intra- or intermolecular), such as hydrophobic and electrostatic (either attractive or repulsive), among the three polymeric segments. The group found conditions for the formation of thermosensitive centrosymmetric core-shell-corona micelles, compact spheres, polyelectrolyte flowerlike micelles, a charged pH-sensitive 3D network, toroidal nanostructures, and finite size clusters (microgels). Apart from triblock terpolymers with one or two stimuli-responsive blocks, also triple-responsive polymers were synthesized and their micellization and aggregation behavior thoroughly examined by the groups of Aoshima,⁴⁷ Zhu⁴⁸ and Laschewsky.⁴⁹

1.3.2 Multicompartment micelles with a compartmentalized corona

Compared to the diversity of multicompartment micelles with a compartmentalized core, the examples of multicompartment micelles with a compartmentalized corona are few. This is already indicated by the fact that very often the term “multicompartment micelles” (MCMs) is used when the exact denomination was “multicompartment core micelles”. Indeed many triblock terpolymers with two solvophilic outer blocks result in a core-corona structure with a non-segregated corona; a micellar structure related to the ones formed by

AB diblock copolymers²² which will not be discussed here. However, there are also some very interesting investigations into multicompartiment micelles with a compartmentalized corona.

The group of Liu has explored a number of micelle-like aggregates (MAs) with segregated corona compartments.⁵⁰⁻⁵² The micellization behavior of poly(*tert*-butyl acrylate)-*block*-poly(2-cinnamoyloxyethyl methacrylate)-*block*-poly(glyceryl monomethacrylate) (PtBA₁₀₇-PCEMA₁₉₃-PGMA₁₁₅) was examined in pyridine/methanol mixtures.⁵⁰ While pyridine is a solvent for all three blocks, methanol is selective for PtBA and PGMA. With increasing methanol content, the polymer first formed spherical, then cylindrical micelles with mixed coronas and then vesicular and tubular MAs again with PCEMA in the core but with segregated PtBA patches in the PGMA corona (Figure 1-6a).

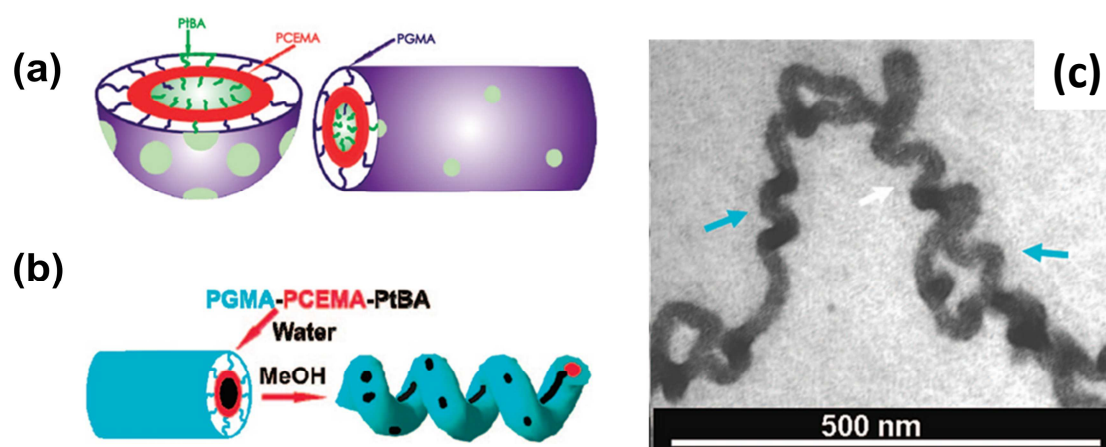


Figure 1-6. Cross-sectional schematics of structures of vesicular and tubular MAs of PtBA-PCEMA-PGMA (a), schematic of the chain packing in the cylindrical MAs and twisted cylinders of PGMA-PCEMA-PtBA (b) and TEM image thereof (c, stained with RuO₄). Adapted with permission from Ref [50,51]. Copyright 2008 American Chemical Society.

The same blocks in a different composition (PGMA₃₁₀-PCEMA₁₃₀-PtBA₁₁₀) were dissolved in water where the polymer formed core-shell-corona cylinders with the insoluble PtBA and PCEMA blocks making up the core and shell and the soluble PGMA block forming the corona. Then the solution was dialyzed against methanol and the cylinders with PCEMA cores twisted in water/methanol with high methanol contents, e.g., >90 vol%, probably to create more space to accommodate the segregated PGMA chains, which were longer, better solvated, and more crowded than the PtBA chains.⁵¹ For a PtBA-PCEMA-PDMAEMA triblock terpolymer

similar chain segregation and twisting was observed in the first stages of the morphological evolution when water was added to a solution of the polymer in methanol.⁵²

From polystyrene-*block*-polyethylene-*block*-poly(methyl methacrylate) (PS-PE-PMMA) cylindrical micelles with a crystalline PE core and a patched corona formed by microphase-separated PS and PMMA chains were obtained in organic media.⁵³ The patchy corona could be clearly visualized by selective staining in transmission electron microscopy. The worm-like micelles can be formed by seeded growth of triblock terpolymer unimers from spherical crystalline-core micelles and even subsequent epitaxial growth to triblock co-micelles can take place.⁵⁴

Du and Armes used a primary amine based triblock terpolymer, poly(ethylene oxide)-*block*-poly(3-caprolactone)-*block*-poly(2-aminoethyl methacrylate) (PEO-PCL-PAMA), to prepare patchy multicompartiment micelles by dissolution in purely aqueous solution at pH 7.⁵⁵ At lower pH (pH 5) a mixture of patchy MCMs and even Janus micelles (complete lateral segregation) was obtained.

Fang et al. presented micelles with a compartmentalized corona prepared from poly(4-*tert*-butoxystyrene)-*block*-polybutadiene-*block*-poly(*tert*-butyl methacrylate) (PtS-PB-PtBMA).⁵⁶ For this purpose the PB block was fluorinated so that in dioxane this block was insoluble and formed the core of the micelles with initially a mixed corona of PtS and PtBMA. During annealing a rearrangement occurred that resulted in micelles with different degrees of chain segregation, from various patchy to again even some Janus micelles (Figure 1-7). Further, bamboo-like, undulated cylindrical assemblies were obtained by stacking of the micelles in ethanol, which is a selective solvent for PtBMA.

Walther et al. investigated the extent of compartmentalization in micelles formed by a series of bishydrophilic block terpolymers with two outer water-soluble segments, PEO-PnBA-PNIPAM.⁵⁷ Here, the LCST behavior of PNIPAM was used to artificially increase the incompatibility within the corona-forming blocks. Consequently, phase separation of the corona was triggered by the collapse of the PNIPAM blocks via temperature raise. Repeating heating cycles increased the extent of phase separation, but regardless of the length of the thermoresponsive block, a full transition to Janus micelles could not be induced. This was attributed to the energetic penalties in the core and the very minor energetic differences between multicompartiment and Janus micelles inside the corona, which cannot counterbalance the entropic penalty.

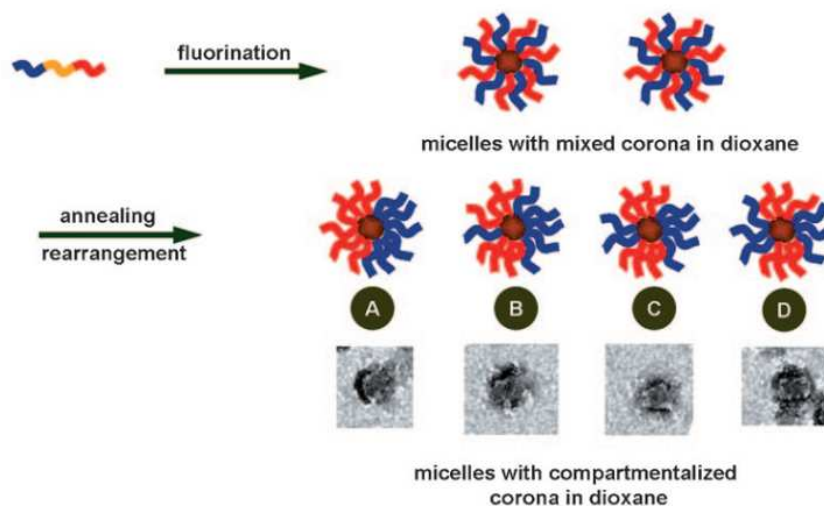


Figure 1-7. Preparation of micelles with compartmentalized corona from PtS-PB-PtBMA by fluorination of the PB block and solvent annealing. Reprinted with permission from Ref [56].

Recently, Borisov and Zhulina presented a theoretical paper about the self-assembly of triblock terpolymers in selective solvent towards corona-compartmentalized (Janus) micelles,⁵⁸ in which they examined the interplay of the many variables that influence chain segregation in multicompartiment corona micelles.

1.3.3 Multicompartiment micelles by precise hierarchical self-assembly

While a vast variety of MCMs has been presented so far, the lack of a general understanding of what governs MCM morphologies prepared from linear triblock terpolymers and a straightforward concept how to manipulate their formation and their hierarchical superstructures becomes apparent.^{23,59} This gap has been closed to a certain extent by Müller and coworkers who introduced a concept of directed self-assembly via pre-assembled subunits and the sequential reduction of the degrees of freedom.⁵⁹ It largely contrasts most of the other present approaches that use one-step dissolution or direct dialysis. Here, the ABC triblock terpolymers are first dissolved in a non-solvent for B which yields well-defined micellar subunits with a collapsed but dynamic B core and a mixed or compartmentalized corona of blocks A/C (first reduction of conformational freedom). Subsequently, the micelle solution is dialysed against a non-solvent for A. The collapse of A happens slowly during dialysis and due to the thus increased phase separation of A and C, rearrangements, possible because of the dynamic core, occur. Finally, the soluble C blocks

cannot solubilize the rearranged subunits anymore and consequently they aggregate into hierarchical MCMs to reduce the exposure of the A domains to the surrounding solvent (second reduction of conformational freedom). In the resulting MCMs the collapsed block A forms the core, the B block forms the patches at the surface of the central core and the C block forms the corona (Figure 1-8).

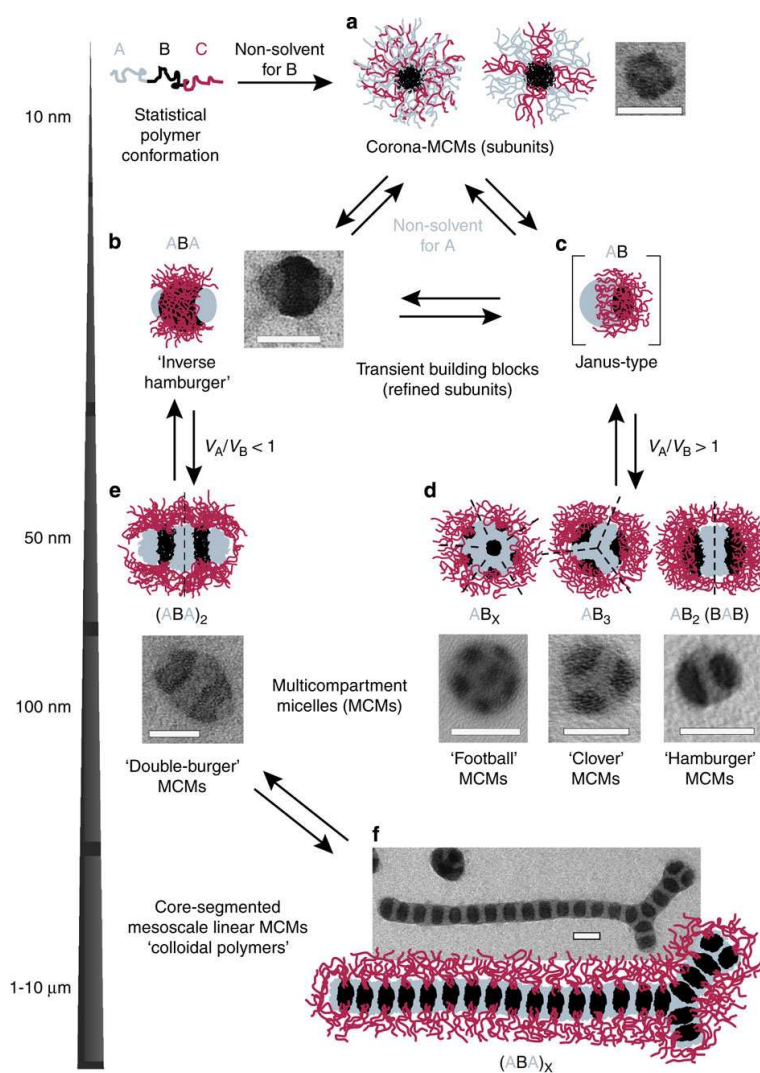


Figure 1-8. Detailed mechanism for the preparation and directed hierarchical self-assembly of well-defined MCMs. Reprinted with permission from Ref [59].

The formation of different MCM structures like “football”, “clover”, “hamburger” and “double-burger” MCMs, is governed by different factors such as the volume (V) ratio of the core-forming A and B blocks, the solvent quality for the C block and the length of the corona-forming C chains. In particular, spherical or linear MCMs occur when V_A/V_B is greater or less

than unity, respectively and the number of patches increases with increasing V_A/V_B ratio. This concept was verified for a range of triblock terpolymers differing in block components, polarity of the final solvent and dynamics of the middle block (T_g varying from -51 to +100 °C). Thus, it is a truly general concept, allowing the prediction and manipulation of MCM structures. Compared to other approaches clear advantages of the step-wise procedure are the rapid preparation (in contrast to protocols with equilibration times up to days) and the access to unique architectures with highly homogenous populations. Further, the control over the hierarchical step-growth polymerization of MCMs into micron-scale segmented supracolloidal polymers was also demonstrated. In a follow-up work it could be shown, how two additional steps, cross-linking of the B block in the MCMs and subsequent dispersion of the thus fixated micelles in a good solvent for all three blocks, open up the possibility of Janus sphere preparation with controllable corona ratios.⁶⁰

1.4 Janus particles

A special subclass of MCMs are Janus particles (JPs). They are bicompartimentalized, non-centrosymmetric colloids. Their two sides or surfaces are different in terms of their chemical and/or physical properties and they were named after the two-faced Roman god Janus.^{61,62} First synthesized by Casagrande et al. in 1989,⁶³ the term “Janus” became popular after deGennes mentioned “Janus grains” in his Nobel lecture about soft matter in 1991.⁶⁴ Now JPs have gained much interest during the last years. Several general reviews⁶⁵⁻⁶⁹ and ones concerning their synthesis,^{70,71} supramolecular organization^{72,73} and with a special focus on inorganic⁷⁴ or polymeric JPs^{72,75} appeared in recent years.

1.4.1 Synthesis of Janus particles

In contrast to other anisotropic morphologies the synthesis of JPs remains more challenging.¹ However, a whole range of possible Janus synthesis protocols exists today. They can be divided into three main categories: masking techniques, phase separation approaches and self-assembly (Figure 1-9).⁶⁶

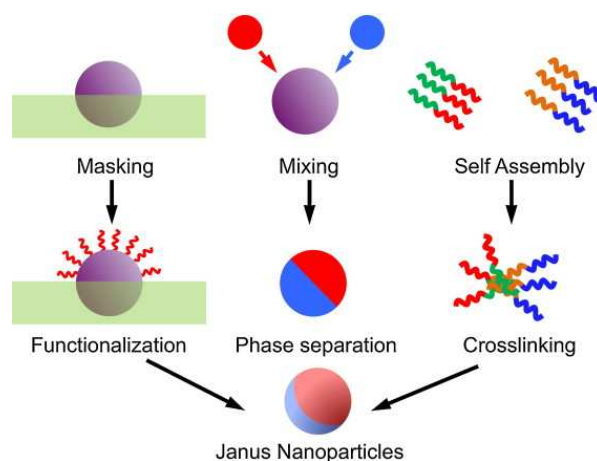


Figure 1-9. Scheme illustrating the three main strategies for the preparation of Janus particles: masking, phase separation and self-assembly. Reprinted with permission from Ref [66].

Masking processes mostly consist of the desymmetrization of spherical homogeneous particles in the micro- and nanometer range. For this purpose the particles are often adsorbed on a solid surface.⁶⁶ The deposited particles can then be chemically functionalized and released, if desired also functionalized on the hemisphere inaccessible before.⁷⁶ Instead of chemical functionalization also metal deposition on the adsorbed particles is often employed.⁷² Apart from a planar surface, particles can also be adsorbed on larger particles, for example PAA coated nanoparticles that were electrostatically adsorbed onto positively charged silica beads and then functionalized on their non-masked hemispheres.⁷⁷ Nie et al. used hybrid nanotubes as the desymmetrization tool that were coated with crosslinked divinylbenzene spheres in situ. On the sphere surface exposed to the surrounding solution, NIPAM polymerization took place.⁷⁸ A very important masking approach was developed by the Granick group. It is based on the formation of an oil-in-water Pickering emulsion of silica particles, using a paraffin wax as the oil phase. Again, the exposed hemispheres of the silica particles can be functionalized and the Janus particles easily obtained after dissolution of the wax.^{66,79,80} Amounts on the gram scale can be prepared with this method that was also used by other groups, e.g. Perro et al.⁸¹

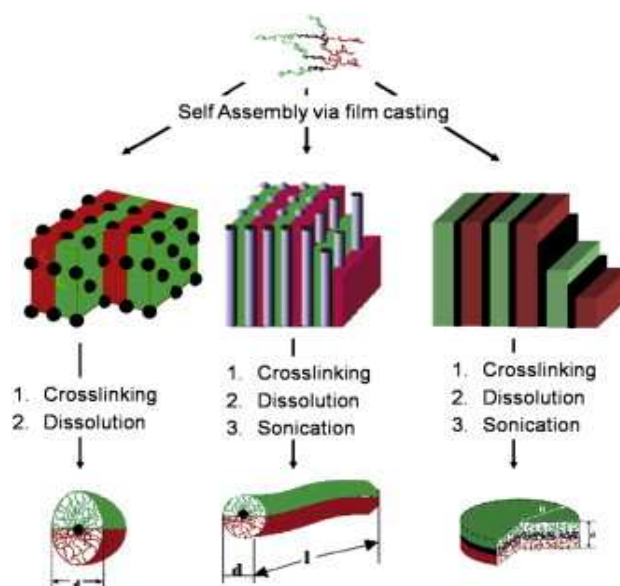
The concept of JP synthesis by phase separation is applied for the preparation of purely inorganic, polymeric-inorganic and purely polymeric particles. The synthesis of so-called “heterodimers” consisting of two inorganic materials to combine their different properties is a wide scientific field with many different mechanisms and many accessible particle morphologies, among them a number of Janus-like ones, such as dumbbell or matchstick shapes.^{66,82-84} Polymer-inorganic heterodimers can be synthesized by techniques like

mini-emulsion polymerization,⁸⁵ dewetting processes⁸⁶ and simple approaches like adding inorganic colloids during the polymerization.⁸⁷ In all cases, the incompatibility of the polymeric and the inorganic component lead to Janus morphologies. For purely polymeric JPs, phase separation processes are the essential characteristic in electrohydrodynamic co-jetting of polymer solutions⁸⁸ and photopolymerization or photolithographic polymerization in microfluidic devices.⁷² Another interesting approach is oil-in-water mini-emulsion, where the oil phase consisted of two immiscible polymers. After emulsification, the solvent was evaporated, leading to phase separation of the two polymers.^{66,89} The group of Shimomura explored a variety of morphologies prepared by a similar protocol. Two polymers or diblock copolymers with a common block were first dissolved in organic solvent and subsequently precipitated in water under stirring to remove the solvent resulting in spherical particles with e.g. lamellar or Janus structure depending on the employed polymers and their respective concentrations.^{90,91}

Self-assembly resulting in JPs can occur for diblock copolymers and triblock terpolymers. Pairs of diblock copolymers either have a common block to form the Janus micelle core⁹² or two compatible blocks like PAA and poly(2-methylvinylpyridinium iodide) (P2MVP). In a mixture of P2MVP-*b*-PEO and PAA-*b*-PAAm (polyacrylamide), electrostatic interactions between the negatively charged PAA blocks and the positively charged P2MVP lead to the self-assembly of disc-like Janus micelles with PAA and P2MVP in the core and phase-separated PEO and PAAm as the hemispheres.^{93,94} Two approaches of solution-self-assembly of triblock terpolymers that partly yielded Janus micelles population were already introduced in section 1.3.2.^{55,57} Sfika et al. observed intermediate Janus micelles during the ageing of P2VP-PMMA-PAA particles in aqueous solution at low pH.⁹⁵ Dupont and Liu utilized the aggregation of a triblock terpolymer with a photo-cross-linkable middle block into “hamburger” micelles and core-segregated cylinders to cross-link block B, followed by dissolution of the aggregates to yield JPs. As already presented in section 1.3.3, Gröschel et al. used a similar approach when they cross-linked the B domains in MCMs assembled from Janus-like triblock terpolymer subunits and subsequently dispersed the particles in a solvent for all three blocks to gain the according JPs.⁶⁰

A self-assembly method that successfully accomplished both tasks, the synthesis of spherical as well as non-spherical JPs and of particles in the nanometer range is based on converting triblock terpolymer bulk structures via selective crosslinking of the middle block.⁹⁶⁻⁹⁸ The self-assembly of triblock terpolymers has already been discussed in section 1.2. Among the multitude of possible bulk morphologies three, namely lamella-sphere (ls), lamella-cylinder (lc) and lamella-lamella (ll), are most suitable for JP synthesis. The non-centrosymmetric

orientation of the terminal blocks A and C can be preserved by cross-linking of the inner block B. Subsequent dissolution of the bulk material yields the according JPs. For cylinders and discs, originating from lc and ll morphologies, the additional step of ultrasound-sonication might be necessary to break down large particles (Scheme 1-1).⁹⁹ The concept was first used by the groups of Ishizu¹⁰⁰ and Müller.⁹⁶ Ishizu and coworkers synthesized spherical JPs by cross-linking the P2VP microdomains of the ls-morphology of a PS-P2VP-PtBMA triblock terpolymer with 1,4-diiodobutane while Müller and coworkers prepared spherical micelles from a PS-PB-PMMA triblock terpolymer by cross-linking the PB domains in the ls-morphology by cold vulcanization with S₂Cl₂ and radical cross-linking (by co-casting of radical initiator in the polymer film). Apart from spherical particles,⁹⁶ the Müller group also produced cylinders^{101,102} and sheets or discs.^{73,103} The accessible particle sizes depend on the total molecular weights of the precursor triblock terpolymers and are between 10 and 50 nm for the cross-section of the resulting colloids.⁹⁹ The molecular weight fraction of the inner block is responsible for the resulting particle shape. While the symmetrical volume fractions of the outer blocks maintain the overall lamellar structures, the increase in the volume fraction of the inner block causes the phase transitions from ls to lc to ll.



Scheme 1-1. Overview of the pathway for the preparation of different Janus particles via selective crosslinking of microphase-segregated structures of triblock terpolymers. Reprinted with permission from Ref [97].

Further, external influences, e.g. the film-casting solvent, the addition of swelling solvents or cross-linking agents, can also trigger changes in the structure. However, this can be utilized in certain cases when these influences help to tailor the microphase-segregated structure into a desirable non-equilibrium morphology.⁹⁹ The resulting JPs are rather monodisperse in size due to their origin in defined bulk morphologies and can be produced on a multigram scale.

1.4.2 Applications of Janus particles

Their non-centrosymmetric architecture provides JPs with unique properties not accessible for homogeneous analogs. For instance, the broken symmetry leads to the formation of a variety of complex superstructures,^{65,73,102,104} which cannot be obtained from simple particles, thus representing fascinating building blocks for the constructions of hierarchical assemblies and materials. Further, they have a high tendency to adsorb and assemble at interfaces due to their bicompartiment character, thereby lowering interfacial tension significantly further as compared to homogenous particles or block copolymers.^{105,106,107} This enhanced interfacial adsorption capabilities of JPs were first predicted by Binks and Fletcher.¹⁰⁸ They predicted an up to threefold stronger adsorption of JPs compared to homogeneous particles.⁹⁹ These predictions were confirmed by Glaser et al.¹⁰⁵ who examined the oil-water interfacial tension via pendant drop tensiometry and observed a remarkable reduction caused by bimetallic JPs compared to homogenous metallic gold or iron oxide nanoparticles. In further studies Walther et al.¹⁰³ and Ruhland et al.^{106,109} studied the interfacial behavior of polymeric Janus spheres, discs and cylinders, examining the influence of their shape and their performance compared to linear non-crosslinked precursor triblock terpolymers compared to which the JPs are significantly more powerful in reducing the interfacial tension.⁹⁹ The same supremacy of JPs compared to their linear precursor triblock terpolymers was observed in the utilization as compatibilizer for polymer blends.¹⁰⁷ With their enhanced adsorption due to their biphasic particle character, JPs remained located exclusively at the interface of the two polymer phases despite high temperature and shear conditions while also providing a smaller domain size of the dispersed phase. The same polymeric JPs were also successfully employed as stabilizers in emulsion polymerization.¹¹⁰ Janus micelles synthesized via cross-linking of MCMs⁶⁰ proved to be well suited as supracolloidal dispersants for carbon nanotubes.¹¹¹ Inorganic JPs have been investigated for their unique optical, magnetic and catalytic properties.^{66,82} For instance, Au/MgO heterodimer crystals presented a catalytic activity higher than that of the traditional catalyst.^{112,113} The different

compartments make JPs also attractive for biological applications. Hosting different enzymes or metal nanoparticles they could be used as (bio)nanoreactors⁵⁸ or for drug delivery of two different drugs to achieve synergistic effects.¹¹² Already reported applications include polystyrene-magnetite JPs that combined optical detection by a fluorescent dye in the PS compartment with magnetolytic therapy^{67,114} and silver-maghemite JPs coated with silica to use as biocompatible cellular biomarkers that unite optical detection and magnetic recovery.¹¹⁵ A real hands-on application was shown by Synytska et al. who coated poly(ethylene terephthalate)-based textile fibers with amphiphilic JPs to render them water-repellent.¹¹⁶

1.5 Objective of this thesis

The general objective of this thesis is the synthesis of triblock terpolymers with functional moieties via living anionic polymerization, followed by the multicompartment micelle and Janus particle synthesis from the prepared triblock terpolymers.

Up to now Janus particles synthesized via selective cross-linking of microphase-segregated bulk structures of triblock terpolymers were mainly prepared from polystyrene-*block*-polybutadiene-*block*-poly(methyl methacrylate) and polystyrene-*block*-polybutadiene-*block*-poly(*tert*-butyl methacrylate). In terms of chemical alterations and stimuli-responsiveness these offer only the possibility of hydrolysis of the C block to yield water-soluble PMAA. Therefore, new suitable monomers with more functionality and stimuli-responsiveness have to be identified, their suitability for anionic polymerization tested and the resulting building blocks characterized. The next step is their application in the synthesis of triblock terpolymers and investigation of the derived bulk morphologies.

Where applicable, Janus particles are to be synthesized from the bulk structures via selective cross-linking of the middle block by cold vulcanization and radical cross-linking.

Further, solution structures of the triblock terpolymers will be investigated. Here, especially the new concept of multicompartment micelles by precise hierarchical self-assembly will be used. This pathway will be further utilized for the synthesis of spherical Janus particles via cross-linking of multicompartment micelle domains.

First results of the solution properties of obtained particles will also be included in this thesis.

2 Experimental Part and Methods

2.1 Materials

4-(*tert*-butoxy)styrene, *tert*-butyl methacrylate and 2-(dimethylamino)ethyl methacrylate (all Aldrich) were degassed, treated with dibutyl magnesium (*tert*-butoxystyrene), trialkylaluminium (*tert*-butyl methacrylate) or tri-*n*-octylaluminium (2-(dimethylamino)ethyl methacrylate) and distilled or condensed, respectively.¹⁰² 4-(dimethylaminomethyl)styrene (90 %, Acros) was isolated via column chromatography, dried over calcium hydride, degassed and purified with *n*-dibutylmagnesium via distillation. Tetrahydrofuran for anionic polymerization (≥ 99.9 %, Sigma-Aldrich) was refluxed three times over calcium hydride and three times over potassium. 1,1-Diphenylethylene (98 %, Acros) was distilled from *sec*-butyllithium under reduced pressure. 2,2'-azobis(isobutyronitrile) (AIBN, Aldrich, 98 %) was recrystallized twice from methanol prior to use. *Sec*-butyllithium (1.4 M in cyclohexane, Aldrich and 1.4 M in cyclohexane, Acros), benzene (p.a. grade, Sigma Aldrich), *N,N'*-dicyclohexylcarbodiimide (≥ 99 %, Fluka), 4-(dimethylamino)pyridine (≥ 99 %, Aldrich), 4-pentynoic acid (98 %, ABCR), 1,4-butanediol (p.a. grade, Sigma Aldrich), 1,3-propanediol (98 %, Aldrich), dimethylformamide (waterfree 99.8 %, Sigma-Aldrich), calcium hydride (≥ 95 %, Fluka), *n*-dibutylmagnesium (1.0 M in heptane, Aldrich), *n*-hexane (98.9 %, AnalaR NORMAPUR), ethyl acetate (> 99.5 %, Sigma-Aldrich), methanol (≥ 99.8 %, Fisher Scientific), buffer solution (pH 2 – 8, AVS Titrimorm), hydrochloric acid (32 wt%, Sigma-Aldrich and 37 wt%, Grüssing), sodium hydroxide (1.0 M, Fluka; 0.1 M, Merck; pellets, Riedel de Haën), acetonitrile (anhydrous 99.8 %, Aldrich), chloroform (p.a. grade, Fisher Scientific), 1,4-dioxane (p.a. grade, Fisher Scientific and Riedel de Haën), *tert*-butanol (p.a. grade, Merck), tetrahydrofuran (technical grade for soxhlet extraction; p.a. grade, VWR; 99.9 % AnalaR NORMAPUR), dimethylacetamide (≥ 99 %, Roth), ethanol (technical grade), dichloromethane (technical grade), sulphur monochloride (98 %, Aldrich), photoinitiator 2,4,6-trimethylbenzoyldiphenylphosphine oxide (Lucirin® TPO (kindly provided from BASF)), trimethylsilyl iodide (p.a. grade, Fluka and 97%, Aldrich) and dialysis membranes (Spectra/Por) were used as received. Water was purified with a Milli-Q water purification system by Millipore.

2.2 Instrumentation

Nuclear magnetic resonance (NMR). ^1H -NMR spectra were obtained either with a Bruker AC 250-spectrometer at an operating frequency of 250 MHz or with a Bruker Ultrashield-300 at 300 MHz. Various deuterated solvents from Deutero GmbH were used depending on the solubility of the samples and tetramethylsilane was used as internal standard. The data was evaluated using the programs 1D WIN-NMR and SpinWorks 3.

Size exclusion chromatography (SEC). SEC measurements in THF were performed with a set of 30 cm SDV-gel columns of 5 μm particle size having pore sizes of 10^5 , 10^4 , 10^3 , and 10^2 Å with a refractive index (RI) and UV ($\lambda = 260$ nm) detection. THF containing toluene as internal standard was used as eluent (flow rate 1 mL min^{-1}). Data evaluation was carried out with WinGPC using a polystyrene calibration. Measurements in DMAc were performed at 60 °C using a SEC system with a set of PSS GRAM columns (7 μm particle size with pore sizes of 10^2 and 10^3 Å). The Agilent 1200 system was equipped with RI and UV ($\lambda = 260$ nm) detection. DMAc containing 0.5 M LiBr was used as eluent (flow rate 0.7 mL min^{-1}). Data evaluation was carried out with WinGPC using a polystyrene-poly(methyl methacrylate)-poly(2-(dimethylamino)ethyl methacrylate) calibration. Poly(*tert*-butoxystyrene)-*block*-polybutadiene-*block*-poly(2-(dimethylamino)ethyl methacrylate) and (for comparison) its precursors were characterized with a system using THF with additional 0.25 wt% tetrabutylammonium bromide (TBAB) as eluent. (flow rate 0.5 mL min^{-1}). The Waters instrument was equipped with PSS SDV gel columns (30 x 8 mm, 5 μm particle size) with 10^5 , 10^4 , 10^3 , 10^2 Å pore sizes, using RI and UV ($\lambda = 254$ nm) detection. Data evaluation was carried out with WinGPC using a polystyrene calibration.

Size exclusion chromatography - multi angle light scattering (SEC-MALS). Measurements were performed at room temperature using a SEC system with three 30 cm PSS SDV columns (10^4 , 10^5 , 10^6 Å), equipped with a Wyatt DAWN HELEOS light scattering detector (50 mW solid state laser; $\lambda = 658$ nm) and an Agilent HPLC-assembly. THF was used as eluent (flow rate 0.8 mL min^{-1}). Data evaluation was carried out with the Astra Software.

Small-angle X-ray scattering (SAXS). Measurements of a solvent cast free-standing polymer film of tSBT of ca. 200 nm thickness were performed with a rotating anode Bruker Microstar microfocus X-ray source (Cu K_α radiation, $\lambda = 1.54$ Å) with Montel Optics with a measurement time of 4 h. The beam was further collimated with four sets of slits, resulting in a beam area of about 1 x 1 mm at the sample position. Scattering intensities were measured using a Bruker AXS 2D area detector. The sample-to-detector distance was 1.5 m. SAXS measurements of solvent-cast films of tSBD were performed on a Bruker AXS Nanostar

(Bruker, Karlsruhe, Germany), equipped with a microfocus X-ray source (Incoatec I μ SCu E025, Incoatec, Geesthacht, Germany), operating at $\lambda = 1.54 \text{ \AA}$. A pinhole setup with 750 μm , 400 μm , and 1000 μm (in the order from source to sample) was used and the sample-to-detector distance was 107 cm. Samples were mounted on a metal rack and fixed using tape. The scattering patterns were corrected for the beam stop and the background (Scotch tape) prior to evaluations. Measurement time was 4 h.

Photo-cross-linking. Cross-linking was induced with a HOENLE UVA HAND 250 lamp (cut-off < 350 nm).

Sonication. Treatment was performed with a Branson model-250 digital sonifier with a 1/8 inch diameter tapered microtip (200 watt at 100% amplitude).

Scanning force microscopy (SFM). Images were taken on a Veeco Digital Instruments Inc. Dimension 3100 closed loop microscope in tapping mode. Offline data processing was done using the Nanoscope Software V6.14R1.

Transmission electron microscopy (TEM). Images were recorded in bright field mode with a Zeiss CEM 902 transmission electron microscope operated at 80 kV and a LEO 922 OMEGA transmission electron microscope operated at 200 kV. Polymer films were cut into thin sections at room temperature using a Reichert-Jung Ultracut E microtome equipped with a diamond knife. Data evaluation and processing was carried out with Soft Imaging Viewer, Digital Micrograph 365 Demo software and Image Tool.

Scanning electron microscopy (SEM). For SEM investigations, samples were fixed via a double-sided adhesive conductive carbon tape on a SEM sample holder and carbon-coated utilizing a MED 010 coating machine from Baltzer. SEM micrographs were recorded using a Zeiss 1530 FESEM equipped with an Inlens detector (acceleration voltage: 5 kV).

Fourier transform infrared spectroscopy (FTIR). Measurements were performed with a Perkin Elmer Spectrum 100 FT-IR Spectrometer in ATR modus. After four background measurements the sample was analyzed four times between 650 cm^{-1} and 4000 cm^{-1} .

Near-infrared spectroscopy (NIR). Measurements were performed with a ZEISS ECCU MCS611 NIR 2,0 HR CLH600 spectrometer. The change of absorbance of the overtone vibration of the vinyl groups at 1630 nm was measured by using the program ZEISS procXplorer Version 1.3. After recording a background measurement of the solvent and injection of (4-dimethylamino)methylstyrene measurements were started when adding *sec*-BuLi. The program Aspect Plus was used for the evaluation of the data and the raw data were corrected.

Turbidity measurements. Measurements were performed with an 809 Titrand from Metrohm at 25 °C working with the program Tiamo 1.3. Changes of the pH value were ascertained under stirring via a micro-pH electrode and changes of the transmission via a turbidity sensor Spectrosense 523 nm from Metrohm. During temperature dependent measurements, an Aquatrode Plus sensor from Metrohm was used to measure changes of temperature and pH. Here, the solutions were heated with a heating rate of 1 K min⁻¹.

Dynamic light scattering (DLS). DLS measurements were performed on an ALV DLS/SLS-SP 5022F compact goniometer system with an ALV 5000/E cross-correlator and a He-Ne laser ($\lambda = 632.8$ nm). The measurements were carried out in cylindrical scattering cells ($d = 10$ mm) at an angle of 90° and a temperature of 20 °C. For temperature-dependent measurements, the temperature of the decaline bath of the instrument was controlled using a LAUDA Proline RP 845 thermostat. The temperature was increased in steps of 2 K followed by an equilibration time of 5 min prior to each measurement. The CONTIN algorithm was applied to analyze the obtained correlation functions. Apparent hydrodynamic radii were calculated according to the Stokes-Einstein equation.

2.3 Methods

Anionic polymerization of *tert*-butoxystyrene. Living anionic polymerization is meanwhile a standard method and the general procedure of this polymerization technique is described in detail elsewhere.¹⁰² In short, poly(*tert*-butoxystyrene) was synthesized in tetrahydrofuran at -78 °C. The calculated amounts of *tert*-butoxystyrene and *sec*-butyllithium were injected to the cooled solvent. After the polymerization was finished, one milliliter degassed methanol was added. The solution was concentrated, precipitated in water and dried in vacuo.

Free radical polymerization of *tert*-butoxystyrene in bulk. 5.6 mL distilled *tert*-butoxystyrene (29.7 mmol) and the respective amount of AIBN (30.8 mg (0.19 mmol) and 15.6 mg (0.095 mmol)) were stirred at 70 °C under inert gas for 16 h.¹¹⁷ Afterwards, the polymer was dissolved in tetrahydrofuran and precipitated in water. Then the colorless polymer was filtered off and dried in vacuo at 80 °C overnight.

Free radical polymerization of *tert*-butoxystyrene in solution. 5.6 mL distilled *tert*-butoxystyrene (29.7 mmol) and 15.6 mg AIBN (0.095 mmol) were stirred in 10 mL benzene at 70 °C under nitrogen atmosphere for 13 h.¹¹⁸ The solution was dialyzed against 1,4-

dioxane (regenerated cellulose Spectra/Por membrane, MWCO = 1000 g mol⁻¹) and freeze-dried.

Hydrolysis of poly(*tert*-butoxystyrene) with HCl. 1250 mg PtS (7.1 mmol) were dissolved in 1,4-dioxane. 2.5 mL hydrochloric acid (37 %, 3*10⁻² mol) were added under stirring. Then the solution was stirred under reflux at 120 °C for 24 h. The colorless polymer solution was then concentrated (to ca. 50 mL), precipitated in water and dried in vacuo at 80 °C overnight.

Hydrolysis of poly(*tert*-butoxystyrene) with TMSI. 400 mg PtS (2.3 mmol) were dissolved in CDCl₃. After degassing for approximately 20 minutes, a 1.3-fold excess of trimethylsilyl iodide (TMSI) regarding the amount of addressed *tert*-butoxy groups was introduced to the solution with a syringe under nitrogen. Afterwards, the mixture was stirred for 2 h at room temperature and for 2.5 h at 60 °C and then treated with few mL of basic MilliQ-water (pH 12-14, addition of NaOH). Subsequent dialysis against 1,4-dioxane, water/1,4-dioxane (1/1) and water of different pH values was used for the work up.

Etherification of PHS with 1,3-propanesultone. 50.2 mg NaOH (1.3 mmol) were dissolved in 38.5 mL methanol. 100 mg PHS (0.8 mmol) were added and the solution was stirred for 30 min. Then, a solution of 1.1 ml 1,3-propanesultone (1.3 mmol) in 1.6 ml 1,4-dioxane was added and the resulting solution was refluxed at 91 °C for 48 h. Afterwards, the polymer product was precipitated in dichloromethane, filtered off and washed with dichloromethane. The remaining solid was dried in vacuo, thoroughly washed again with water and dried in vacuo overnight.

Esterification of PHS with 4-pentynoic acid. 100 mg PHS (80.8 mmol) were dissolved in a mixture of 5 mL THF and 2.5 ml DMF and degassed with argon. 4-pentynoic acid, DCC and DMAP were added under stirring (see Table 2-1 for the respective amounts).

Table 2-1. Used amounts of reagents for esterification of PHS.

sample	m (4-pentynoic acid) [mg]	m (DCC) [mg]	m (DMAP)[mg]
1	424.9 (4.3 mmol)	903.3 (4.4 mmol)	56.4 (0.5 mmol)
2	112.1 (1.1 mmol)	247.9 (1.2 mmol)	15.1 (0.1 mmol)

The solution was stirred at RT for 48 h. Then, precipitated DCC urea was filtered off and the THF was removed under vacuum. The remaining suspension containing newly precipitated

DCC urea was filtered with a 0.45 μm PTFE syringe filter. Then the polymer solution was precipitated in water to remove the excess pentynoic acid and the polymer was filtered off. After redissolving in THF the polymer was precipitated in *n*-hexane to remove the excess DCC and DCC urea and again filtered off.¹¹⁹

Purification of DMAMS. 4-(dimethylaminomethyl)styrene was purified via column chromatography with silica gel (size: 0.063 mm – 0.200 mm) and an ethyl acetate/*n*-hexane (1:3) solution as eluent. After evaporation of the solvent DMAMS was dried over calcium hydride overnight and distilled: bp 60 °C – 66 °C [10^{-4} mbar]. *N*-dibutylmagnesium was added to the distilled monomer until the solution became yellow and the distillation of DMAMS was repeated.

Anionic polymerization of DMAMS. In short, poly(4-(dimethylaminomethyl)styrene) was synthesized in THF at -72 °C. The calculated amounts of 4-(dimethylaminomethyl)styrene and *sec*-butyllithium were injected to the cooled solvent. After the polymerization was finished, one milliliter degassed methanol was added. The solution was concentrated, dialyzed against 1,4-dioxane (regenerated cellulose Spectra/Por membrane, MWCO = 1000 g mol⁻¹) and freeze-dried.

Preparation of PDMAMS solutions for temperature dependent turbidity measurements. For solutions of pH 6, 7 and 8, an acidic PDMAMS solution of pH 3 was prepared first. Then buffer solutions of pH 6, 7 or 8, respectively, were added until the desired pH value was reached. Before measurements, all solutions were degassed in vacuo to prevent the generation of bubbles at higher temperatures.

Synthesis of poly(*tert*-butoxystyrene)-*block*-polybutadiene-*block*-poly(*tert*-butyl methacrylate) (tSBT), poly(*tert*-butoxystyrene)-*block*-polybutadiene-*block*-poly(2-(dimethylamino)ethyl methacrylate) (tSBD), poly(4-(dimethylamino)methylstyrene)-*block*-poly(allyl methacrylate)-*block*-poly(*tert*-butyl methacrylate) (DSAT). tSBT, tSBD and DSAT were synthesized via living anionic polymerization. Having become a standard method by now, the general procedure of this polymerization technique is described in detail elsewhere.¹⁰² In short, for tSBT the calculated amount of *sec*-butyl lithium initiator (0.22 mL, 0.31 mmol) was added to the *tert*-butoxystyrene solution in THF at -78 °C, and after 1 h butadiene was added to the mixture at -78 °C and polymerized at -30 °C for 5 h. Thereafter, the reaction mixture was treated with a 5-fold excess of 1,1-diphenylethylene (DPE) relative to the amount of initiator before the addition of tBMA at 60 °C and subsequent polymerization at -40 °C for 2 h. For tSBD the calculated amount of *sec*-BuLi initiator (0.23 mL, 0.29 mmol) was added to the *tert*-butoxystyrene solution in THF

at -75 °C, and after 1.5 h butadiene was added to the mixture at -75 °C and polymerized at 10 °C for 6 h. Then the reaction mixture was treated with a 3-fold excess of DPE relative to the amount of initiator at -50 °C. After 1 h DMAEMA was added at -70 °C and subsequently polymerized at -40 °C for 1.5 h. For DSAT the calculated amount of *sec*-BuLi initiator (0.10 mL, 0.14 mmol) was added to the DMAMS solution in THF at -72 °C, and after 7 minutes a 10-fold excess of DPE relative to the amount of initiator was added to the mixture. After 2 h AMA was added and polymerized at the same temperature. Subsequently, tBMA was added and polymerized overnight at -50 °C. All polymerizations were terminated with 1 mL of degassed methanol and the solutions concentrated. tSBT was then precipitated in water and dried in vacuo, while tSBD and DSAT were dialyzed against 1,4-dioxane and subsequently freeze-dried.

Film casting. The respective amount of triblock terpolymer (with Lucirin® TPO) was dissolved in the desired solvent in a crystallization dish or small glass vial. After that, evaporation of the solvent took place for two weeks (crystallization dish) or several days (vial) at room temperature and the films were dried in vacuo for 24 h at room temperature.

Photo-cross-linking with Lucirin® TPO. Polymer films, co-cast with 30 wt% of Lucirin® TPO, were exposed to the radiation of a UV-lamp for 3.5 h.

Cross-linking with sulphur monochloride (S₂Cl₂). A piece of polymer film was swollen in acetonitrile for one day. 5-10 vol% of S₂Cl₂ were added via a syringe and the cross-linking took place at room temperature overnight. In the case of Janus ribbons, films were swollen in an acetonitrile/decane emulsion that needed constant, not too strong stirring (ca. 130 rpm) to avoid large-scale demixing of the two solvents for 14 h. Cross-linking time was 7 h. After the reaction, the films were washed three times with aprotic solvents acetonitrile and 1,4-dioxane and purified via Soxhlet extraction with THF for 1-3 days.

Sonication. Cross-linked material was dispersed in dioxane to give dispersions of an approximate concentration of 1 g L⁻¹. Portions of about 20 mL were then treated with an ultrasound sonication tip under water cooling. The typical settings were a pulse of 2 sec, 5 to 10 sec of pause, sonication time of 30 to 90 sec and amplitude of 30 %. Afterwards, the solutions were filtrated using a 5 µm PTFE filter and freeze dried.

Hydrolysis of Janus cylinders. Janus cylinders were dissolved in CHCl₃ to give a solution of ca. 1.5 wt%. After degassing for approximately 20 minutes, a 1.3-fold excess of trimethylsilyl iodide (TMSI) regarding the amount of addressed *tert*-butoxy groups was introduced to the solution with a syringe under nitrogen. Afterwards, the mixture was stirred for 3 h at 60 °C

and then treated with few mL of basic MilliQ-water (pH 12-14, addition of NaOH). Subsequent dialysis against 1,4-dioxane, water/1,4-dioxane (1/1) and water of different pH values was used for the work up. A regenerated cellulose Spectra/Por dialysis membrane with molecular weight cut-off of 50000 was used.

Preparation of tSBD micelles. Solutions of tSBD in 1,4-dioxane were prepared with a concentration of 1 or 10 g L⁻¹ and dialyzed against water of the desired pH value.

Preparation of multicompartment micelles. tSBD and tSBT were dissolved in DMAc with an initial concentration of 1 g L⁻¹ to form the subunits with collapsed PB cores. Then, the resulting solutions were dialyzed against a selective solvent for the corona block, MilliQ-water in the case of tSBD and EtOH for tSBT.

Preparation of Janus spheres from tSBT MCMs. To a solution of tSBT MCMs in EtOH 2 equivalents of the photo-cross-linker Lucirin® TPO per double bond were added and thoroughly dissolved. Then the solution was irradiated with a UV-lamp for 8 h. Afterwards it was dialyzed against 1,4-dioxane to break up the MCMs into single Janus particles.

Hydrolysis of Janus spheres from tSBT MCMs. A solution of Janus spheres in 1,4-dioxane of a concentration of about 0.5 g L⁻¹ was degassed for about 30 min and then a 5-fold excess of hydrochloric acid (32 %) relative to the amount of present *tert*-butoxy groups was added under stirring. Then the solution was stirred under reflux at 120 °C for 24 h and subsequently dialyzed against 1,4-dioxane.

Preparation of TEM samples. Microtome-cut ultrathin film sections were exposed to OsO₄ vapour for 60 sec for preferential staining of the polybutadiene block (appears black). Liquid TEM samples were solvent evaporated from solutions with a concentration of 1 g L⁻¹ on carbon-coated copper grids. For aqueous solutions, grids were rendered hydrophilic via a plasma treatment and the sample was blotted after 30 sec. For cryogenic transmission electron microscopy (cryo-TEM) studies, a drop of the sample, dissolved in water or toluene, was put on a lacey carbon-coated copper grid, where most of the liquid was removed with blotting paper, leaving a thin film stretched over the lace. The specimens were instantly vitrified by rapid immersion into liquid ethane (aqueous samples) or nitrogen (toluene) and cooled to approximately 90 K by liquid nitrogen in a temperature controlled freezing unit (Zeiss Cryobox, Zeiss NTS GmbH, Oberkochen, Germany). The temperature was monitored and kept constant in the chamber during all of the sample preparation steps. After freezing the specimen it was inserted into a cryo-transfer holder (CT3500, Gatan, München, Germa-

ny) and transferred to the Zeiss LEO 922 OMEGA TEM. Examinations were carried out at temperatures around 90 K.

3 Building Blocks

3.1 Poly(*tert*-butoxystyrene)

3.1.1 Anionic and free radical polymerization

In contrast to its skeletal analog styrene, 4-*tert*-butoxystyrene (for convenience called *tert*-butoxystyrene in the following) has a functional group attached to the benzene ring. This *tert*-butoxy unit itself does not yet dramatically change the monomer's properties. The interesting feature is the possibility of hydrolysis after polymerization, which yields polyhydroxystyrene (PHS).¹¹⁷ Unlike polystyrene (PS) and poly(*tert*-butoxystyrene) (PtS), PHS is water-soluble at high pH.¹¹⁷ Therefore, if it is used as a building block in triblock terpolymers, it opens up the possibility to synthesize water-soluble and amphiphilic Janus particles (JPs).

Tert-butoxystyrene is a monomer suitable for all types of polymerization. Reports about free radical,^{117,120} controlled radical,^{121,122} and cationic¹²³⁻¹²⁵ polymerization exist while the predominantly chosen method is living anionic polymerization in tetrahydrofuran (THF).^{117,126,127} Consequently, it is perfectly suitable to serve in the synthesis of triblock terpolymers via living anionic polymerization just like styrene.

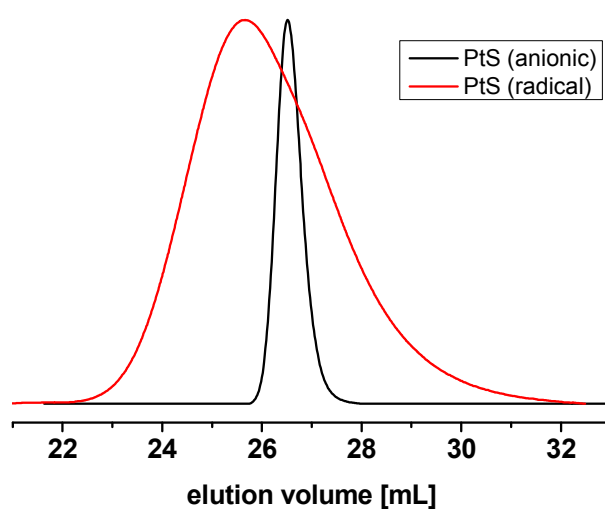
With the living anionic polymerization technique in THF, using *sec*-butyllithium (*sec*-BuLi) as initiator, we were able to synthesize PtS with polydispersity indices (PDIs) as low as 1.01 (Table 3-1 and Figure 3-1). However, to synthesize PtS homopolymers for the execution of model hydrolysis and functionalization reactions, we used free radical polymerization (FRP) with 2,2'-azobis(isobutyronitrile) (AIBN) as initiator as alternative method with less preparative effort.¹¹⁸ While FRP in bulk resulted in bimodal polymers with accordingly high PDIs, FRP in benzene, combined with dialysis against dioxane as work-up, yielded a polymer with a satisfying PDI of 1.51 (Figure 3-1). The NMR spectrum (Figure 3-2) reveals that residual monomer is present. However, the amount is in the range of a molar fraction of 8% and therefore was not expected to disturb the model reactions.

Table 3-1 shows a comparison of the conditions and results of the living anionic and free radical polymerization of PtS.

Table 3-1. Anionic and free radical polymerization of PtS.

	$[I]_0 \times 10^3$ [mol L ⁻¹]	$[M]_0$ [mol L ⁻¹]	$M_{n,th} \times 10^{-3}$ [g mol ⁻¹]	$M_n \times 10^{-3}$ [g mol ⁻¹]	PDI
PtS (anionic)	0.52	0.18	60	53.8 ^a	1.01 ^a
PtS (radical)	9.5	2.97	-	52.8 ^a	1.51 ^a

a) SEC in THF, PS calibration

**Figure 3-1.** SEC traces of PtS synthesized via anionic (black) and free radical polymerization (red).

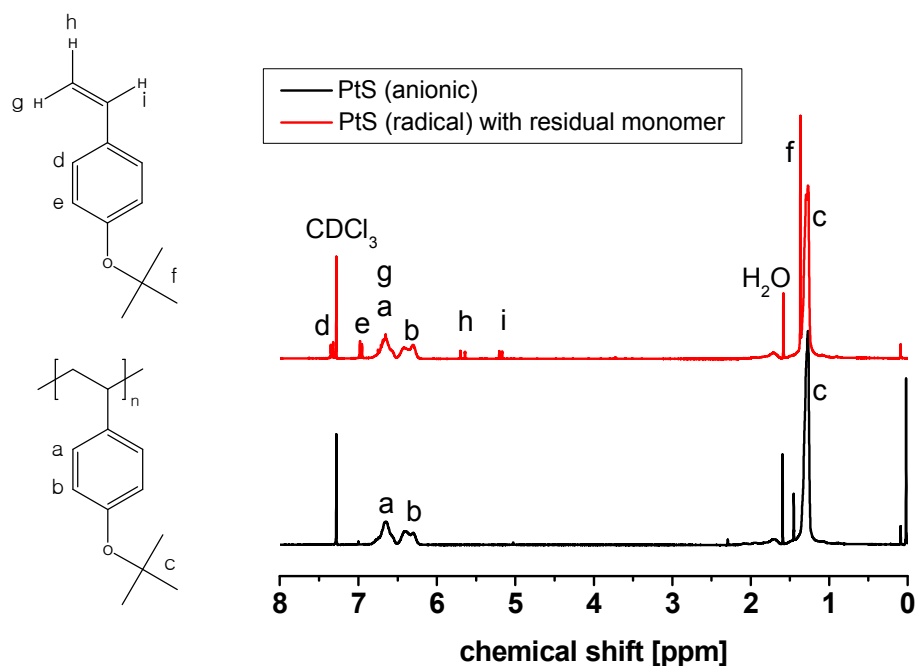


Figure 3-2. NMR spectra of PtS synthesized via anionic (black) and free radical polymerization (red).

3.1.2 Hydrolysis

As mentioned above, PtS can be hydrolyzed to polyhydroxystyrene (PHS), a pH-sensitive weak polyelectrolyte. In contrast to PS, PHS is soluble in water at high pH and as such represents a stimuli-responsive segment.^{128,129} Some isolated reports exist on the utilization of PHS in the field of block copolymers and for stimuli-responsive micelles because of this interesting property.¹²⁸⁻¹³⁶

The simplest method for the hydrolysis of PtS is refluxing with hydrochloric acid in dioxane. Figure 3-3 shows the NMR spectra of PtS and of PHS prepared by this procedure, Figure 3-4 the accordant IR spectra. The NMR of PHS exhibits the signal of the hydroxyl group at 8.9 ppm while the *tert*-butoxy signal around 1.3 ppm has vanished. In the IR, a large water-signal around 3318 cm^{-1} that is caused by the hydroxyl group is visible and at 1365 cm^{-1} the *tert*-butoxy signal is largely diminished.

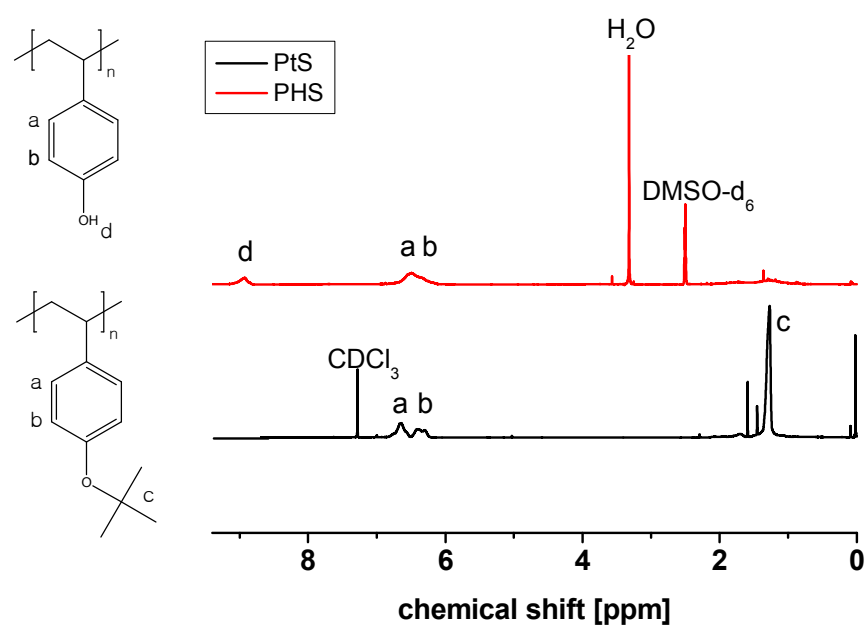


Figure 3-3. NMR spectra of PtS (black) and its hydrolyzed analog PHS (red).

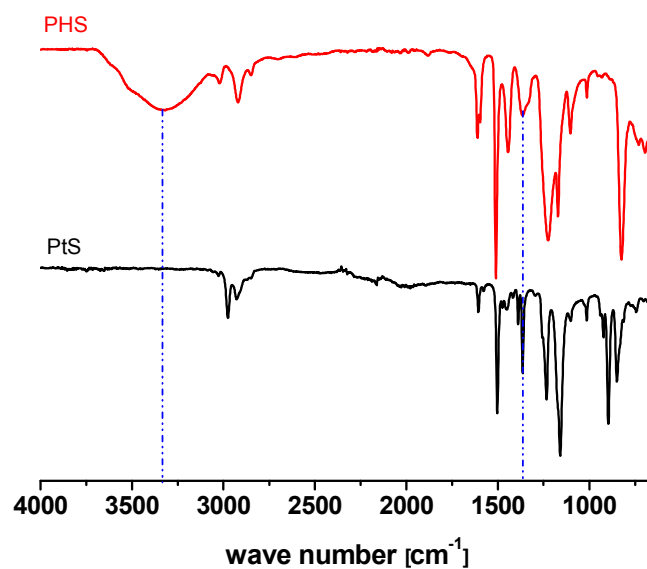


Figure 3-4. IR spectra of PtS (black) and PHS (red).

However, when we intended to use the same approach for Janus cylinders with a PtS and a poly(*tert*-butyl methacrylate) (PtBMA) hemisphere, the reflux at high temperatures (~110

°C) in only a small batch volume (~ 5 mL) caused a significant amount of material to decompose and stick at the side of the reaction vessel.

So, as alternative route we chose the hydrolysis with trimethylsilyl iodide (TMSI) that takes place at room temperature. This reaction was introduced in 1977 by Jung and Lyster for esters¹³⁷ as well as ethers.¹³⁸ As it is tolerant of a lot of functional groups, e.g. amines, amides or ketones, it remains an important mild and efficient hydrolysis method in organic synthesis to this day.¹³⁹ The principle of this method is the treatment of the ester or ether with TMSI, resulting in a silyl ester or ether, followed by the actual hydrolysis with water or methanol. In the field of polymer chemistry it has been successfully used for the hydrolysis of poly(*tert*-butyl acrylate) (PtBA)¹⁴⁰ and PtBMA.¹⁴¹

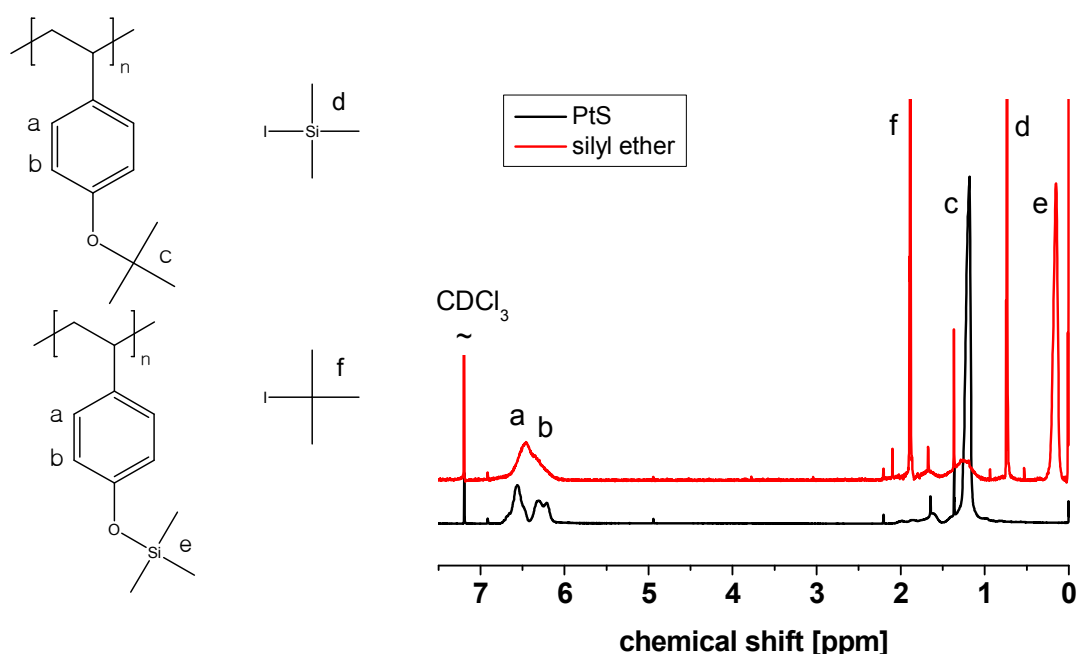
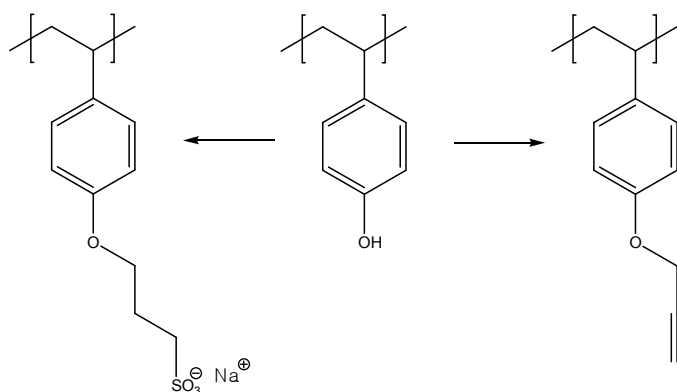


Figure 3-5. NMR spectra of PtS (black) and its corresponding silyl ether (red) after reaction with TMSI.

3.1.3 Functionalizations

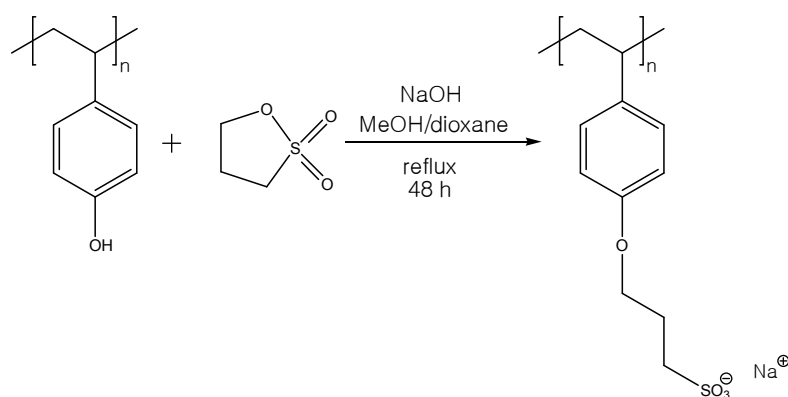
As a main benefit, the hydroxyl group of PHS allows chemical modifications in different directions, which further increases the versatility of this polymer. Two examples from literature are the functionalization with 1,3-propanesultone to obtain a polymer with sulfonate groups¹⁴² and with propargylbromide to introduce alkyne groups (Scheme 3-1).¹⁴³



Scheme 3-1. Possible functionalization reactions of PHS.

A polymer with sulfonate groups is a strong anionic polyelectrolyte. Further, the sulfonate groups can be hydrolyzed to thiol groups or esterified with alcohols (after transformation to sulfonic acid with HCl). The alkyne group can be used for “Click” reactions with azides.^{144,145}

For the reaction with sultone we followed a procedure described by Dimitrov et al.¹⁴² shown in Scheme 3-2. First, we used the less toxic 1,4-butanedisulfone for our functionalization reaction, but could only reach degrees of functionalization under 5%. Consequently, we switched back to the original instruction of the etherification using 1,3-propanedisulfone.



Scheme 3-2. Etherification of PHS with 1,3-propanedisulfone.

Figure 3-6 shows the NMR spectrum of the etherified polymer clearly exhibiting the signals of the methylene groups at 2.0 ppm, 2.6 ppm and 3.95 ppm. However, also the signal of the unfunctionalized hydroxyl groups is clearly visible. A calculation shows that a degree of

functionalization of still only 20.4 % was reached while 100 % have been described in literature.¹⁴²

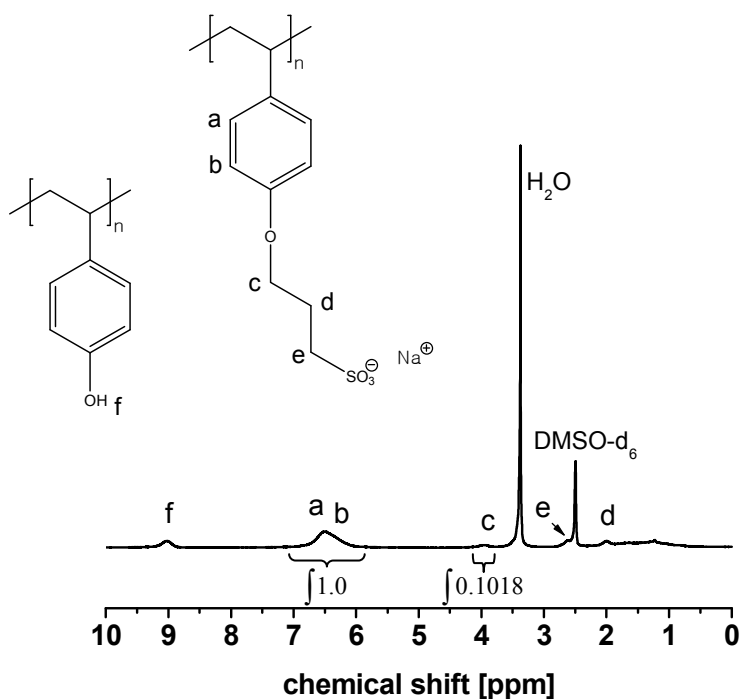


Figure 3-6. NMR spectrum of PHS etherified with 1,3-propanesultone.

The incomplete functionalization is also qualitatively visible in the IR spectrum (Figure 3-7). The broad water signal around 3318 cm⁻¹ is caused by the remaining hydroxyl groups while the sulfonic group is visible through its symmetrical and asymmetrical O=S=O valence oscillations at 1036 cm⁻¹ and 1170 cm⁻¹.

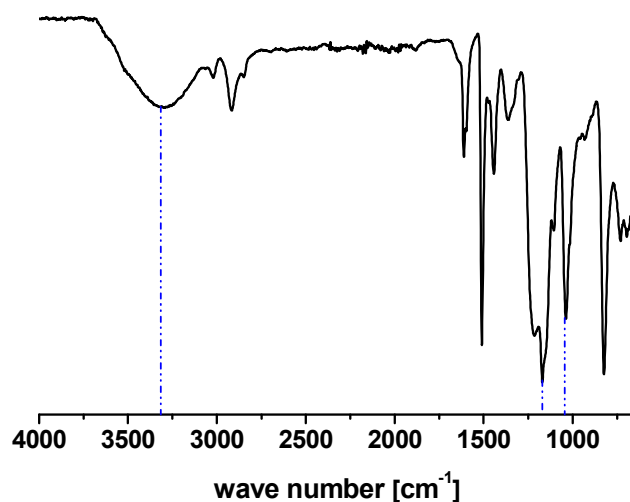
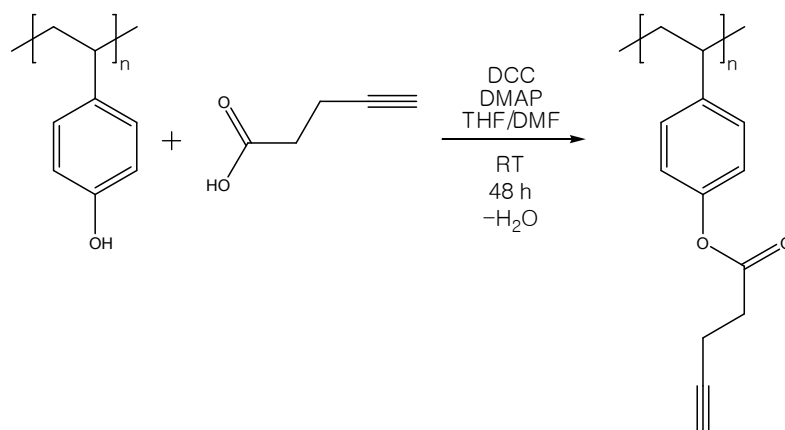


Figure 3-7. IR spectrum of PHS etherified with 1,3-propanesultone.

A general method to introduce a wide range of functional groups into the PHS polymer is the esterification of the hydroxyl groups with carboxylic acids or carboxylic acid halides. The Steglich esterification is a mild method at room temperature that uses dicyclohexylcarbodiimide (DCC) as coupling reagent and 4-(dimethylamino)pyridine (DMAP) as catalyst to accomplish the reaction.¹⁴⁶ After the unsuccessful attempt to introduce an alkyne group via a Williamson-type etherification with propargyl bromide,¹⁴³ PHS was esterified with 4-pentynoic acid via the Steglich method to insert alkyne groups.¹¹⁹ Using a 5-fold excess of 4-pentynoic acid and DCC, PHS could be functionalized successfully.



Scheme 3-3. Steglich esterification of PHS with 4-pentynoic acid.

Figure 3-8 shows the NMR spectra of the esterified PHS. The characteristic signals of the 4-pentynoic moiety can be seen in the range of 2.30 to 2.85 ppm. Further, the signal of the hydroxyl group is gone. The degree of functionalization calculated from the spectrum is 100 %. This fact is proven further by the IR spectrum of the esterified sample (Figure 3-9). Here, the O-H valence oscillation at 3318 cm^{-1} does no longer exist. Instead, new signals of the C-H valence oscillation at 3290 cm^{-1} and of the C=O valence oscillation of the ester bound at 1750 cm^{-1} are visible.

A second batch with only a 1.5-fold excess of 4-pentynoic acid and DCC resulted in a degree of functionalization of 88.8 %, demonstrating the importance of a sufficient excess of the pentynoic acid.

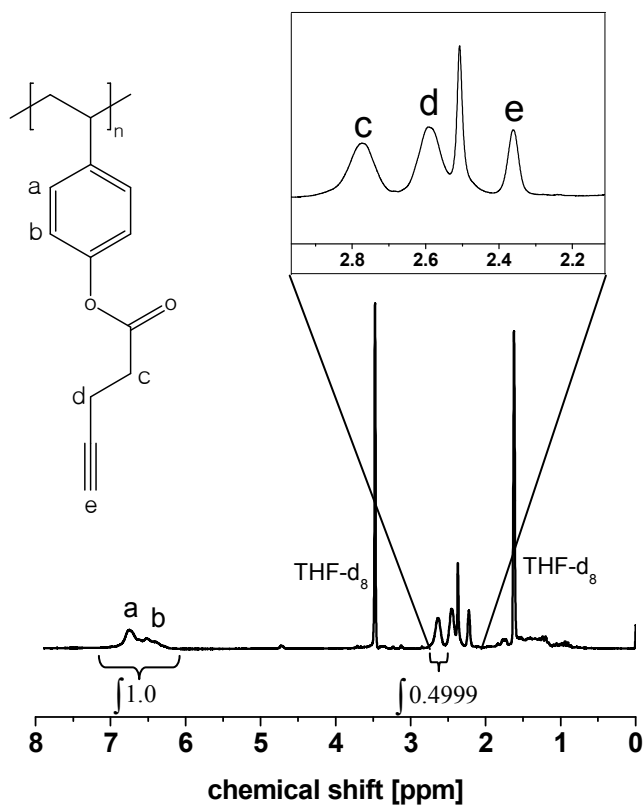


Figure 3-8. NMR spectrum of PHS esterified with 4-pentynoic acid.

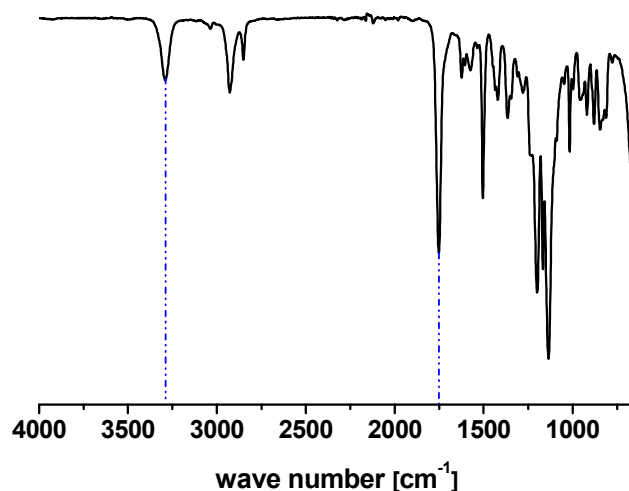


Figure 3-9. IR Spectrum of PHS esterified with 4-pentynoic acid.

Other attempted Steglich esterifications included reactions with succinic anhydride (to introduce acidic groups), 3-(tritylthio)propionic acid (for thiol groups) and different amino acids. However, problems occurred regarding the solubility of the according products and consequently a thorough characterization was prevented.

3.1.4 Conclusion

We could successfully synthesize PtS with a very low PDI of 1.01 via living anionic polymerization in THF with *sec*-BuLi as initiator. With less preparative effort, we obtained PtS with a PDI of 1.51 via free radical polymerization in benzene. It contained around 8 mol% of residual monomer, which however did not influence its suitability for model reactions. A fitting hydrolysis method for PtS is refluxing with hydrochloric acid in dioxane. It is less applicable for very small reaction volumes. Here, a good alternative is provided by the hydrolysis via reaction with TMSI. Hydrolyzed PtS was successfully functionalized with 1,3-propanesultone to incorporate sulfonate groups and with 4-pentynoic acid to introduce alkyne groups suitable for “Click”-reactions. However, a desired larger library of functionalized PtS was not achieved due to solubility and consequential characterization problems.

3.2 Poly(4-(dimethylaminomethyl)styrene)

3.2.1 Anionic polymerization

Monomers suitable for anionic polymerization must not carry any acidic protons. Therefore, many functional groups, e.g. hydroxyl and carboxyl groups, have to be protected during the polymerization process. In contrast, tertiary amino styrenes like 4-(dimethylaminomethyl)styrene (DMAMS) combine a polymerizable vinyl group with an interesting functional unit while not carrying any labile protons that would cause the termination of the living ends during an anionic polymerization.¹⁴⁷ The resulting polymer, poly(4-(dimethylaminomethyl)styrene) (PDMAMS), shows pH-responsive behavior¹⁴⁸⁻¹⁵⁰ and can be quaternized to obtain strong cationic polyelectrolytes.¹⁵¹

The anionic polymerization of DMAMS has been reported by Se et al.^{147,152} and Higo et al.¹⁵¹ Se et al. polymerized DMAMS using THF as solvent and *n*-butyllithium as initiator. The resulting polymers showed broad MWDs with PDIs higher than 1.38. Se et al. claimed that the polymerization process was disturbed by the amino groups of tertiary amines participating in the solvation of lithium ions during the polymerization. Therefore, they switched to the less nucleophilic initiators cumyl potassium and cumyl cesium and could successfully synthesize PDMAMS with PDIs as low as 1.05. Higo et al. used benzene as solvent and *sec*-BuLi as initiator. They report that PDMAMS with a sharp molecular weight distribution can be obtained with this system provided the monomer concentration is as low as 3 wt%. Polymerizations with higher monomer concentration did not follow a first-order law during the whole process, leading to broadening of the MWD. Polymerization in THF led to PDMAMS with broad MWD. Higo et al. assumed that a presumably very small dissociation constant of the ion-pairs in THF is the reason for this. Hence, no satisfactory reports exist of successful DMAMS polymerization in THF with *sec*-BuLi as initiator. In contrast to the already described polymerizations of DMAMS in benzene¹⁵¹ or with cumyl initiators^{152,147} this well-established system combines a less dangerous solvent with a commercially available initiator. Further, THF is used for polymerization of polybutadiene (PB) with a high fraction of 1,2-PB that allows for efficient cross-linking of the resulting polymer. Therefore, we reattempted the polymerization of a narrowly distributed DMAMS polymer under these very conditions. Prior to the actual polymerization reaction 1 mL *sec*-BuLi per 100 mL solvent was added to the THF solution at -20 °C and then aged overnight. Beside the elimination of residual impurities,¹⁵³ this practice leads to the formation of lithium alkoxides.^{153,154} After thorough purification of the DMAMS monomer it was polymerized in the prepared THF so-

lution at $-72\text{ }^{\circ}\text{C}$ using *sec*-BuLi as initiator. Used concentrations and characteristics of the resulting polymer are shown in Table 3-2.

Table 3-2. Polymerization of DMAMS and styrene.

	$M_{n,th} \times 10^{-3}$ [g mol $^{-1}$]	$M_n \times 10^{-3}$ [g mol $^{-1}$]	PDI	$k_{app} \times 10^2$ [s $^{-1}$]	k_p [L s $^{-1}$ mol $^{-1}$]
PDMAMS	10.2	9.8 ^a	1.03 ^a	3.59	29.67
PS	6.6	6.3 ^b	1.03 ^b	10	82.64

$[I]_0 \times 10^3 = 1.21\text{ mol L}^{-1}$ and $[M]_0 = 0.079\text{ mol L}^{-1}$ for both polymerizations

a) SEC in DMAc, PS-PMMA-PDMAEMA calibration

b) SEC in THF, PS calibration

The NMR and SEC data of the synthesized polymer demonstrate the successful synthesis of PDMAMS with a narrow MWD and a PDI of 1.03 (Figure 3-10).

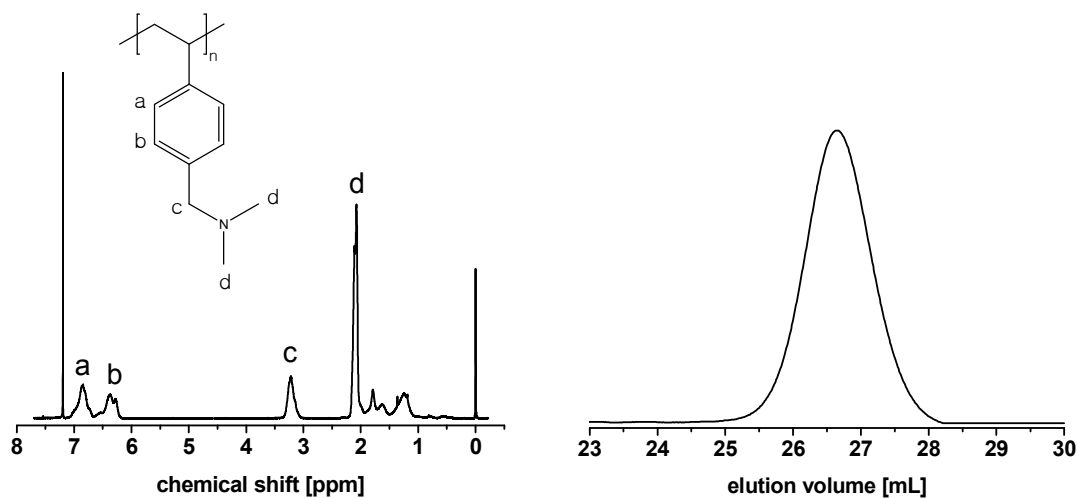


Figure 3-10. $^1\text{H-NMR}$ spectrum (in CDCl_3) and SEC curve for PDMAMS.

To follow the kinetics of the polymerization reaction we used near-infrared (NIR) fibre optics inline spectroscopy and monitored the signal of the overtone vibrations of the DMAMS vinyl groups at the wavelength of 1630 nm. For comparison, we also monitored the polymerization of styrene under the same reaction conditions. Figure 3-11a shows the rapid exponential decrease of the NIR-signal for DMAMS (black) and PS (red).

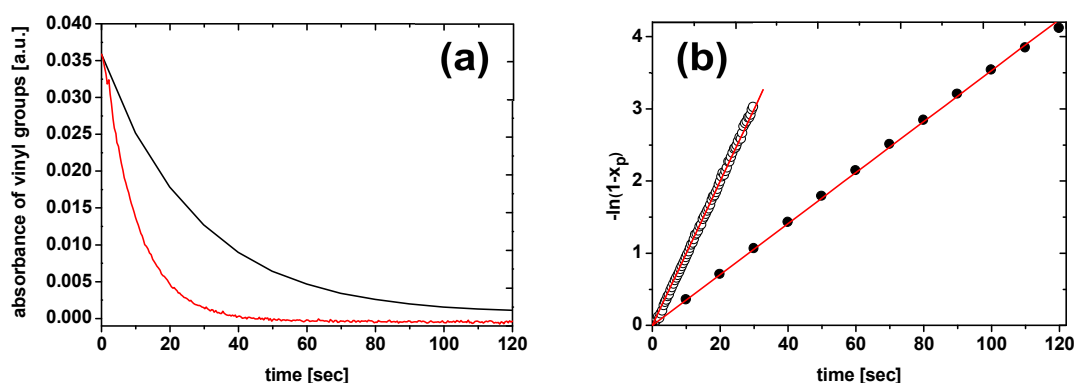


Figure 3-11. Time-dependent decrease of absorbance of the overtone vibration of the vinyl groups depending on time during the polymerization of DMAMS (black) and PS (red) (a). First-order kinetics plots for DMAMS (closed circles) and PS (open circles) polymerization (b).

While the polymerization of DMAMS was finished after 120 seconds with a half life of about 20 seconds, the polymerization of styrene was even faster and took about 55 seconds with a half life of about 7.5 seconds. Thus, in the *sec*-BuLi/THF system the polymerization of PS in THF is about 2.79 times as fast as the polymerization of DMAMS. The corresponding apparent rate constants k_{app} were determined from the slope of the first-order kinetic plots (Figure 3-11b and Table 3-2).

In comparison to earlier attempts to polymerize DMAMS, the two main differences in our approach are the monomer concentration and the pretreatment of the solvent with *sec*-BuLi. For DMAMS polymerization in THF, Se et al. used monomer concentrations around 0.2 mol L⁻¹.¹⁵² Higo et al. report that the success of DMAMS polymerization in benzene depends on a low monomer concentration of around 3 wt% which equals 0.18 mol L⁻¹.¹⁵¹ In contrast, we used a monomer concentration as low as 0.079 mol L⁻¹. More important, the polymerization took place in the presence of alkoxides, which were generated on purpose by addition of *sec*-BuLi to the THF on the day before polymerization. Lithium alkoxides, except linear ones, generally slow down the polymerization reaction while stabilizing the living chain end through complexation.^{153,155} Apart from Se's assumption that the polymerization process of DMAMS was disturbed by the amino groups of tertiary amines participating in the solvation of lithium ions during the polymerization,¹⁵² there is also a report about the polymerization of (dialkylamino)isoprenes which suggests that in polar solvents like THF the tertiary amino groups strongly coordinate to the Li⁺ counterion at the living chain end and therefore hinder

the addition of monomer.¹⁵⁶ Consequently, the presence of alkoxides is vital for the successful anionic polymerization of narrowly distributed PDMAMS in the *sec*-BuLi/THF system.

3.2.2 Solution properties of PDMAMS

For PDMAMS pH-responsiveness has been reported¹⁴⁸⁻¹⁵⁰ while any temperature-responsive properties have not yet been communicated. Yet, it bears a tertiary amino group like poly(2-(dimethylamino)ethyl methacrylate) (PDMAEMA) and the structurally similar poly(2-(diethylamino)ethyl methacrylate) (PDEAEMA) which both show pH- as well as temperature-responsive behavior.¹⁵⁷ Thus, for PDMAMS we expected LCST behavior like exhibited by PDMAEMA and PDEAEMA at least in a certain pH range.

To verify the pH-responsive behavior an acidic (pH = 2.5) PDMAMS solution (1 g L⁻¹) was titrated with 0.1 M NaOH to pH 10. The titration process was monitored via a turbidity sensor. At a critical pH value, pH_{cr}, the polymer became insoluble and a significant change in the transmittance could be observed (Figure 3-12a). The critical pH value was defined as the intercept of the tangents at the onset of turbidity and was 7.1. The apparent pK_a value could be determined from the titration curve (Figure 3-12b) analogous to the method used by Plamper et al.¹⁵⁸ and pK_{a,app} was 6.8.

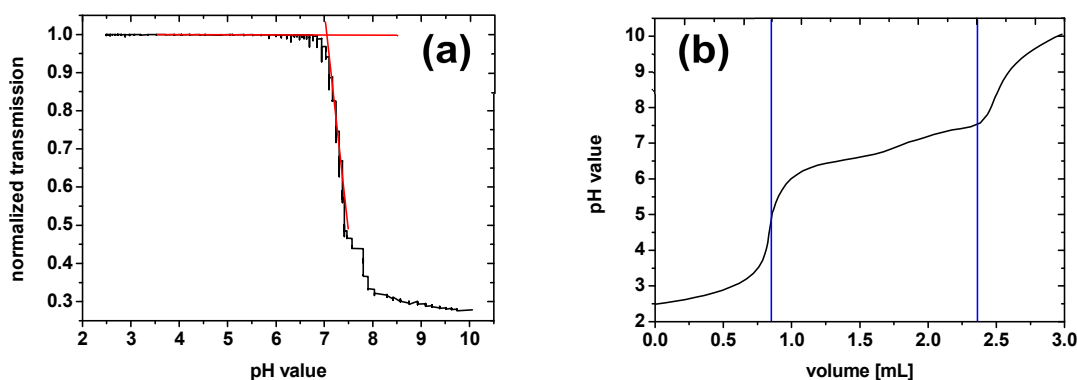


Figure 3-12. pH dependent turbidity titration (a) and titration curve of PDMAMS (b).

This is in the same range as reported values pK_{a,app} = 7.3 and 7.1 for a random and a block copolymer of PDMAMS with poly(*ar*-vinylbenzyl)trimethylammonium chloride)¹⁴⁹ and corresponds with the theory that the protonated block copolymer behaves as a stronger acid than the random copolymer because the protonated DMAMS units are more densely confined to a limited space in the block copolymer than in the random copolymer and

should be even more so in a homopolymer. Consequently, the pK_a value for PDMAMS homopolymer is even lower than for the mentioned block copolymer.

To investigate a possible LCST behavior of PDMAMS, several temperature-dependent turbidity measurements were performed. PDMAMS solutions (1 g L^{-1}) with the pH values of 2, 3, 4 and 6 were heated with a heating rate of 1 K min^{-1} . No significant change of transmittance could be observed for these samples up to a temperature of $85 \text{ }^\circ\text{C}$. PDMAMS could also be dissolved in buffer solutions of pH 7 and even 8. The temperature-dependent changes of transmittance for the pH 7 solution are shown in Figure 3-13a.

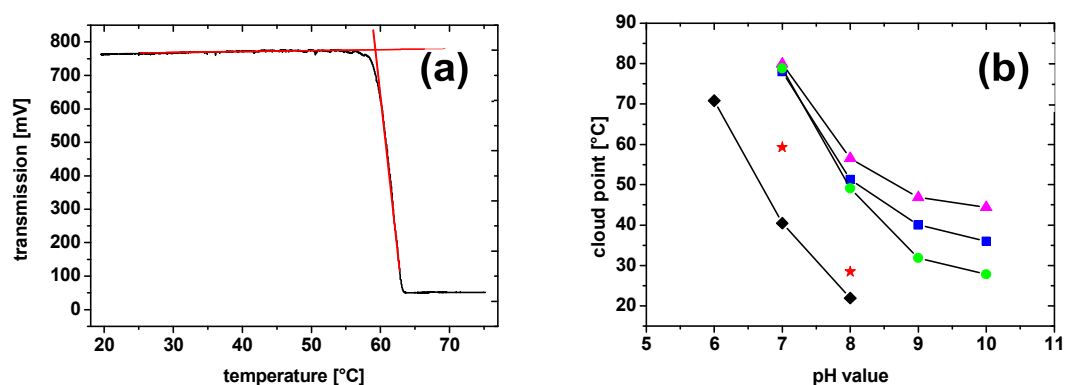


Figure 3-13. (a) Temperature-dependent change of transmittance for PDMAMS with initial pH of 7. (b) pH-dependent cloud points for (\blacktriangle) $(\text{PDEAMA}_n)_x$ stars, (\star) PDMAMS_{61} , (\bullet) $(\text{PDMAEMA}_{170})_{18}$, (\blacksquare) $(\text{PDMAEMA}_{100})_{3.1}$, (\blacklozenge) PDMAEMA_{108} . Cloud points of $(\text{PDEAMA}_n)_x$ stars are independent of M_n and arm number x .

The cloud point was defined as the intercept of the tangents at the onset of turbidity. For pH 7 the cloud point is $59.3 \text{ }^\circ\text{C}$. At pH 8 PDMAMS is less protonated than at pH 7. Consequently, the cloud point is significantly lower, namely $28.5 \text{ }^\circ\text{C}$.

Interestingly, Figure 3-13b shows that the cloud points of PDMAMS determined at pH 7 and 8 are located between the corresponding cloud points of PDEAEMA and PDMAEMA. Therefore, PDMAMS containing a benzene ring is more hydrophobic than PDMAEMA.

3.2.3 Conclusion

In conclusion, we conducted the first successful living anionic polymerization of DMAMS with a narrow MWD (PDI 1.03) in a *sec*-BuLi/THF system. Besides using even lower mono-

mer concentrations than in previous anionic polymerizations of DMAMS, the important feature in our polymerization is the presence of alkoxides. They hinder the coordination of the tertiary amino groups to the Li⁺ counterions which would otherwise disturb the addition of monomer. Now it is possible to synthesize well-defined homo- and block copolymers of PDMAMS. The latter is especially interesting as in THF PB polymerizes with a high 1,2-PB content that allows for the synthesis of cross-linkable polymers. Triblock terpolymers containing both PDMAMS and 1,2-PB could be used for the synthesis of Janus particles from bulk morphologies.¹⁵⁹ This is interesting due to the pH- and temperature-responsive behavior of PDMAMS. We could affirm the pH-responsive behavior and now for the first time also show the LCST behavior of the homopolymer with cloudpoints of 59.3 °C at pH 7 and 28.5 °C at pH 8.

4 Triblock Terpolymers: Synthesis and Bulk Morphologies

After determining suitable building blocks for the preparation of JPs from bulk structures, the polymerization of the triblock terpolymers was the next step. Living anionic polymerization was the method of choice because it leads to block copolymers with high molecular weights and very narrow molecular weight distributions.¹⁶⁰ Most important is the fact that for the crucial step of fixation of the JPs, a cross-linkable middleblock is inevitable. PB carries cross-linkable double bonds in both its 1,2- and 1,4-type; the 1,2-structure is preferred as its pendant vinyl groups can be cross-linked more efficiently than the double bonds within the 1,4-structure. Consequently, the polymerizations of the triblock terpolymers were conducted in the polar solvent THF.¹⁶¹ However, attempts to synthesize a polymer with PDMAMS and PB as the first two blocks were not successful; polymerization of the PB block stopped after about 10 % conversion, possibly due to some unclear termination reactions of the chain end with the PDMAMS block. As a substitute, allyl methacrylate was used. During anionic polymerization it grows via the methacryloyl moiety while the allyl groups do not react.¹⁶² Therefore, the latter can be used for cross-linking of the corresponding polymers.

The poly(*tert*-butoxystyrene) was used as first block in two different terpolymers, poly(*tert*-butoxystyrene)-*block*-polybutadiene-*block*-poly(*tert*-butyl methacrylate) (tSBT) and poly(*tert*-butoxystyrene)-*block*-polybutadiene-*block*-poly(2-(dimethylamino)ethyl methacrylate) (tSBD). PDMAMS was used for poly(4-(dimethylaminomethyl)styrene)-*block*-poly(allyl methacrylate)-*block*-poly(*tert*-butyl methacrylate) (DSAT).

4.1 Poly(*tert*-butoxystyrene)-*block*-polybutadiene-*block*-poly(*tert*-butyl methacrylate) (tSBT)

The triblock terpolymer tSBT was modeled after the already investigated polystyrene-*block*-polybutadiene-*block*-poly(*tert*-butyl methacrylate) (SBT). SBT has successfully been used for the synthesis of Janus sheets and discs.¹⁰³ The PtBMA block can be hydrolyzed to water-soluble poly(methacrylic acid). While this lead to amphiphilic colloidal particles in the case of SBT Janus discs,⁷³ with PtS in its hydrolyzed form, PHS, the synthesis of water-soluble JPs from triblock terpolymer bulk structures is possible for the first time.

Size exclusion chromatography combined with multi-angle light scattering (SEC-MALS) showed a molecular weight of 163,000 g mol⁻¹ and a PDI of 1.01 for the tSBT terpolymer

(Figure 4-1b). The weight fractions of the three blocks were calculated from NMR (Figure 4-1a) to be $tS_{46}B_{16}T_{38}$ and degrees of polymerization are $tS_{425}B_{482}T_{430}$.

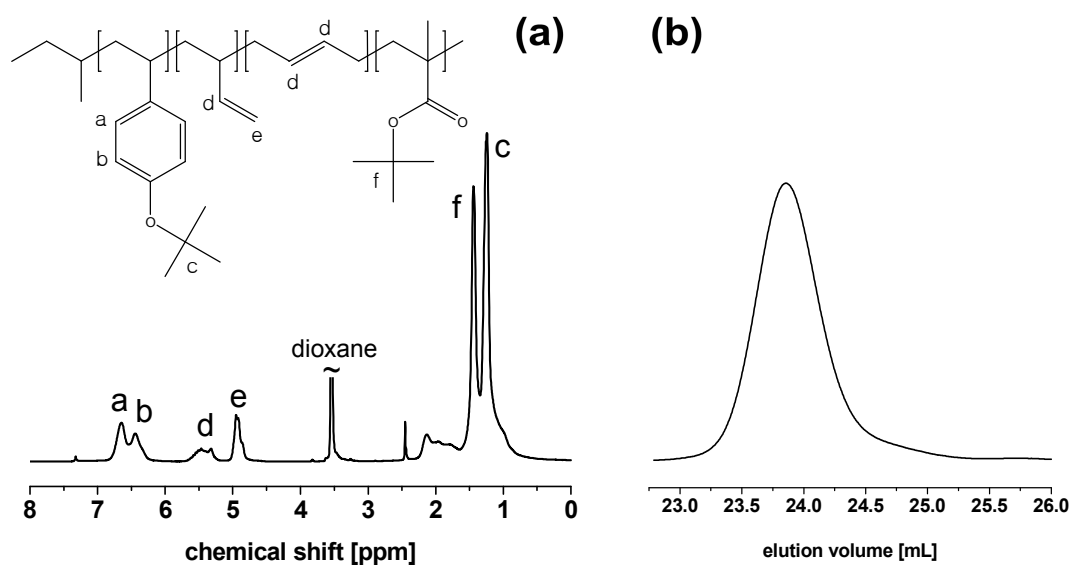


Figure 4-1. NMR spectrum (a) and SEC curve (b) of tSBT.

After film-casting from chloroform, we examined the resulting bulk structure of tSBT by transmission electron microscopy (TEM) and small-angle X-ray scattering (SAXS). Figure 4-2 shows a TEM-micrograph of an OsO_4 -stained ultrathin section of tSBT. The PB cylinders (appearing black) are surrounded by alternating lamellae of PtS (gray) and poly(*tert*-butyl methacrylate) (PtBMA) (white). The PtBMA phase appears white due to electron-beam induced degradation. The diameter of the polybutadiene cylinders is 14 ± 1.8 nm and the distance between the centers of two cylinders is in the range of 22 nm while the long period of the lamellar structure is 68 nm. Note that the TEM micrograph may not reflect the absolute dimensions as staining and electron-induced degradation of the PtBMA may alter the exact distances to some extent. With respect to the following results, it is important to note that a morphology with undulated lamellae, as shown in Figure 4-2c, could not be observed. The magnified image (see Figure 4-2d) does not indicate any thin lamellar connections between the PB cylinders.

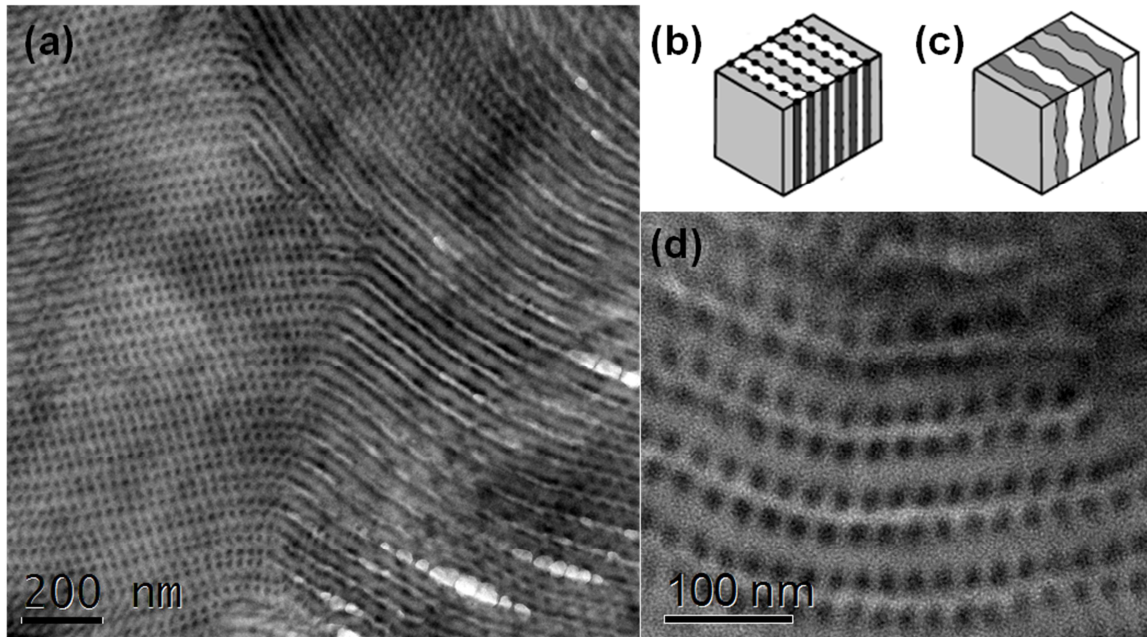


Figure 4-2. TEM micrographs (a and d) of ultrathin sections of a tSBT film stained with OsO_4 (PB appears black, PtS gray and PtBMA white) and two cartoons displaying a lamella-cylinder (b) and an undulated lamellar morphology (c). Reprinted with permission from Ref [159]. Copyright 2011 American Chemical Society.

The result of the SAXS measurements is in agreement with the observed lamella-cylinder (lc) morphology. Figure 4-3 depicts the scattering curve of tSBT exhibiting the typical integer reflexes of a lamellar morphology. Additionally, the 200 peak is rather broad and exhibits a shoulder. Its deconvolution results in three peaks that can be assigned to the 200 and 300 reflexes and the primary reflex of the correlation distance between the cylinders. This characteristic spacing can be calculated to 21.8 nm. The calculated long period is 60 nm. In comparison, the values measured in TEM micrographs are 22 nm for the cylinder distance and 68 nm for the long period and therefore in good agreement.

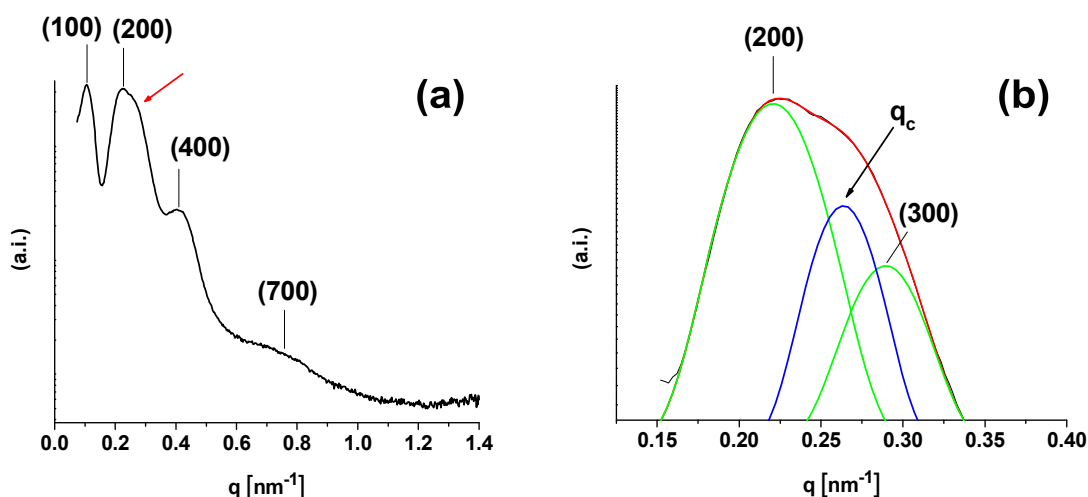


Figure 4-3. SAXS curve of tSBT (a) with a characteristic shoulder indicated by the arrow. Close-up (b) shows the deconvolution of the shoulder revealing the underlying correlation distance of the cylinders. Adapted with permission from Ref [159]. Copyright 2011 American Chemical Society.

4.2 Poly(*tert*-butoxystyrene)-*block*-polybutadiene-*block*-poly(2-(dimethylamino)ethyl methacrylate) (tSBD)

For the second triblock terpolymer poly(2-(dimethylamino)ethyl methacrylate) (PDMAEMA) instead of PtBMA was used. It is a weak polyelectrolyte that exhibits LCST behavior.¹⁵⁸ Further, its tertiary amino groups can be quaternized to result a strong polyelectrolyte.³⁵

The weight fractions of the three blocks as calculated from the NMR (Figure 4-4a) were $tS_{48}B_{16}D_{36}$ at a molecular weight of $116,000 \text{ g mol}^{-1}$ (calculated from NMR and SEC of PtS-precursor) and degrees of polymerization are $tS_{316}B_{343}D_{267}$. The PDI was 1.1 due to a small amount of termination reactions (compare shoulders in Figure 4-4b).

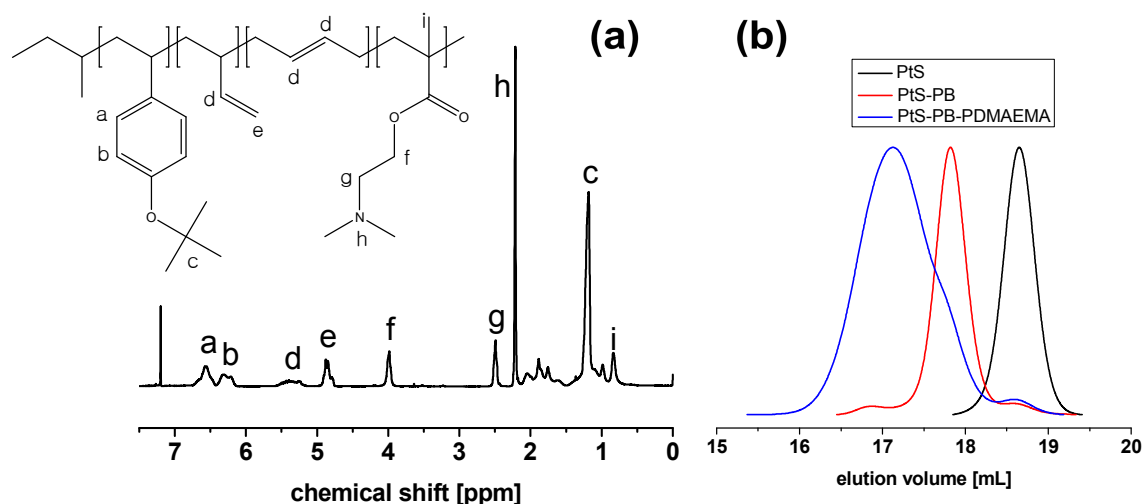


Figure 4-4. NMR spectrum (a) and SEC curve (b) of tSBD and its precursors.

Film-casting from chloroform, dioxane and THF always resulted in a lamellar morphology (Figure 4-5). This morphology did not consist of alternating phases of the three blocks (“ABCBABC”) as desired for Janus particle synthesis, but instead showed a symmetrical “ABCBABCBA” motif. Ultrathin sections of a tSBD film were stained with OsO_4 for PB to appear black. Figure 4-5 shows that the PB lamella forms the core lamella “C” of the pattern.

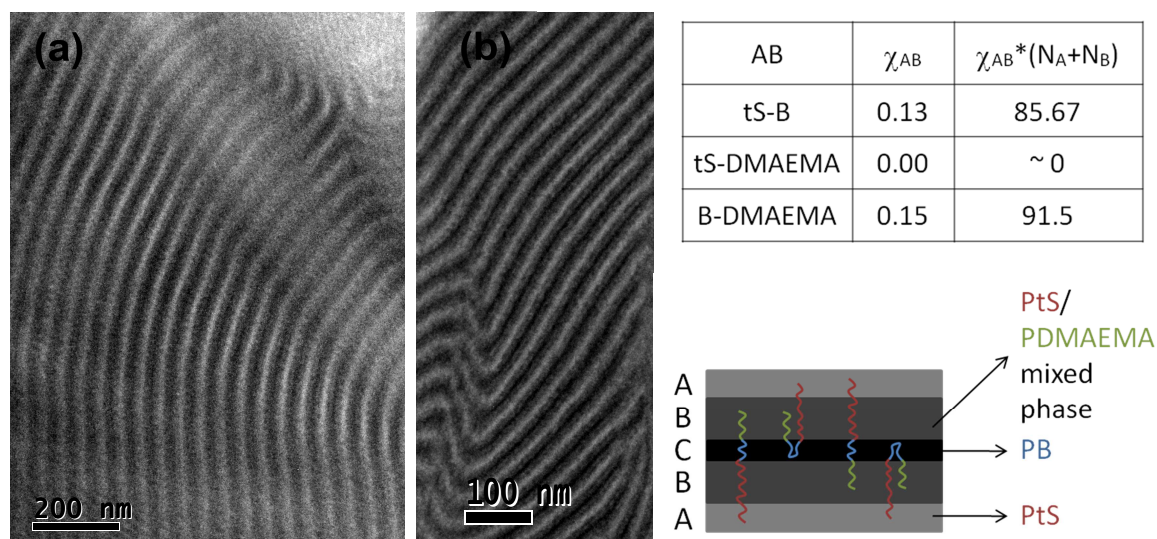


Figure 4-5. TEM micrographs of ultrathin sections of a tSBD film cast from dioxane (a) and THF (b) stained with OsO_4 (PB appears black), table of the respective χ -parameter and scheme of the morphology pattern.

Usually, when a methacrylate is present in the morphology it appears as the lightest colored phase in the TEM due to electron-beam induced degradation. Here this would hint that PDMAEMA resembles phase A and PtS remains to be phase B in the ABCBA motif. However, as the structure of the triblock terpolymer is PtS-PB-PDMAEMA, the PB phase cannot be exclusively neighbored by PtS. It is not possible for the chains to align in such fashion. Therefore, phase B has to be a mixed phase of PDMAEMA and PtS. Indeed, calculations of the respective χ -parameter show that χ_{tSD} is 0 and therefore these two blocks are miscible while χ_{tSB} and χ_{BD} are positive and the corresponding blocks undergo phase separation. As the PtS block exceeds the PDMAEMA block in volume, phase A has to consist of PtS.

The long period of this lamellar structure can be narrowed down to be in the range of 30 to 50 nm. Due to cutting artefacts (compressions and extensions of the film) a more accurate statement is not possible. However, the long period can also be calculated from SAXS measurements. Figure 4-6 depicts the scattering curves for the tSBD films cast from all three solvents. As expected, they exhibit the integer reflexes of a lamellar morphology. The 100 reflex is at the same scattering vector position for all three films. The long period calculated from it is 55 nm and therefore in satisfactory agreement with the measurement made in TEM micrographs.

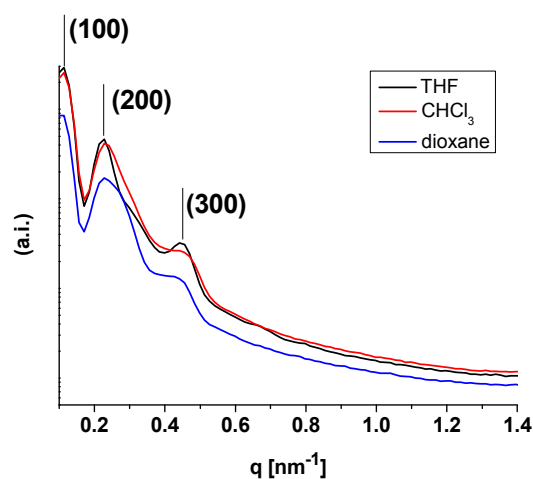


Figure 4-6. SAXS curve of tSBD films cast from different solvents exhibiting the integer reflexes typical for a lamellar morphology.

4.3 Poly(4-(dimethylaminomethyl)styrene)-*block*-poly(allyl methacrylate)-*block*-poly(*tert*-butyl methacrylate) (DSAT)

DSAT aimed to combine the pH- and newly reported thermo-responsivity of PDMAMS with an inherent acidic group through the use of PtBMA. Figure 4-7a shows the NMR spectrum of the polymer which results in a weight composition of DS₄₂A₁₁T₄₇. However, the SEC curves (Figure 4-7b) reveal a significant amount of termination for the diblock PDMAMS-PAMA possibly due to impurities in the tBMA. Therefore, the polymer composition DS₄₂A₁₁T₄₇ actually refers to a polymer mixture of the actual triblock and the precursor diblock. A more detailed analysis of the SEC data shows that the mixture consists of 67 wt% of DS₃₀A₈T₆₂¹²⁰ and 33 wt% DS₇₉A₂₁⁴⁶. This equals 44 mol% DSAT and 56 mol% DSA.

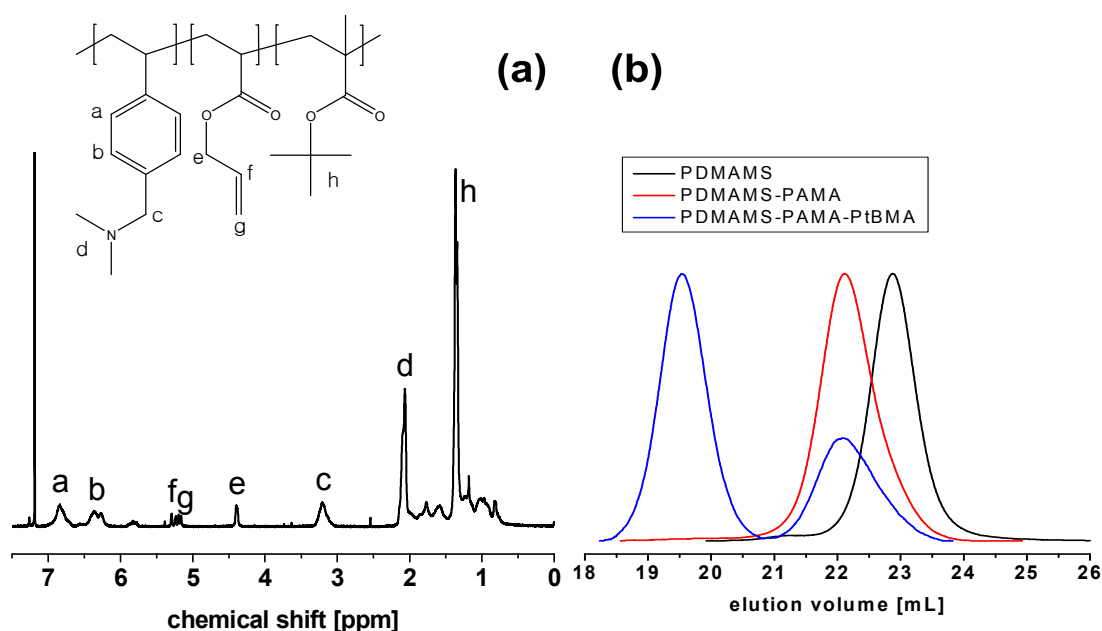


Figure 4-7. NMR spectrum (a) and SEC curves for DSAT polymerization (b).

For the precursor PDMAMS as well as the precursor diblock, the PDI is 1.03. As expected, the overall PDI of the resultant mixture of tri- and diblock rises dramatically and is 1.51.

The analysis of the bulk structures, stained with OsO₄ to give the highest contrast to poly(allyl methacrylate) (PAMA), shows a lamellar morphology at first sight (Figure 4-8); but a closer look into the darker domains also shows black spheres. Consequently, we assume a lamellar morphology of PDMAMS (gray) and PtBMA (lightest phase due to electron

beam irradiation) with PAMA spheres (black appearance due to OsO_4) in the PDMAMS lamella.

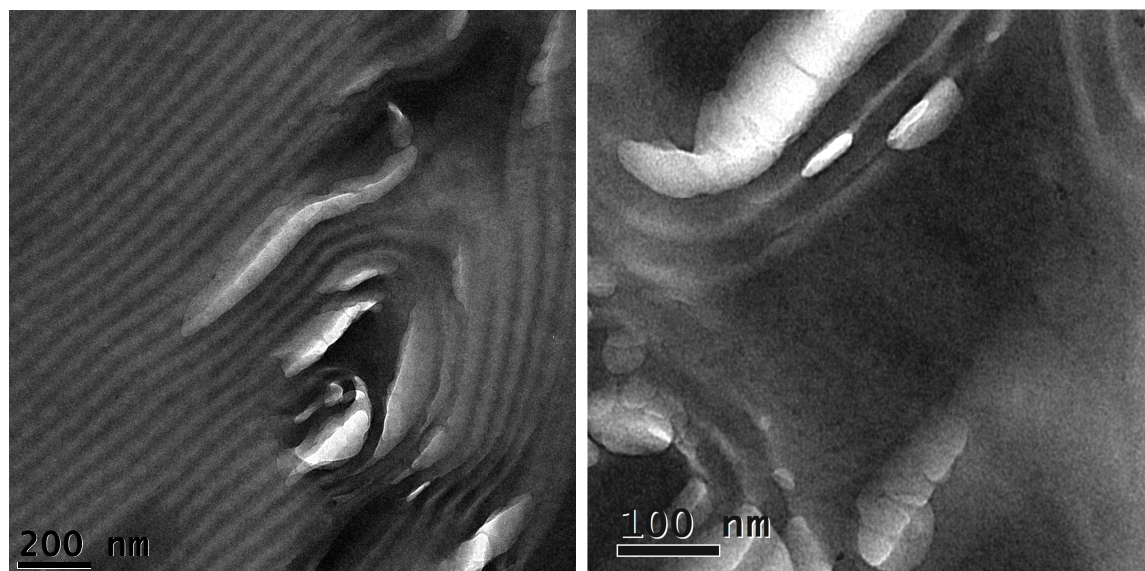


Figure 4-8. TEM micrographs of ultrathin sections of a DSAT film cast from CHCl_3 stained with OsO_4 (PAMA appears black).

4.4 Conclusion

The newly introduced building block for triblock terpolymers, *tert*-butoxystyrene was successfully employed in the synthesis of the two triblock terpolymers tSBT and tSBD. tSBT has a very narrow PDI of 1.01 and exhibits a lamella-cylinder morphology as its bulk structure. The latter is interesting because when PS instead of PtS was used for the same triblock terpolymer, an lc-morphology, or an lamella-sphere (ls)-morphology for very little PB content, could never be realized for SBT.⁹⁷ The PB-cylinders are surrounded by alternating lamellae of PtS and PtBMA, therefore making tSBT an ideal precursor material for Janus particles. tSBD has a slightly broadened PDI of 1.1 due to a small amount of termination reactions. Its bulk morphology is a lamella-lamella (ll) one. Unfortunately, in contrast to other terpolymers with an ll-morphology, e.g. SBT, the bulk structure of tSBD consists of a symmetrical pattern. Due to a χ -parameter value of 0 for tS and D, the two blocks built a centrosymmetric mixed phase on both sides of the PB lamellae. Excess PtS gives the third type of lamella. With this symmetrical structure, tSBD is not suitable for the JP synthesis from bulk material. The synthesis of a triblock terpolymer with PDMAMS as the first block followed by PB was not possible. Instead PAMA was employed as cross-linkable middle block. However, a signif-

ificant amount of termination took place after the polymerization of the DSA diblock. Consequently, the resulting polymer is merely a mixture of diblock and triblock. Although this in itself was not a hindrance for JP synthesis, the bulk material does not exhibit a clear and suitable morphology.

5 Janus Particles from tSBT Bulk Structures

Major parts of this chapter were published in *Macromolecules* **2011**, *44*, 9221-9229 under the title: “Janus Triad: Three Types of Nonspherical, Nanoscale Janus Particles from One Single Triblock Terpolymer” by Andrea Wolf, Andreas Walther and Axel H. E. Müller (<http://pubs.acs.org/doi/full/10.1021/ma2020408>). Text and respective figures are adapted and reprinted with permission. Copyright 2011 American Chemical Society. The actual preparation of the particles was performed during the precedent diploma thesis and is repeated as the base of the further detailed examinations.¹⁶³

5.1 Preparation of Janus particles

After thorough investigation of the bulk morphology of tSBT, which was lamellar-cylindrical, we expected to be able to prepare the according Janus cylinders from the bulk material by cross-linking of PB followed by dissolution in THF.

Two different approaches were used to cross-link the PB domains and prepare Janus particles. Photo-cross-linking was performed using 2,4,6-trimethylbenzoyldiphenylphosphine oxide (Lucirin® TPO) as radical initiator, which was co-cast with the polymer. The incorporation of Lucirin® TPO does not alter the lc-morphology of tSBT-films as concluded from TEM images of the bulk structures (Figure 5-1). The other method employed sulphur monochloride, S_2Cl_2 , as cross-linking agent. Here, the polymer film was swollen in acetonitrile before the introduction of the cross-linking agent.

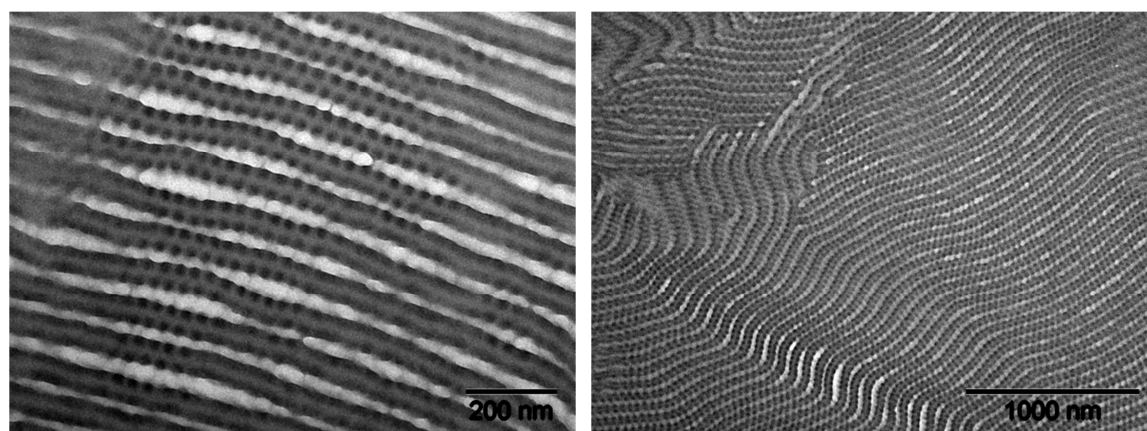


Figure 5-1. TEM micrographs of a tSBT film with 30 wt% of Lucirin® TPO, stained with OsO_4 (PB appears black, PtS gray and PtBMA white).

Photo-cross-linking resulted in well-defined Janus cylinders after dispersing the polymer film in THF, a good solvent for all three blocks of the terpolymer (Figure 5-2a). To decrease the length and thus to enhance the solubility of the resulting particles, the cylinders were sonicated (Figure 5-2b). These and all following TEM images are non-stained if not stated otherwise.

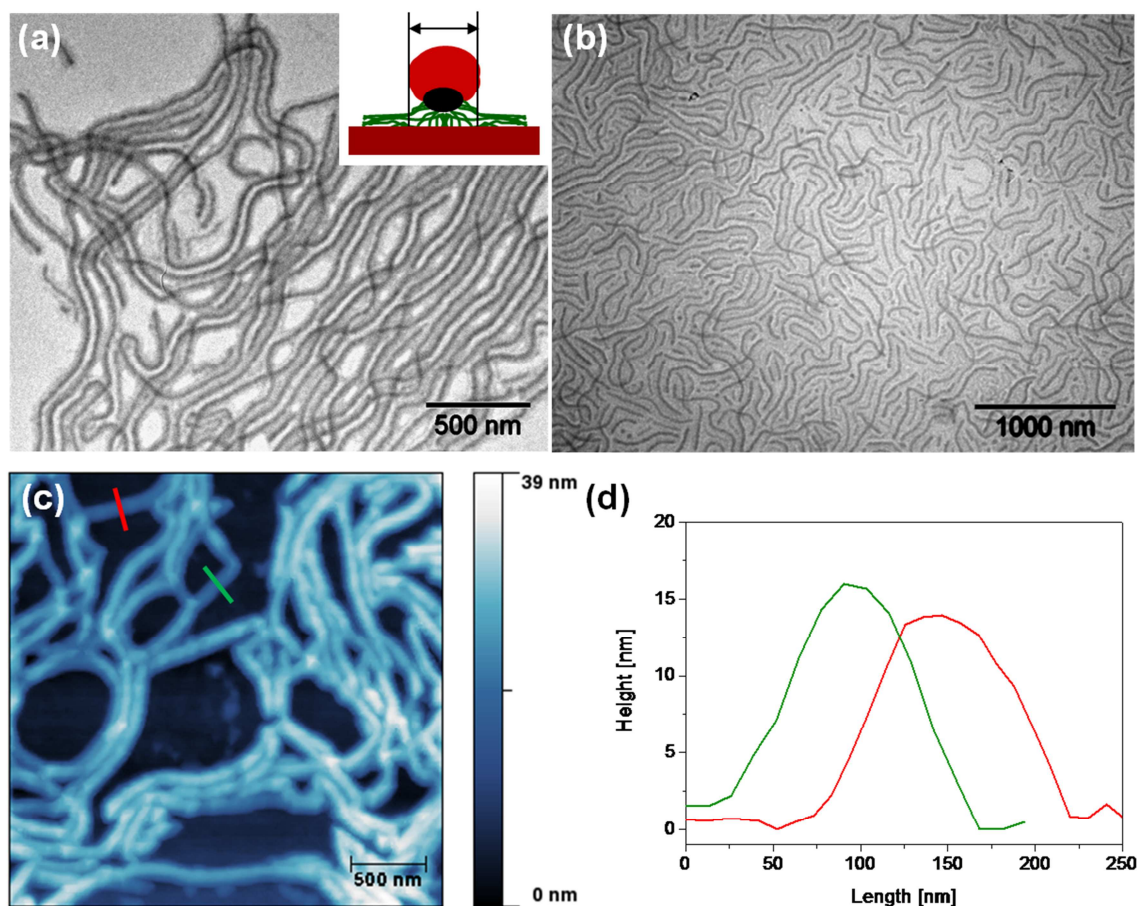


Figure 5-2. TEM micrographs of Janus cylinders before (a) and after (b) sonication and SFM height image of Janus cylinders (c) with corresponding cross-sections (d).

The evaluation of the core diameter of the core-corona structures visible in the TEM images yields values in the range of 22 nm. This value exceeds the measured diameter of the PB cylinders of 14 ± 1.8 nm in the bulk structure. Furthermore, the heights of the structures by scanning force microscopy (SFM) are in the range of 15 nm (Figure 5-2d). Considering the presence of additional corona on top and below of the PB cylinder (Figure 5-2a), a slightly flattened appearance of the PB cylinder is indicated when adsorbed onto surfaces.

In contrast to photo-cross-linking, the procedure of using S_2Cl_2 as cross-linker involves a previous swelling of the polymer film in acetonitrile. After addition of S_2Cl_2 , during the so-called cold vulcanization process, disulfide-bonds between the polybutadiene double bonds form. Similar to the case of photo-cross-linking, we expected the formation of Janus cylinders because of the lc-morphology. Surprisingly however, after cross-linking through cold vulcanization followed by sonication, two-dimensional Janus sheets instead of cylinders were obtained. Interestingly, the TEM micrographs show that the PB lamella is not of uniform thickness. Instead, clear, well-spaced undulations can be observed (Figure 5-3b). PB cylinders (darkest areas) can be observed that are connected by a PB layer, clearly thinner than the cylinders themselves (consequently brighter in the TEM image). Therefore, a phase transition in the morphology has occurred.

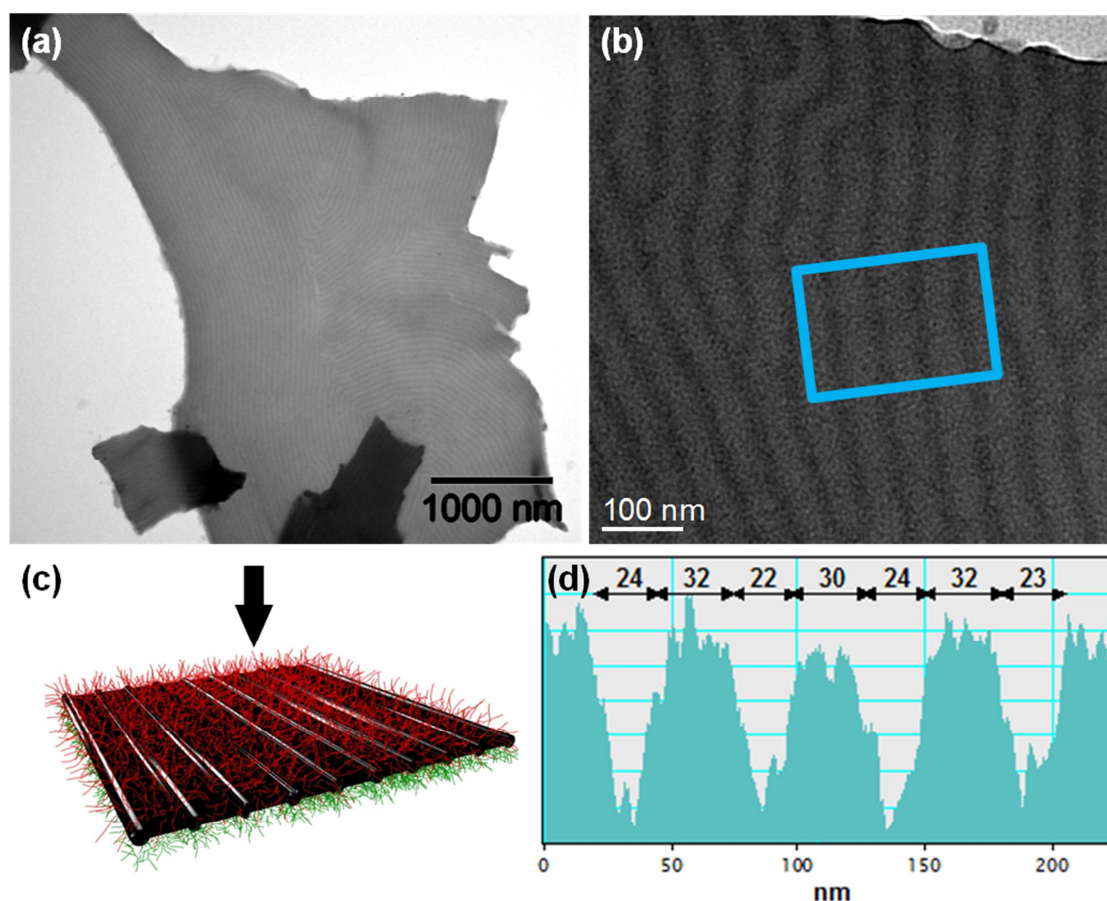


Figure 5-3. TEM images of Janus sheets obtained from tSBT after one (a) and five (b) days of swelling in acetonitrile, cross-linked with S_2Cl_2 , with (d) analysis of the cross section indicated in micrograph (b). The schematic drawing (c) indicates the line of sight onto the Janus sheets.

The structure developing during the process is best described as an undulated-lamellar (ul) morphology. A section analysis further visualizes this structure (Figure 5-3d). The cross section is based on the gray scale originating from the contrast variations within the sample. The thicker and darker cylinders can clearly be distinguished from the thinner and brighter connecting PB parts. The gray-scale analysis shows a diameter of the cylinders of ca. 23 nm and a width of the connecting PB parts in the range of 30 to 32 nm, thus exhibiting slightly larger dimensions than the cylinder packing in the bulk structure. The process of swelling and adding S_2Cl_2 obviously causes an increase of the volume of the PB domains, which is reflected in the final dimensions of a Janus sheet structure. We observed that this transition is solely caused by the reaction with S_2Cl_2 and not already upon addition of the swelling solvent as confirmed by a detailed TEM study (Figure 5-4). The concurrent volume increase of the PB phase during incorporation of the bulky S_2Cl_2 and altered interfacial tensions among the various blocks trigger this phase transition.

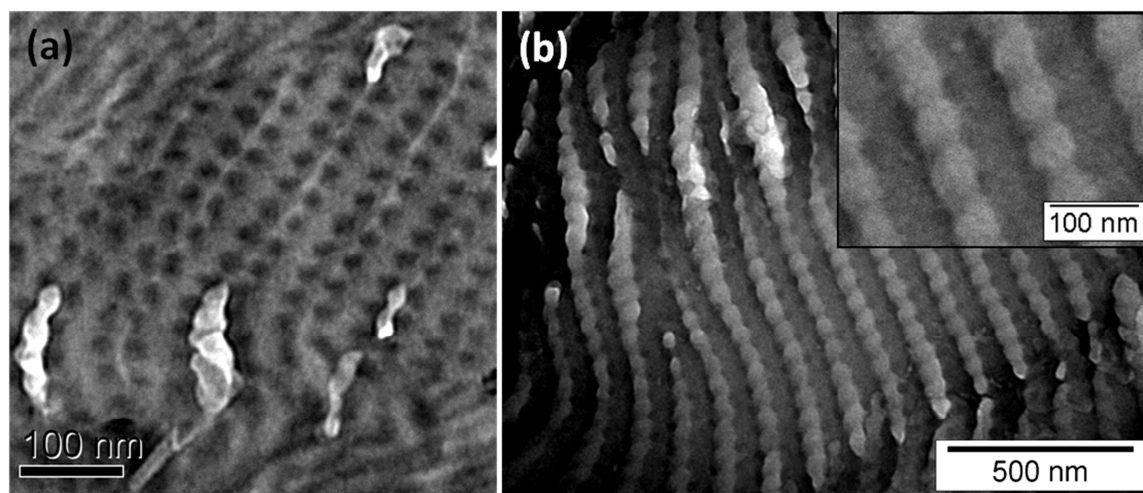


Figure 5-4. TEM micrographs of tSBT bulk morphologies after one day of swelling in acetonitrile (a) and additional treatment with S_2Cl_2 (b), the inset shows the formed PB lamellae in higher magnification). Samples are stained with OsO_4 (PB appears black, PtS gray and PtBMA white).

As the thinner parts of the PB layer are prone to fracture, most of the sheets have very clear particle edges along the cylinder lines and favor rectangular materials upon prolonged sonication. The sheet-like character of the Janus particles is also well visible in SEM pictures where stacks of sheets can be observed (Figure 5-5a). Again, the alternating thicker and thinner parts within the PB layer are clearly visible (Figure 5-5b).

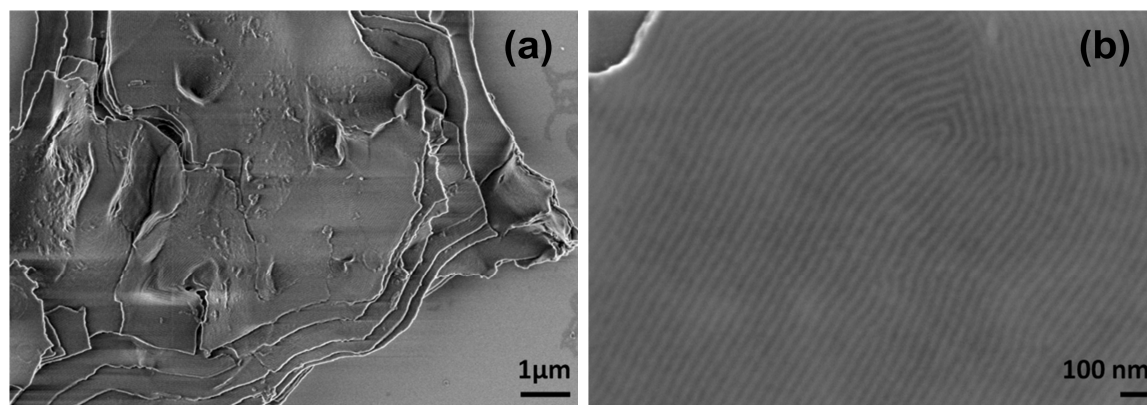


Figure 5-5. SEM images of Janus sheets.

With the aim of achieving a continuous PB lamella to increase the stability of the Janus sheets, we added other solvents (e.g. decane) that have a better ability to swell the PB phase than acetonitrile. However, tSBT is soluble in decane. To prevent the complete dissolution of tSBT while still keeping decane as a good swelling agent for PB, a mixture of decane and acetonitrile was used in a ratio of 1:1. The two solvents are not fully miscible, but form an emulsion upon stirring. After 14 hours of swelling in the steadily stirred acetonitrile/decane emulsion, tSBT was cross-linked with S_2Cl_2 for seven hours. Surprisingly, instead of continuous Janus sheets, a totally new type of Janus particle was obtained, i.e. Janus ribbons (Figure 5-6). Therein, exactly two Janus cylinders are connected along their major axis via a thin PB layer, forming a ribbon-type structure. The population is fascinatingly homogeneous with respect to the exclusive connection of only two cylinders. Individual Janus cylinders are nearly absent and trimeric cylinders do not exist. Additionally, the ends of both connected cylinders terminate at similar distance, indicating that the bands extend throughout the complete domain of the microphase-segregated morphology and that sonication chops fully extended Janus ribbons into shorter pieces.

Unlike in the case of Janus sheets, where a complete phase transition from an lc- to an ul-morphology takes place, a different phase transition occurs during the formation of the Janus ribbons. A connecting PB layer is formed only in every second interspace of the original PB cylinders. Therefore, we suggest that the precise PB layer formation might be influenced by a wave function-like instability occurring during the structure formation in the stirred emulsion. Such hydrodynamic instabilities might be assisted by the shear forces caused by the steady stirring of the emulsion. For cylindrical particles like polymer threads sinusoidal distortions, which lead to a break-up of the particles into spheres, are also known to be caused by Rayleigh-Plateau instabilities.¹⁶⁴

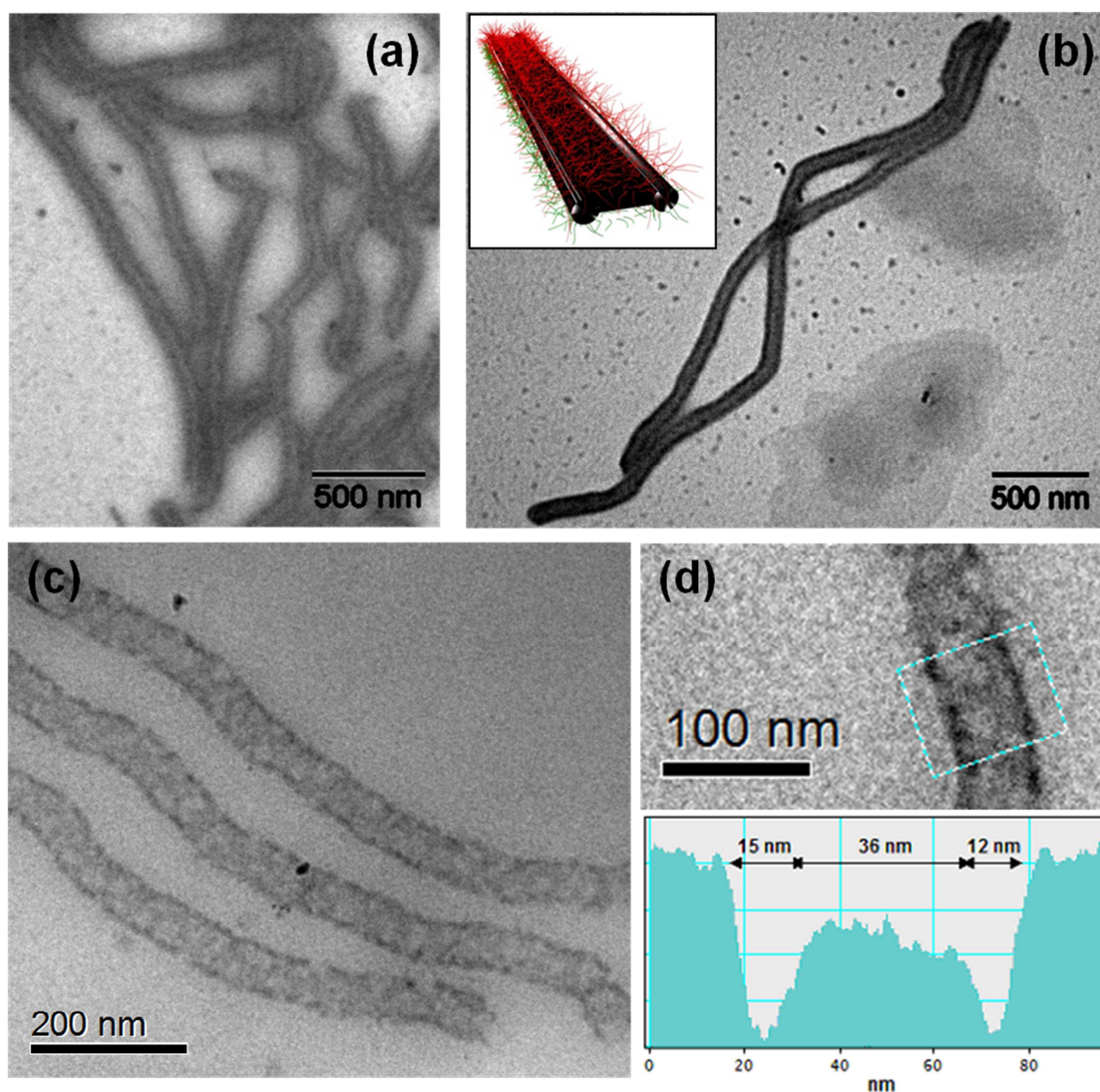


Figure 5-6. TEM images of dried Janus ribbons (a, b) including a scheme of one Janus ribbon (inset in b) and cryo-TEM images in vitrified toluene (c, d) with analysis of the cross section indicated in micrograph (d).

Further investigation of the synthesis pathway showed that a sufficient swelling time is necessary for a complete phase transition. After only seven hours of swelling and subsequent cross-linking TEM micrographs indicate the development of only few Janus ribbons whereas mainly Janus cylinders are present (Figure 5-7).

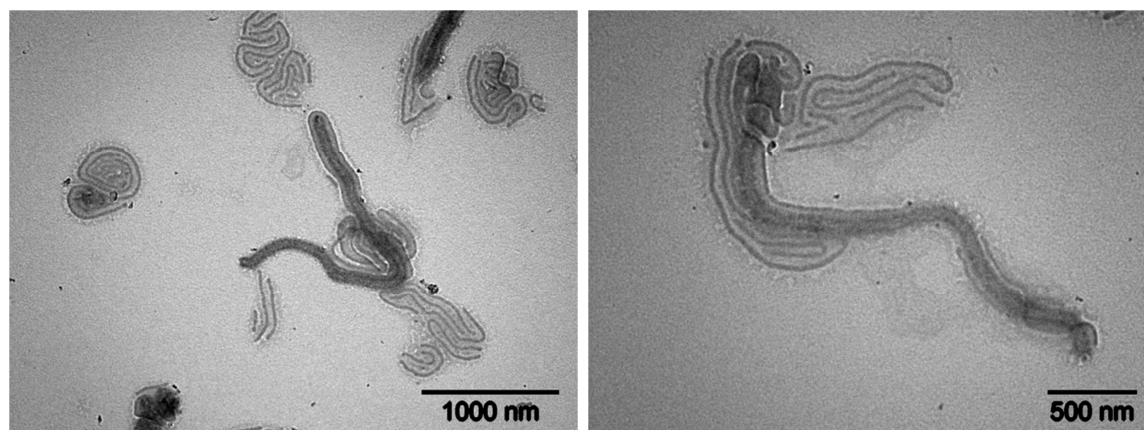


Figure 5-7. TEM micrographs of Janus cylinders transforming into Janus tapes. Sample obtained after seven hours of swelling in acetonitrile/decane and cross-linking with S_2Cl_2 .

This observation together with the TEM images of tSBT (Figure 4-2) which show an lc-morphology supports the above described pathway and opposes the possibility that the Janus ribbons originate from an initially formed undulated lamellar morphology which is then broken in every second interspace. Additionally, the formation of ribbons in acetonitrile/decane emulsion, in contrast to sheet formation in pure acetonitrile (stirred and unstirred), illustrates the strong influence of the swelling agent and the hydrodynamic forces.

Strikingly, despite the challenging conditions, the Janus ribbon synthesis proved to be highly reproducible, thus corresponding to a remarkably defined and robust pathway for the phase transition. This points to the fundamentally important discovery of a defined intermediate phase during the phase transition from a lamella-cylinder to an undulated-lamella morphology.

To gain further insight into the structure of the Janus ribbons and their behavior in solution they were also investigated by cryogenic transmission electron microscopy (cryo-TEM) in toluene solution. Figure 5-6c and d show micrographs taken of a sample of Janus ribbons in toluene and a cross section analysis for one ribbon. The gray scale analysis visualizes the structure of the PB layer of the Janus ribbons with two limiting cylinders at the boundaries (darker in the image, lower gray value) connected by a thinner layer of PB (lighter in the image). It indicates a diameter of 12 to 15 nm for the cylinders and 36 nm for the interspace. Due to swelling and lower contrast in cryo-TEM, the dimensions of the cylindrical parts at the lateral boundaries of the ribbon can be underestimated. In comparison, lateral cylinders of the ribbons in TEM of a dried sample (Figure 5-6a and b) are 24 ± 7 nm and their interspaces 37 ± 9 nm. These ribbon dimensions are similar to the dimensions of the Janus sheets

in TEM of a dried sample (cylinders ≈ 23 nm, interspaces ≈ 31 nm). These were also swollen and treated with S_2Cl_2 , thus illustrating that both structures, ribbons and sheets, originate from the same lc-morphology. Consequently, the higher radius of the cylinders in the final ribbons compared to the bulk phase and the radically cross-linked Janus cylinders is due to the incorporated S_2Cl_2 similar to the case of Janus sheets. The different structure of the two 2-D Janus objects cylinders and ribbons is also visible in SEM images (Figure 5-8). While the Janus cylinder itself appears lightly colored with dark edges, the ribbons exhibit white edges caused by the Janus cylinders in these lateral positions.

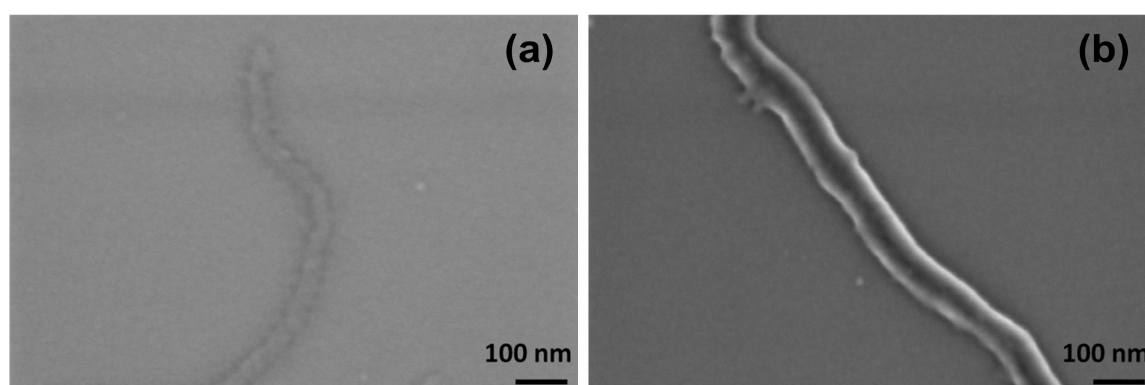


Figure 5-8. SEM micrographs of a Janus cylinder (a) and a Janus ribbon (b).

As Janus sheets (with all original cylinders connected) result after swelling in pure acetonitrile and the Janus ribbons develop in a mixture of acetonitrile (A) and decane (D) in the ratio $A/D = 1/1$, we wondered whether it is possible to influence the number of merging cylinders by increasing the acetonitrile content. We followed the same procedure as for Janus ribbon synthesis with solvent ratios of $A/D = 6/4$, $A/D = 7/3$ and $A/D = 9/1$. However, in all cases the resulting particles more or less resembled sheet-like structures (Figure 5-9). For $A/D = 6/4$, neither real continuous sheets nor Janus ribbons were present in the sample, instead the increase in acetonitrile amplified the swelling of PB in a way that resulted in holey sheet structures. For $A/D = 7/3$ and $A/D = 9/1$ also such holey sheets albeit with less holes are present while also continuous sheets are found (not shown in Figure 5-9). Unsurprisingly, with the portion of acetonitrile increasing from 7 to 9, also the amount of continuous sheets increases.

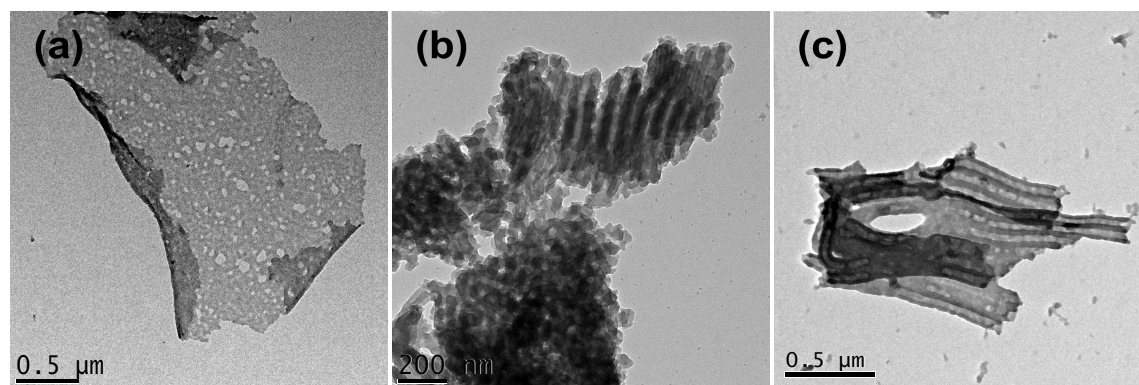


Figure 5-9. Particles from tSBT films swollen in A/D emulsions of the ratios 6/4 (a), 7/3 (b) and 9/1 (c) followed by cross-linking with S_2Cl_2 .

The susceptibility of the lamella-cylinder equilibrium bulk morphology to phase transitions also prompted us to explore whether suitable solvent casting could be used to obtain the lamella-sphere (ls) morphology suitable for the fabrication of Janus spheres. Indeed, it turned out that *tert*-butanol, a good solvent for both end blocks, PtS and PtBMA, and a non-solvent for PB, leads to the development of spherical PB domains at the interface of an overall lamellar structure. Obviously, the strong ability to swell the end blocks of the tSBT triblock terpolymer, while being a non-solvent for the middle block, leads to the development of the ls bulk structure, which is a defined non-equilibrium state that cannot relax into the lc phase due to the slow dynamics in the bulk state. The ls-morphology was present after film casting without and with TPO (Figure 5-10a and b). Further investigations revealed that micelles with a PB core and a mixed corona of the soluble blocks PtS and PtBMA do already form during the dissolution of tSBT in *tert*-butanol (Figure 5-10c). The outer blocks then undergo phase separation during the evaporation of *tert*-butanol and the final ls-morphology is formed. In a TEM sample stained with OsO_4 the PB core of the observed micelles is visible and has the same size as the PB domains in the later bulk morphology, 17 ± 3 nm. After photo-cross-linking, the PB core of the obtained Janus micelles in dioxane is 21 ± 6 nm. The size is slightly increased now because PB is no longer collapsed in a non-solvent, but swollen in dioxane.

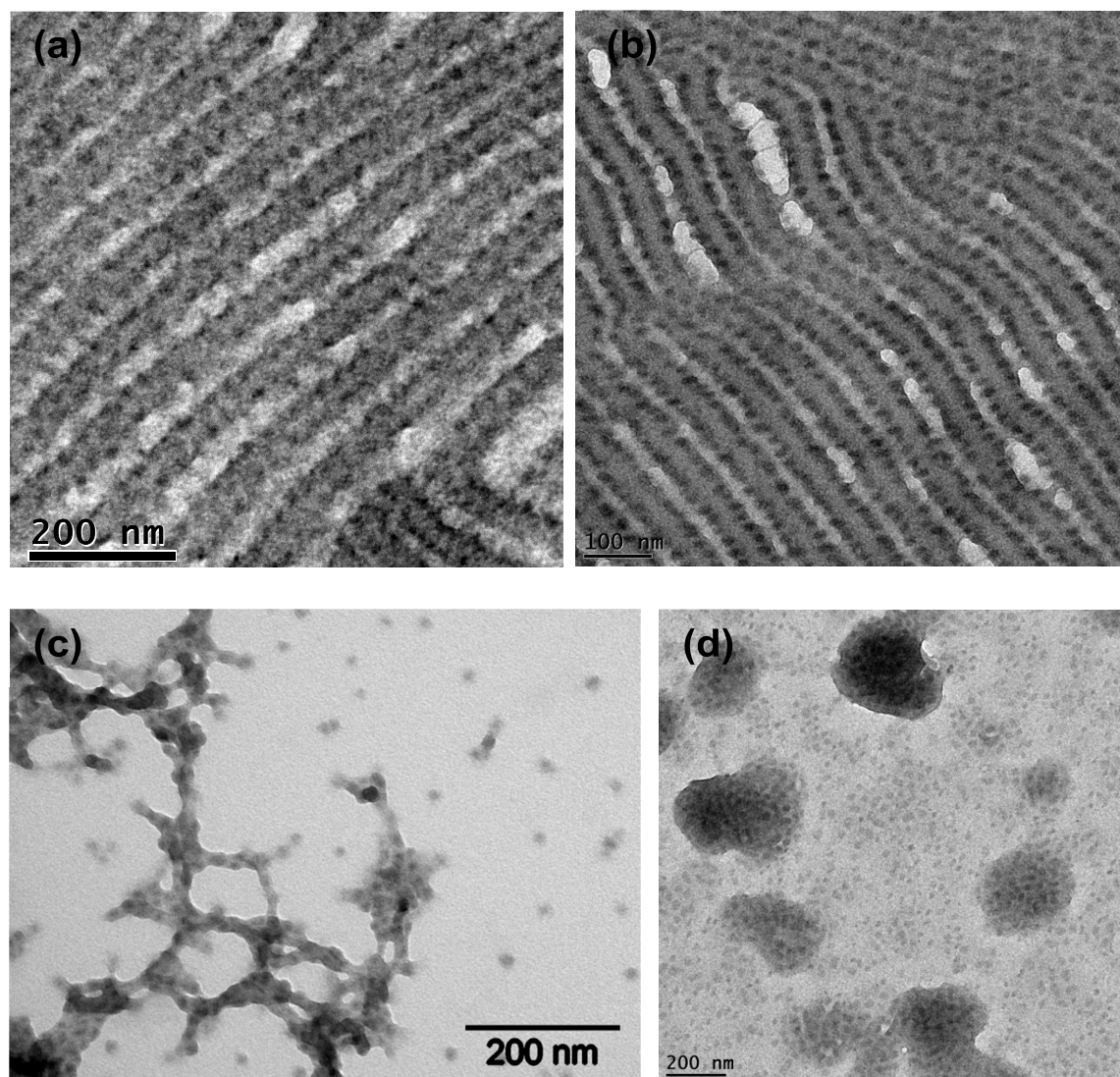


Figure 5-10. TEM micrographs stained with OsO_4 of tSBT bulk *l*s-morphologies without (a) and with TPO (30 wt%, b), tSBT micelles formed in *tert*-butanol (c) and tSBT Janus micelles after photo-cross-linking and dissolution in dioxane (d).

In summary, we were able to synthesize nanosized JPs with three different non-spherical topologies from one single tSBT triblock terpolymer, which are Janus cylinders, Janus ribbons and structured Janus discs, in addition to spherical Janus beads. This represents a significant simplification of the production of different Janus architectures. We accomplished that by the careful adjustment of pre-treatment and cross-linking conditions of its bulk morphology. Photo-cross-linking without prior swelling led to Janus cylinders. This was expected because tSBT showed an *l*c-morphology after film-casting from chloroform. However, if the polymer film was swollen in acetonitrile prior to cross-linking with S_2Cl_2 , the morphology changed to an undulated-lamella one in which the original cylinders still exist

in the form of thicker parts in the newly formed PB lamella. After cross-linking and sonication, this morphology results in sheet-like JPs. Most surprising is the discovery of the novel topology of Janus ribbons (with a flattened dimension compared to cylinders). They formed when the original polymer film was swollen in a stirred acetonitrile/decane emulsion. Exclusively two cylinders became connected by a newly developed PB-layer. This ribbon-like structure was then preserved by cold vulcanization.

5.2 Hydrolysis and solution structure of Janus cylinders

Apart from the versatility of the tSBT triblock terpolymer concerning the synthesis of different Janus structures, it also features the interesting PtS block, which was chosen for the possibility of hydrolysis into pH-responsive PHS. The pK_a of linear PHS is reported at approximately 10,^{129,165} and Janus particles with a pH-dependent water-soluble PHS side can be created. Furthermore, the hydrolysis of PtBMA results in poly(methacrylic acid) (PMAA) hemicylinders, which are well water-soluble at $pH \geq 4$. Consequently, HSBT Janus particles made from tSBT are potentially water-soluble and pH-responsive which extends the range of self-assembly and enables applications in aqueous media. Additionally, the hydroxyl group allows further functionalization of the Janus particles. In the following we focus on the solution properties of the Janus cylinders.

When we attempted to hydrolyze them by the standard protocol of refluxing in dioxane with HCl, a significant amount of material decomposed and stuck at the side of the reaction vessel; probably due to the small batch volume (~ 5 mL). Therefore, we chose the reaction with trimethylsilyl iodide (TMSI) as alternative. This mild method can be used for esters and ethers and works already at room temperature or at slightly elevated temperatures.^{137,138} First, the *tert*-butoxy group is converted to a silyl ester (PtBMA) or ether (PtS), respectively, by TMSI, then the actual hydrolysis follows through addition of water or methanol.

Figure 5-11 presents the 1H -NMR spectra of Janus cylinders before and after reaction with TMSI at 60 °C, yet before the final hydrolysis took place.

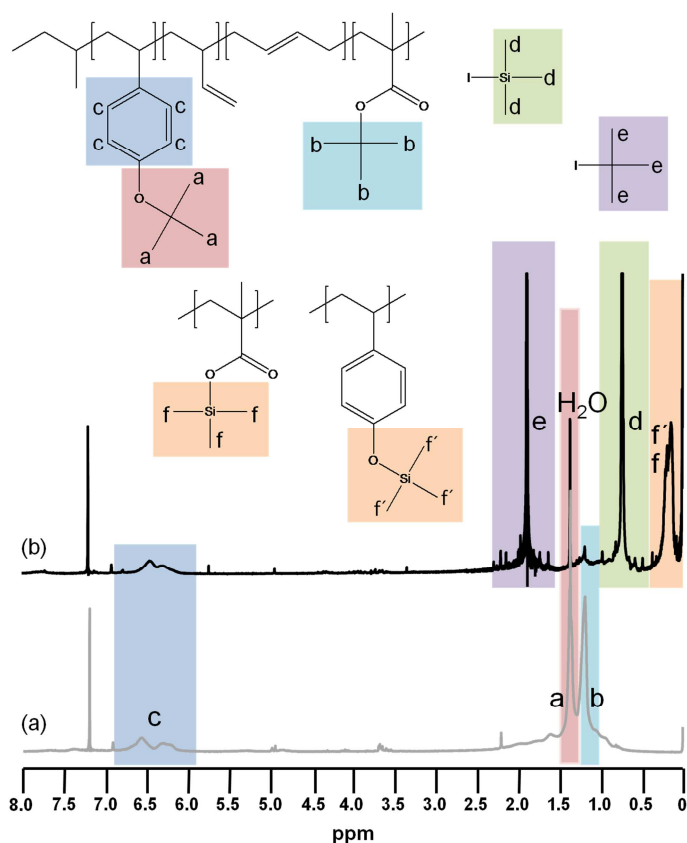


Figure 5-11. $^1\text{H-NMR}$ spectra illustrating the hydrolysis of Janus cylinders recorded in CDCl_3 : before hydrolysis (a) and after addition of TMSI and three hours at 60°C (b).

The spectra clearly show the substitution of the *tert*-butoxy group to a near quantitative degree, which then hydrolyze fully upon addition of aqueous methanol. Both peaks corresponding to the *tert*-butyl groups are strongly diminished and only signals of the polymer backbone remain. A comparison of the silyl ester/ether signal f/f' with the signals of the aromatic units results in a conversion of above 90 %. The very sharp peak at 1.36 ppm in the spectra (b) originates from residual water.

To investigate the solution structure of these hydrolyzed Janus cylinders, cryo-TEM images in water ($\text{pH} \approx 10$ and $\text{pH} \approx 13$) in the presence of 100 mM CsCl were recorded. Cryo-TEM has the distinct advantage that the extent of staining with heavy ions depends on the degree of ionization of the polyelectrolyte brushes, their brush density and thus the overall tendency to confine counterions within the brush. This is the reason why poly(ethylene oxide) or other non-ionic water-soluble polymer coronas (of micelles or particles) can often not be visualized due to the unfavorable staining behavior and contrast, whereas strong polyelectrolyte brushes are rather easy to resolve using appropriate ionic additives. We herein applied this principle with the aim to visualize the biphasic character of fully water-soluble

Janus cylinders at appropriate pH values, where both corona sides are differently stained simply for their different degrees of ionization.

Figure 5-12 displays images of the Janus cylinders at pH 10, where the PHS block only carries a minor fraction of charges, in particular compared to the basically quantitatively deprotonated PMAA side. Various unimolecularly dispersed cylinders can be observed in which a corona is solely visibly on one side. Figure 5-12c and d display a further close up on one cylinder and the complementing cross-sectional gray-scale analysis. The Janus character of the cylinders is remarkably well visible. At the lower side of the well-visible dark cylinder in Figure 5-12c, a corona part with condensed Cs⁺ counterions is evident, whereas no corona can be observed at the upper side. Given the large difference of the pK_a values of PMAA and PHS, we can reasonably suggest that the visible corona consists of the completely deprotonated PMAA. Due to its high charge density at pH 10, a large amount of Cs⁺ counterions is condensed inside its corona. In contrast, PHS with its pK_a around 10 is far less ionized, especially as it was shown that the pK_a can increase for brush-like structures as compared to linear analogous. This behavior was found earlier for multi-arm star-shaped polyanions.¹⁶⁶ Thus, at pH 10, the fraction of deprotonated PHS units is small and consequently very little Cs⁺ ions can accumulate within the PHS corona. Therefore, it is not visible adjacent to the dark PB core and PMAA corona. It is also important to note that the calculated diameter of the dark cylinder only amounts to 23 ± 3 nm. This corresponds to the PB cylinder alone and further indicates that the PHS part is dissolved and not part of the dark cylindrical core.

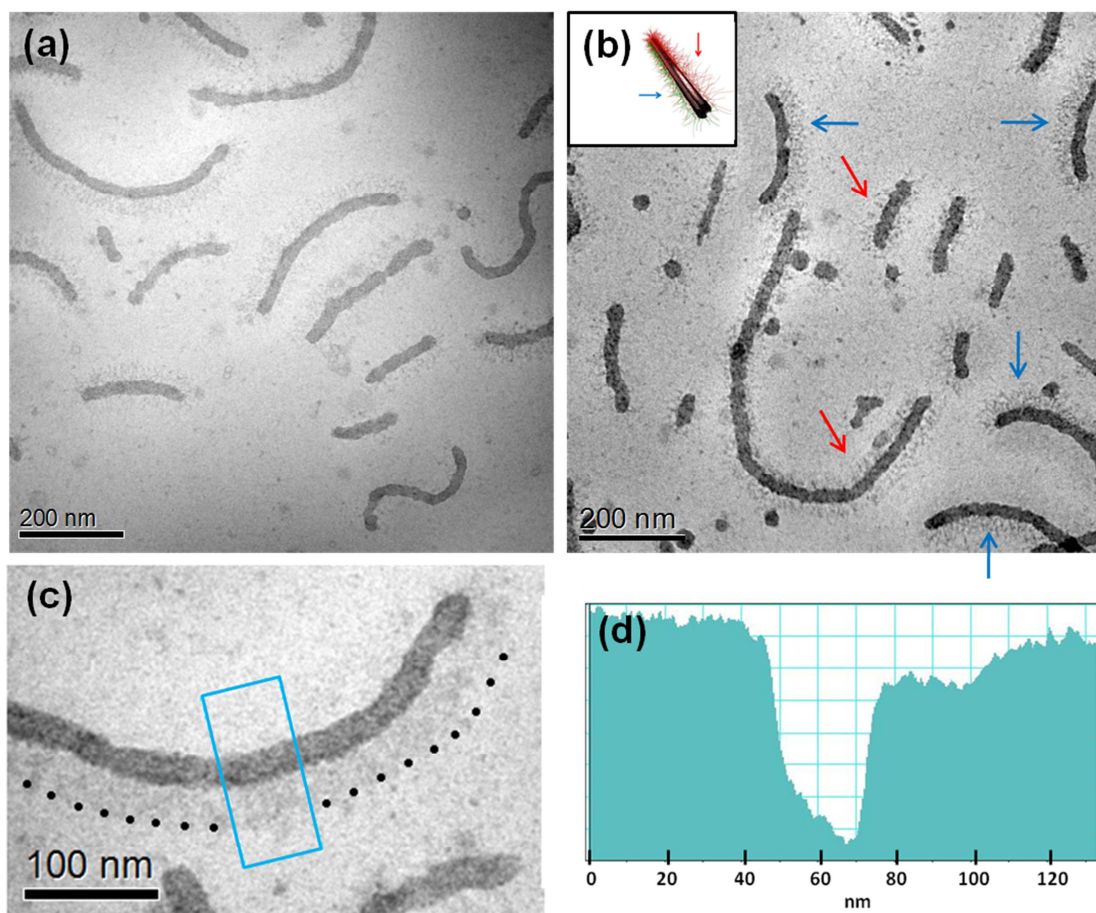


Figure 5-12. Cryo-TEM images of hydrolyzed Janus cylinders at $\text{pH} \approx 10$ (a,b,c) with gray-scale analysis (d) of the cross section indicated by blue line in the micrograph (c). Dotted line in micrograph (c) visualizes the boundary of the PMAA corona.

The exclusive visibility of the PMAA corona at one side of the cylinder represents one of the most convincing real-space proofs of the biphasic character of water-soluble polymeric Janus nanoparticles. It furthermore establishes that the phase segregation is fully retained during the transfer of the cross-linked bulk structure into solution and does not vanish due to a potential entropically favored chain mixing of the two sets of brush arms on the cross-linked PB cylinder. The PMAA corona can be found at the cylinders in all four directions with respect to the image (Figure 5-12, blue arrows). This confirms the absence of any artifacts of the imaging process. Cylinders that seem to have a corona on both sides are simply imaged from the top (red arrows), because of the rotational freedom of the cylinders within the thin water film.

The situation looks different when studying cryo-TEM images of hydrolyzed Janus cylinders at $\text{pH} 13$ (recorded in the presence of 100 mM CsCl). Figure 5-13 shows two typical images.

As anticipated, in contrast to the cylinders shown above, every cylinder displays a corona on both sides, fully surrounding the central PB cylinder. This is due to the fact that now not only PMAA, but also PHS is deprotonated to a high degree and therefore binds large amounts of Cs⁺ ions. The average diameter of the cylindrical cores is 22 ± 2 nm and therefore the same as for pH 10. This underlines the fact that the PHS corona is soluble for both pH values, it just remains invisible at pH 10 because of insufficient counterion capture at lower ionization.

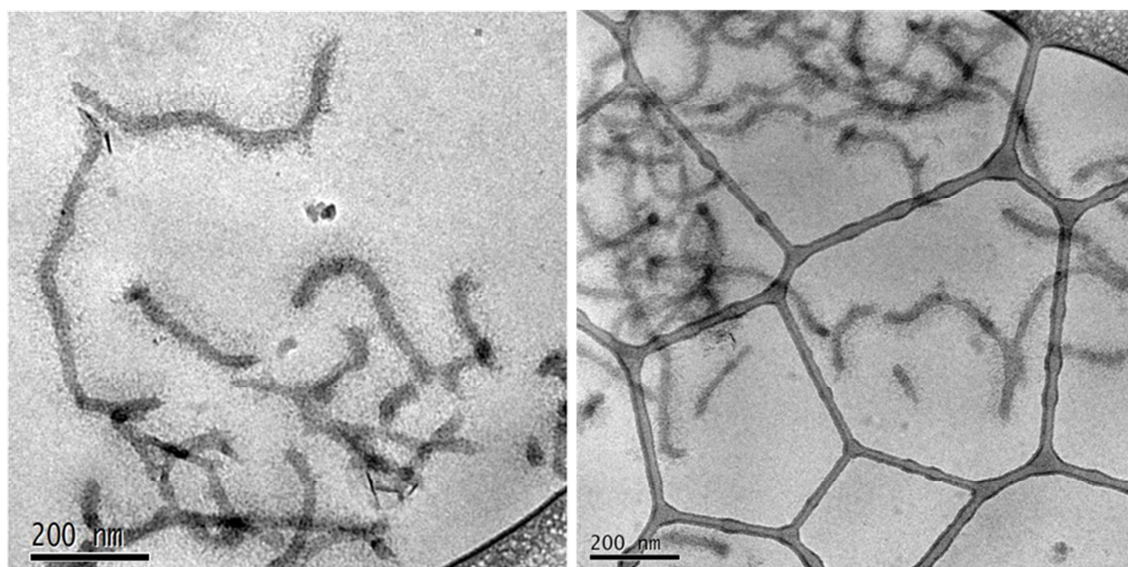


Figure 5-13. Cryo-TEM images of hydrolyzed Janus cylinders at pH 13.

5.3 Conclusion

We have demonstrated how the careful choice of solvent and cross-linking conditions can be used to manipulate triblock terpolymer bulk structures in a way that allows synthesizing three different types of non-spherical Janus particles as well as spherical ones from one single triblock terpolymer. We were able to obtain Janus sheets, Janus cylinders and an intermediate new structure, Janus ribbons. The successful preparation of all these structures relies on a thorough understanding of how to manipulate the bulk morphologies into equilibrium and non-equilibrium structures. The intermediate fraction of PB of 16 wt% facilitates transformations into spherical and lamellar domains that would usually be only stable at much smaller or larger weight fractions (at moderate interfacial tension/incompatibility between A and C), respectively. Selective solvent casting proved useful to access the non-equilibrium ls-morphology and generate Janus spheres. On the other hand, the surprising

observation of Janus ribbons points to the fundamentally important discovery of a defined intermediate phase during the phase transition from the lamella-cylinder to the undulated-lamella morphology. Overall, this beneficial and simple way to tune bulk morphologies drastically simplifies the access routes towards asymmetric soft Janus particles with nanometer dimensions on the multigram scale. We expect that the considerations herein can be applied to other terpolymer systems and allow to generate Janus particles of higher functionality from a single triblock terpolymer with moderated efforts. We also introduced the use of poly(*tert*-butoxystyrene) instead of polystyrene in the synthesis, which can be hydrolyzed to polyhydroxystyrene, featuring stimuli-responsiveness and water-solubility and opening possibilities for the modification of the PHS hydroxy group towards tailored functionalities in the future. The water-solubility and stimuli-responsiveness expand possible fields of application for such Janus particles to aqueous media.

6 Solution Structures of tSBD and tSBT

6.1 Stimuli-responsive micelles from tSBD

Poly(2-(dimethylamino)ethyl methacrylate) is a water-soluble polymer which is thermo-responsive due to its balance of hydrophilicity and hydrophobicity and pH-responsive because of its tertiary amino-group. Above a certain transition temperature hydrated DMAEMA segments undergo dehydration which leads to precipitation of the polymer. This critical point of phase separation is called cloud point and is dependent on the polymer concentration. At a critical concentration we find the cloud point with the lowest temperature. This temperature is defined as lower critical solution temperature (LCST). As for pH, with a higher amount of protonated tertiary amino groups, the polymer hydrophilicity as well as the electrostatical repulsion increases and consequently the cloud point increases with decreasing pH value.^{167,168}

When tS₃₁₆B₃₄₃D₂₆₇, completely dissolved in dioxane, is dialyzed against water, the PtS and PB block become insoluble and micelles with a core of PtS and PB held in solution by a corona of PDMAEMA were expected. Because of PDMAEMA's described properties, the micelles were supposed to be pH- and thermo-responsive.

After complete dissolution of tSBD in dioxane, a solvent for all three blocks, dialysis against water with pH 5 took place. As expected this resulted in the formation of micelles (Figure 6-1) which were observed with TEM and cryo-TEM. The size of the visible core is 26 ± 3 nm in TEM micrographs and 27 ± 4 nm in the cryo-TEM. In both cases the core of collapsed PtS and PB is visible while PDMAEMA does not contribute to the contrast. For the core, phase separation of PtS and PB was expected as already observed in tSBT and tSBD bulk structures (see chapter 4). Due to the block sequence a core of PtS should be surrounded by a PB shell. However, the TEM micrographs only show a uniform core, probably due to the low thickness of the PB shell. To gain information about the full hydrodynamic radius of the micelles, it was measured with DLS and was 110 nm, clearly showing the large corona of well-protonated PDMAEMA (around 95 nm) (Figure 6-2).

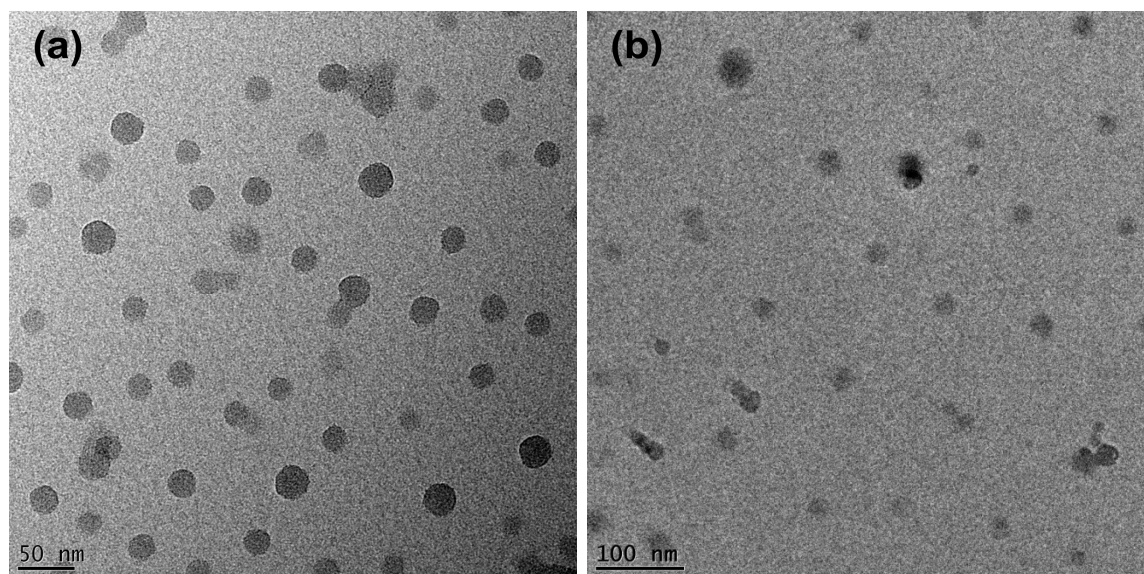


Figure 6-1. TEM (a) and cryo-TEM (b) micrographs of tSBD micelles at pH 5. The TEM micrograph is stained with OsO_4 (PB appears black).

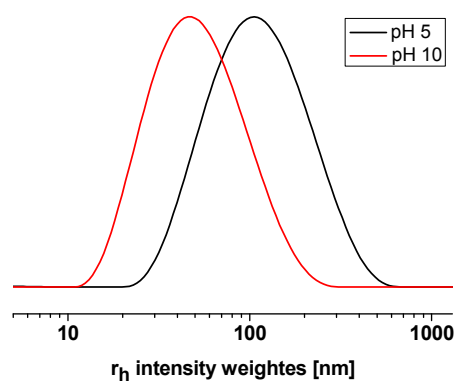


Figure 6-2. DLS CONTIN plot of tSBD micelles at pH 5 (black) and pH 10 (red) showing the hydrodynamic radius r_h .

For pH 10 the particle sizes in TEM and cryo-TEM are 28 ± 3 and 34 ± 3 nm (Figure 6-3). In DLS measurements a hydrodynamic radius of only 50 nm was observed. The differences in size of core and corona are due to the different degree of protonation. While at pH 5 PDMAEMA is partially protonated, it is deprotonated at pH 10. Therefore, no more repulsive interactions due to charged polymer chains exist in the corona and between tSBD molecules. Consequently, the aggregation number of the micelles rises which causes an increase in core size. At the same time the corona size decreases.¹⁶⁹ It is now only around 35 nm, only about

37 % of the original 95 nm at pH 5. For the TEM sample this leads to some aggregation of the micelles during the drying process of the sample preparation while the cryo-TEM micrograph shows that they are still existent as single particles in solution.

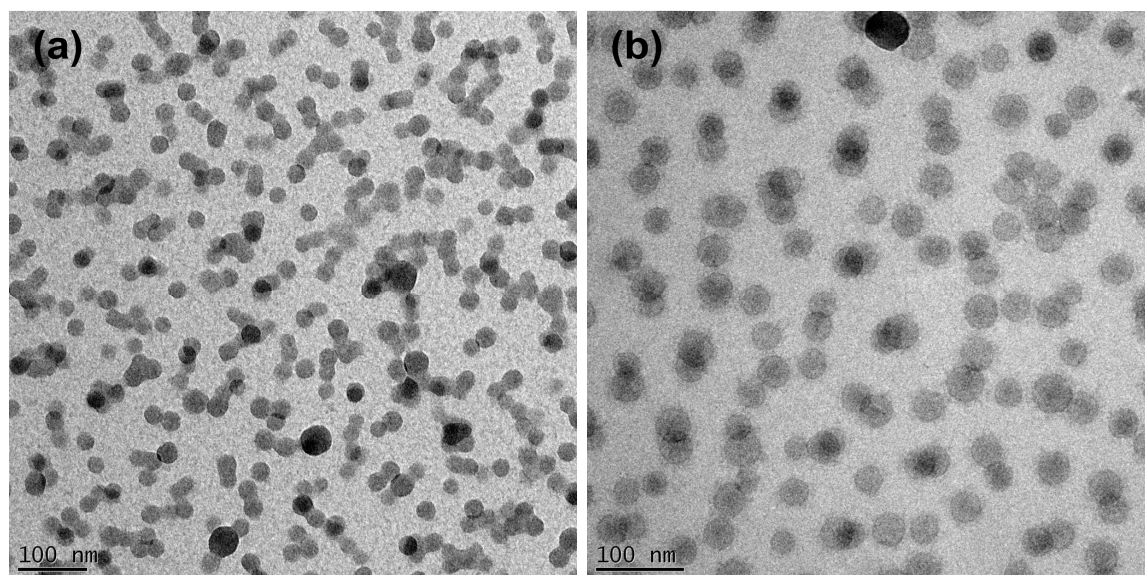


Figure 6-3. TEM (a) and cryo-TEM (b) micrographs of tSBD micelles at pH 10. TEM micrograph is stained with OsO_4 (PB appears black).

To detect the cloud points of the tSBD micelles, we measured DLS temperature ramps for micelles in buffer solutions of pH 8, 9 and 10. The results are shown in Figure 6-4. Here, we can observe the same decrease of the T_{cl} with increasing pH as reported for linear and star-shaped PDMAEMA by Plamper et al.¹⁵⁸

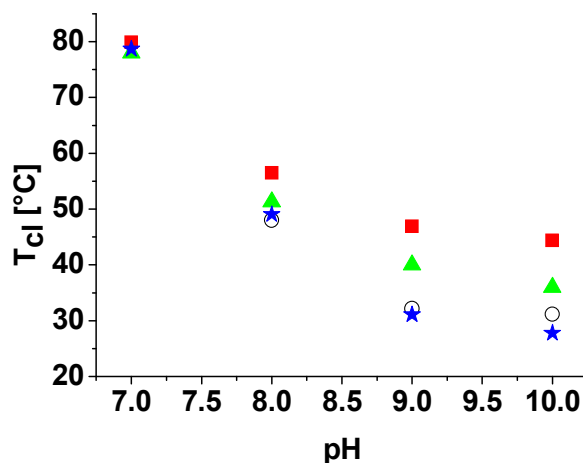


Figure 6-4. pH dependent cloud points for linear and star-shaped PDMAEMA , (!) PDMAEMA₁₀₈, (7) (PDMAEMA₁₀₀)_{3.1}, (ξ) (PDMAEMA₁₇₀)₁₈ and for (-)tSBD micelles. Adapted with permission from Ref [158]. Copyright 2007 American Chemical Society.

6.2 Multicompartment micelles from tSBD

Apart from micelle formation by a one-step dialysis procedure, also multicompartment-core micelles could be obtained from tSBD. This was achieved by directed self-assembly by step-wise reduction of the degree of freedom of the multicompartment micelle (MCM) formation of triblock terpolymers.⁵⁹ In this two-step process first pre-assembled subunits are formed by dissolution of the terpolymer in a non-solvent for the middle-block or dialysis against such a solvent, followed by dialysis against a non-solvent for both the middle block and one of the outer blocks to obtain the final multicompartment micelles. Accordingly, tSBD was first dissolved in dimethylacetamide (DMAc), a non-solvent for PB, then the solution was dialyzed against untreated Milli-Q water (pH 5), so that PtS collapsed as well while the water-soluble PDMAEMA built the corona. The volume ratio of the A and B block, V_{PtS}/V_{PB} is 2.62 which should result in spherical MCMs like in all cases where $V_A/V_B > 1$.⁵⁹ The large value further suggests an MCM structure with more than three subunits, so-called “football” MCMs (Figure 1-8).⁶⁰ Indeed, Figure 6-5 shows the obtained MCMs with their football-like shape. Dialysis against pH 3 and 4 instead of 5 resulted in the same structures.

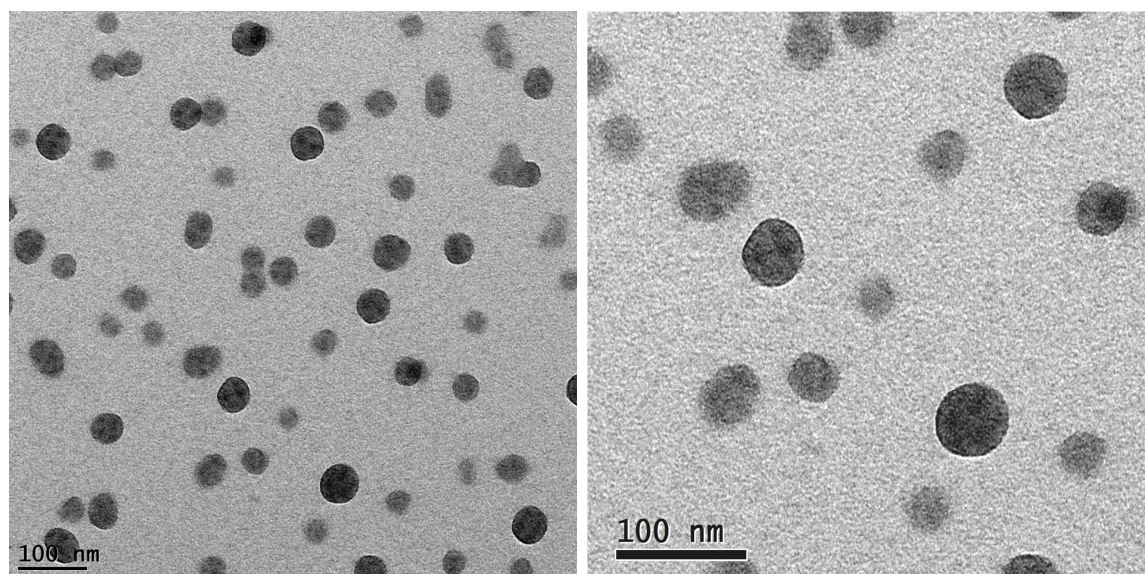


Figure 6-5. MCMs of tSBD at pH 5, stained with OsO_4 ; visible is the multicompartment core of PtS and PB (darker areas indicating PB).

Gröschel et al. were successful in the self-assembly of different MCMs (inverse “hamburger”, “double-burger”, linear MCMs) from the same poly(*tert*-butyl methacrylate)-*block*-poly(2-(cinnamoyloxy)ethyl methacrylate)-*block*-poly(2-(dimethylamino)ethyl methacrylate) (TCD) by varying the pH of the solution against which the final dialysis was performed.⁵⁹ Like in tSBD, PDMAEMA is the corona-block for these different MCMs. Due to its pK_a at 6.2,¹⁵⁸ it is fully protonated at pH = 3, partially protonated at pH = 6 and sparsely charged at pH = 8; consequently, the size of the PDMAEMA corona decreases in this order. To keep the micelles solubilized, their assembly changes from inverse “hamburger” to “double-burger” to linear MCMs as this way the surface area that has to be covered by the contracting corona is decreased.

We investigated whether the decrease in size of the PDMAEMA corona also leads to different MCM formation in the case of tSBD MCMs. For this purpose MCMs were examined with TEM and cryo-TEM after the dialysis against pH 6 and pH 8 (Figure 6-6 and Figure 6-7). In contrast to the TEM micrographs of MCMs at pH 5 (Figure 6-5), at pH 6 merged MCMs are visible albeit no distinctive pattern is recognizable. At pH 8 similar objects are visible in the TEM micrograph. However, when investigated with cryo-TEM, only single (“football”) MCMs are observed. Consequently, the size of the corona decreases with increasing pH which causes increased aggregation of the individual MCMs during the drying process in the sample preparation for conventional TEM; but it does not lead to a real merging of the MCMs

and formation of MCMs shaped differently from the original “football” micelles. Only in some isolated spots, large linear MCMs are visible in the TEM samples at pH 8 (Figure 6-7a).

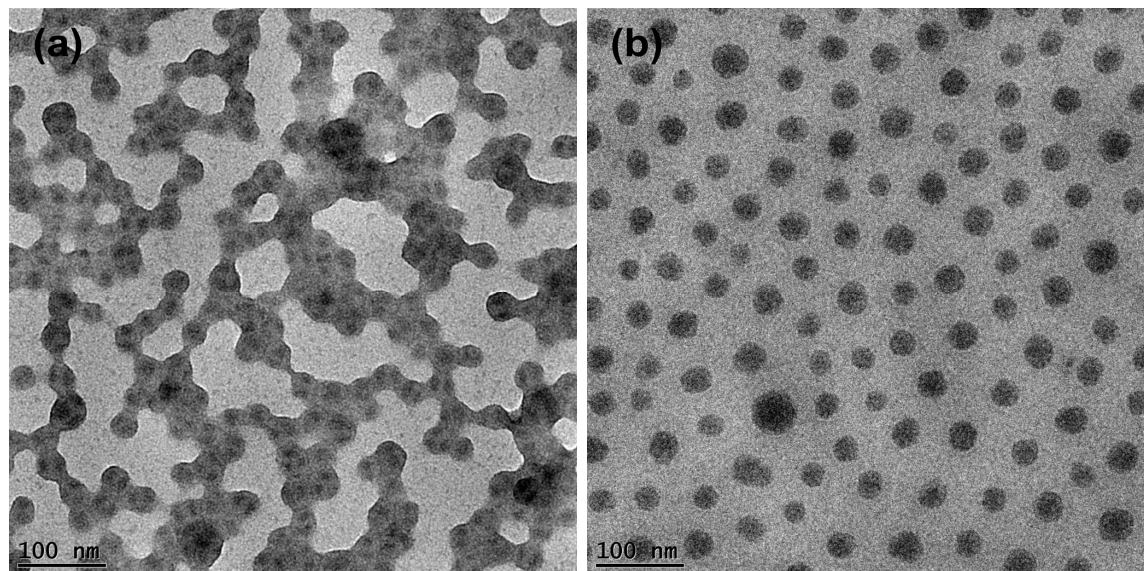


Figure 6-6. TEM (a) and cryo-TEM (b) micrographs of tSBD MCMs at pH 6. TEM micrograph is stained with OsO_4 (PB appears black).

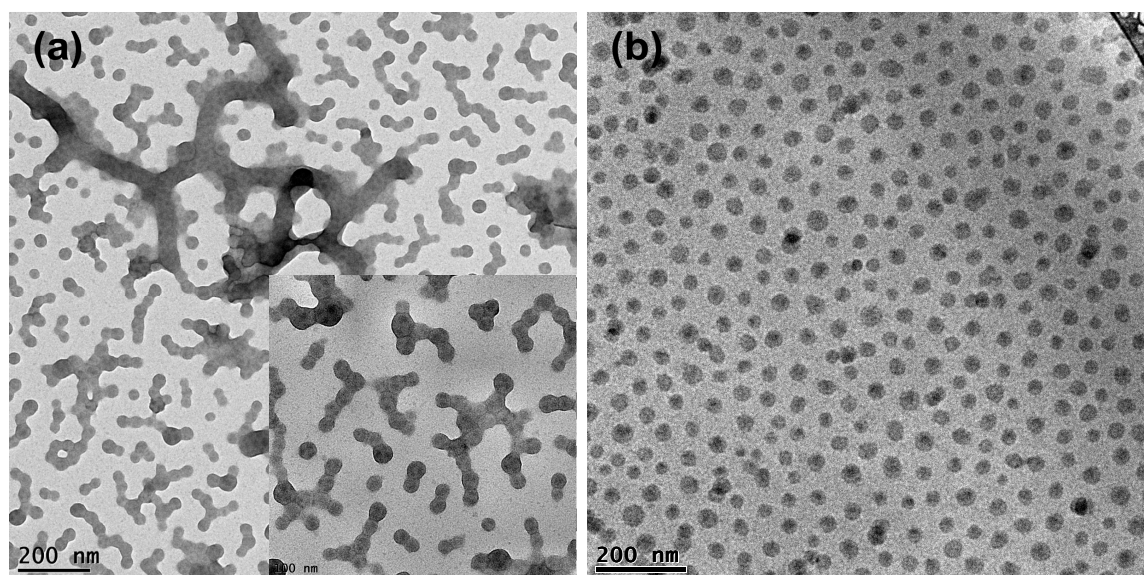


Figure 6-7. TEM (a) and cryo-TEM (b) micrographs of tSBD MCMs at pH 8. TEM micrograph is stained with OsO_4 (PB appears black).

The next step was the cross-linking of the tSBD MCMs. Cross-linking of the B compartments in MCMs fixates the phase segregation of blocks A, B and C as present in the MCMs and subsequent dissolution in a good solvent for all three blocks results in Janus particles (Figure 6-8).⁶⁰

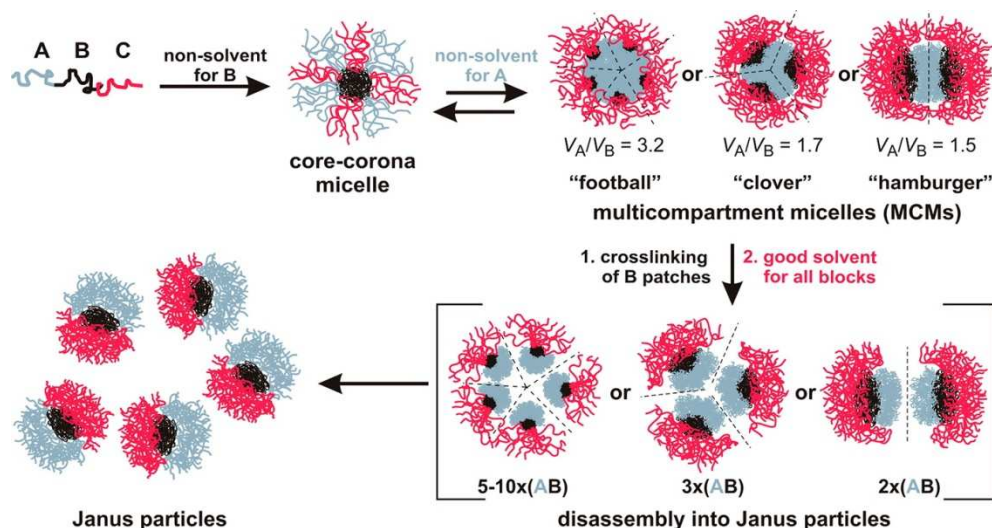


Figure 6-8. Self-assembly of ABC triblock terpolymers into multicompartment micelles and subsequent disassembly into Janus particles. Reprinted with permission from Ref [60]. Copyright 2012 American Chemical Society.

In the most common case where MCMs with a PB compartment are present in organic solvents, the photo-cross-linker Lucirin® TPO can be added to the solution and cross-linking of the PB domains takes place under UV light. However, the tSBD MCMs could only be obtained in aqueous solution and Lucirin® TPO is therefore not soluble. On the other hand, a water-soluble UV-cross-linker has no affinity to the lipophylic PB domains so that no sufficient cross-linking of that phase can take place. Therefore, we chose to first dissolve tSBD and the cross-linking agent in THF or acetone, then slowly add DMAc to induce the collapse of PB, at the same time incorporating the lipophilic cross-linker, followed by the usual dialysis step against water for the MCM assembly. Apart from TPO (in different ratios from equimolar to excess), also AIBN and AIBN/TRIS (trimethylolpropane mercaptopropionate, should lead to a strong and quantitative cross-linking as it acts as chain transfer agent and is able to react with 1,4-PB in a thiol-ene reaction⁹⁷) were used for cross-linking. However, none of the mentioned approaches resulted in a successful cross-linking process. Only hardly cross-linked and ill-defined structures were the result.

6.3 Multicompartment micelles from tSBT

For the preparation of MCMs from tSBT by directed self-assembly, the terpolymer first had to be dissolved in DMAc to cause the collapse of PB. The subunits then formed MCMs when the DMAc solution was dialyzed against ethanol (EtOH), in which the PtS collapses while PtBMA remains in solution. Due to the volume ratio of $V_{\text{PtS}}/V_{\text{PB}} = 2.51$ spherical MCMs were expected. Although only having a slightly smaller $V_{\text{PtS}}/V_{\text{PB}}$ ratio than tSBD ($V_{\text{PtS}}/V_{\text{PB}} = 2.62$), here, “clover” MCMs with three subunits instead of “football” micelles assembled. Only some isolated inverse “double burgers” could be observed (Figure 6-9).

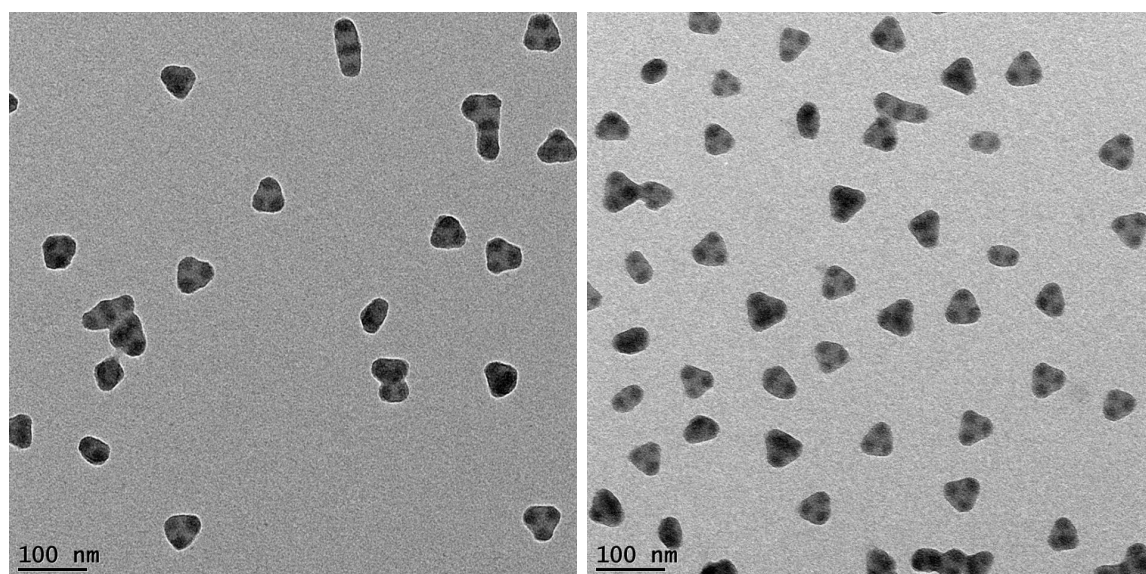


Figure 6-9. Multicompartment micelles of tSBT obtained after dissolution in DMAc and subsequent dialysis against EtOH. TEM micrographs are stained with OsO_4 (PB appears black, PtS gray).

6.4 Janus spheres from tSBT multicompartment micelles

In contrast to the tSBD MCMs, tSBT MCMs exist in an organic solvent, EtOH in this case. Consequently, for cross-linking of the PB domain to prepare Janus particles as depicted in Figure 6-8, the photo-cross-linker Lucirin® TPO could simply be added to the MCM solution. The cross-linked MCMs were then dialyzed against dioxane, a solvent for all three blocks, to obtain dissolved Janus spheres. The Janus particles are well visible in the TEM after staining with OsO_4 (Figure 6-10). The thus visible PB cores have a diameter of 23 ± 2 nm compared to PB domains of 21 ± 3 nm in the prior MCMs. DLS measurements of the Janus particles in

dioxane result in a hydrodynamic radius r_h of 42 ± 0 , consequently a diameter of about 80 nm. Accordingly, the obtained Janus spheres have a core of around 20 nm in diameter and a corona that is about 30 nm thick.

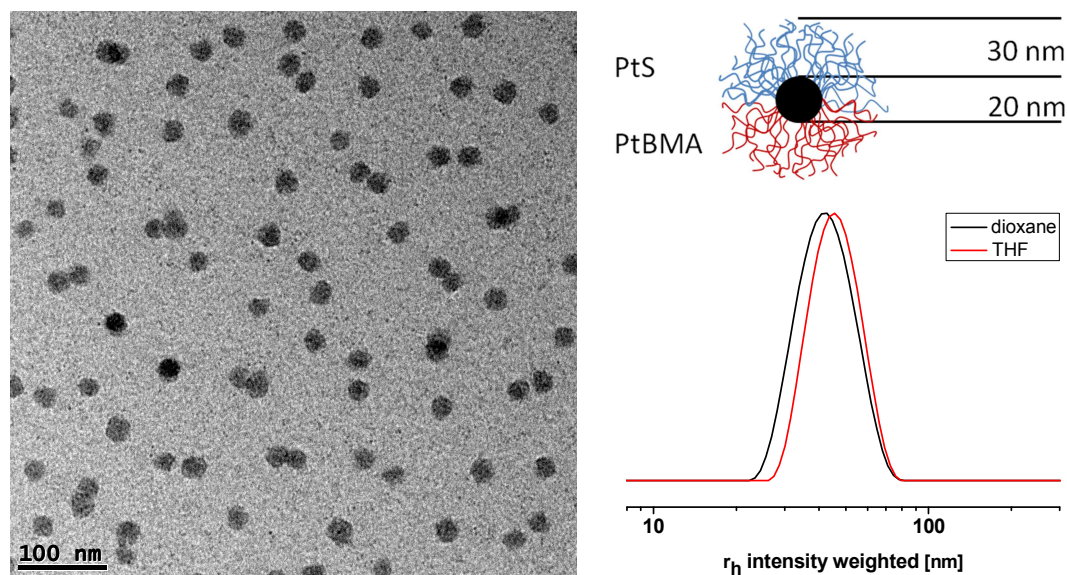


Figure 6-10. TEM micrograph (stained with OsO_4 , PB appears black) and scheme of Janus micelles from tSBT in dioxane and DLS plots in dioxane (black) and THF (red).

In contrast to the TEM micrographs in dioxane where we can observe single JPs by their visible PB core, the JPs have a tendency to aggregate in THF (Figure 6-11). The slightly worse soluble PtS aggregates and this way is now visible in the micrographs due to the higher local concentration. The stained PB cores are 22 ± 2 nm in size and confirm that in dioxane only the core is visible. Although in some places even raspberry-like particles are present (Figure 6-11a), DLS measurements prove that the aggregation solely takes place during the drying process on the TEM grid. DLS measurements show a hydrodynamic radius of 45 ± 1 nm (Figure 6-10).

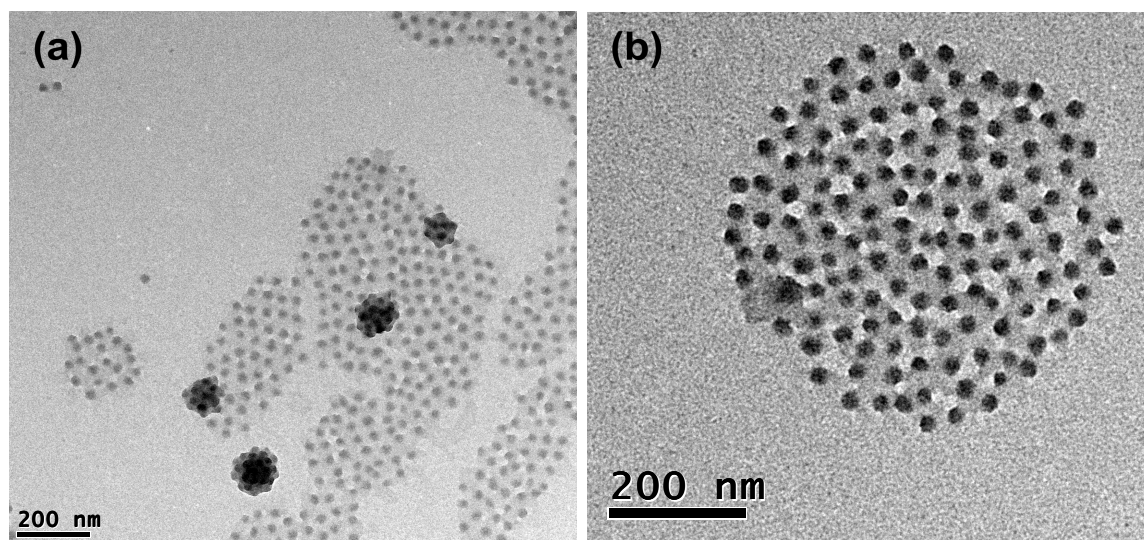


Figure 6-11. TEM micrographs of tSBT JPs in THF stained with OsO_4 (PB appears black, PtS gray).

The obtained tSBT Janus spheres were then hydrolyzed with HCl and afterwards dialyzed against aqueous solutions of pH 5 or 14. At pH 5, the polyhydroxystyrene that resulted from hydrolysis of PtS is fully protonated and therefore insoluble in contrast to the poly(methacrylic acid) that resulted from PtBMA, which is soluble under these conditions. Consequently, we expect aggregation of the JPs due to the collapsed PHS coronas. Indeed, apart from large areas where the JPs aggregated in large numbers probably during the drying process, JPs aggregated into “clovers” as well as “hamburgers” could be observed (Figure 6-12).

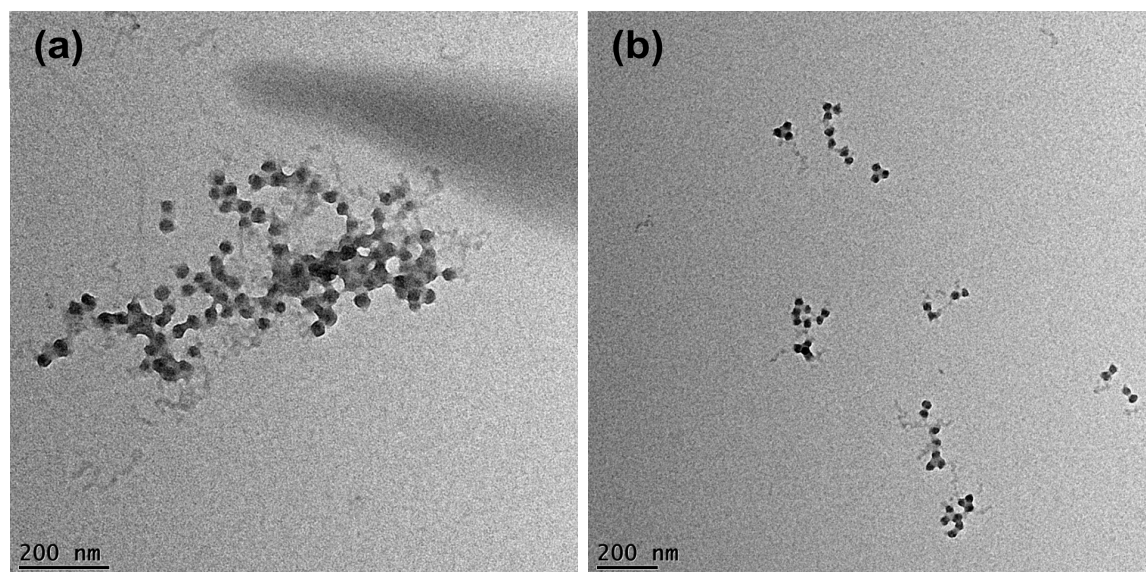


Figure 6-12. TEM micrographs of hydrolyzed Janus spheres in pH 5 showing large aggregates (a) and oligomer formation (b). TEM micrographs are stained with OsO_4 (PB appears black).

In pH 14, both PHS and PMAA should be soluble and single JPs present. However, the TEM micrographs do show only largely aggregated JPs (Figure 6-13). In contrast to pH 5 where a tendency to form burgers and clovers was noticeable, a specific pattern is not noticeable here.

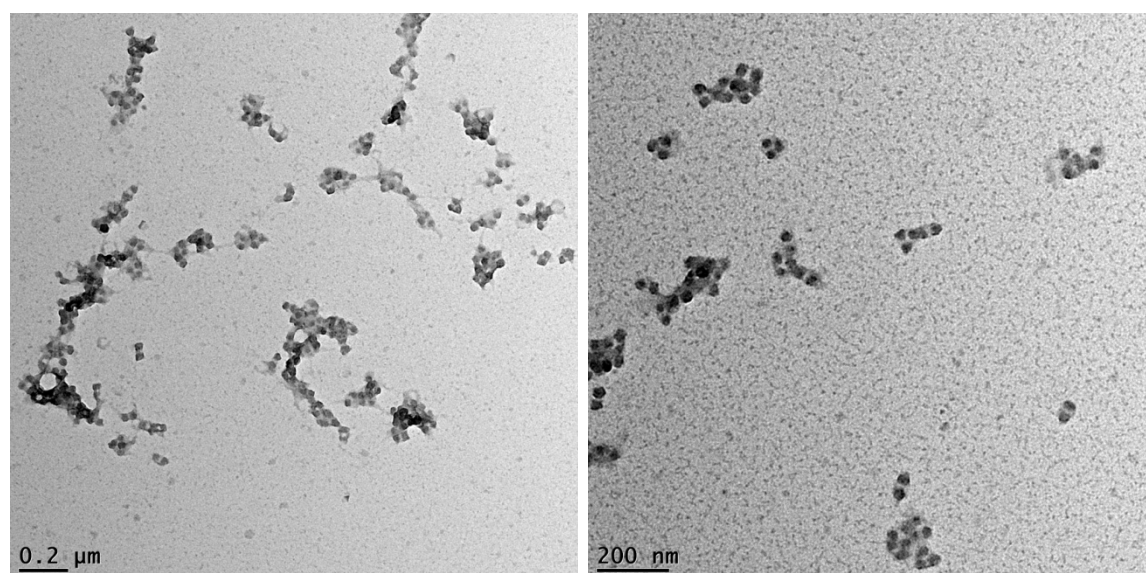


Figure 6-13. TEM micrographs of hydrolyzed Janus spheres in pH 14 showing differently sized aggregates. TEM micrographs are stained with OsO_4 (PB appears black).

As consequence, the sample was also measured under cryo-TEM conditions. Here, together with indeed a small number of single JPs, again trimeric “clovers” and dimeric “hamburgers” were observed. This could be attributed to the slightly better solubility of PMAA. Besides, aggregation even in good solvents has also been reported for SBM Janus micelles⁹⁶ and SBT Janus discs.¹⁰³

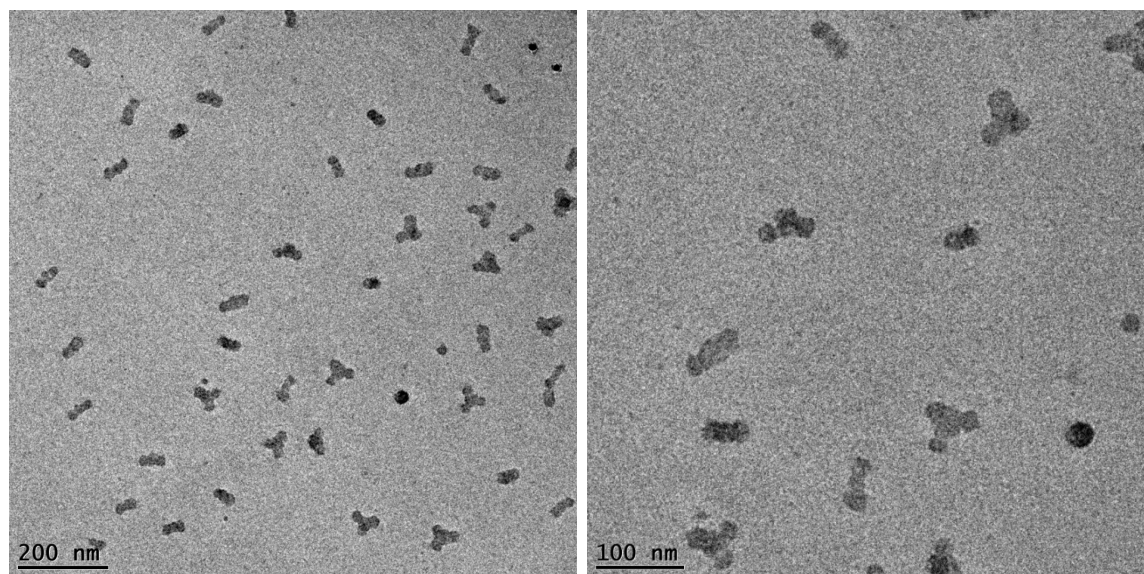


Figure 6-14. Cryo-TEM micrographs of hydrolyzed Janus spheres in pH 14 showing “clover” and “hamburger” formation as well as isolated single JPs.

6.5 Conclusion

By simple dialysis against water (pH 5), micelles with a PtS/PB core and PDMAEMA corona were obtained from dissolved tSBD. Their behavior is characterized by the pH- and temperature-responsive properties of PDMAEMA. Consequently, an increase in pH leads to a contraction of the corona due to the less protonated PDMAEMA. Further, the micelles showed LCST behavior. The observed cloud points were of the same magnitude and followed the same decrease as reported for linear and star-shaped PDMAEMA.¹⁵⁸ With the novel method of directed self-assembly⁵⁹ it was possible to also create football-like MCMs in water from tSBD. We investigated whether the pH-responsive PDMAEMA corona results in different MCM formation depending on the pH like it was observed for TCD.⁵⁹ However, this was not the case and football MCMs were observed for all pH values. In principle, the cross-linking of the PB domains present in the “football” MCMs results in Janus spheres. However, the aqueous solution prevented the use of the hydrophobic photo-initiator Lucirin® TPO and no oth-

er sufficient cross-linking method was found. The MCMs of tSBT are clover-shaped and exist in EtOH. Here, photo-cross-linking with TPO was successfully used for the preparation of Janus spheres which were investigated with TEM and DLS. They were hydrolyzed to JPs consisting of a PHS and a PMAA hemisphere. In pH 5 the particles showed the expected aggregation due to the insoluble PHS part of the corona. “Clover” and “hamburger” MCMs were observed. Although at pH 14 solubility of both hemispheres and consequently single JPs were anticipated, cryo-TEM investigations showed only isolated single particles while the main amount of particles was assembled in trimeric “clovers” and dimeric “hamburgers” possibly due to the slightly better solubility of PMAA. Besides, aggregation even in good solvents has also been reported for SBM Janus micelles⁹⁶ and SBT Janus discs.¹⁰³

7 References

1. Du, J.; O'Reilly, R. K. *Chem. Soc. Rev.* **2011**, *40*, 2402-2416.
2. Fendler, J. H. *Chem. Mater.* **1996**, *8*, 1616-1624.
3. Hadjichristidis, N.; Iatrou, H.; Pitsikalis, M.; Pispas, S.; Avgeropoulos, A. *Prog. Polym. Sci.* **2005**, *30*, 725-782.
4. Tsitsilianis, C., In *Controlled and Living Polymerizations*, Müller, A. H. E.; Matjaszewski, K., Eds. Wiley-VCH Verlag GmbH & Co. KGaA: 2010; pp 445-492.
5. Stadler, R.; Auschra, C.; Beckmann, J.; Krappe, U.; Voight-Martin, I.; Leibler, L. *Macromolecules* **1995**, *28*, 3080-3097.
6. Lecommandoux, S.; Lazzari, M.; Liu, G., In *Block Copolymers in Nanoscience*, Lazzari, M.; Liu, G.; Lecommandoux, S., Eds. Wiley-VCH Verlag GmbH & Co. KGaA: 2008; pp 1-7.
7. Abetz, V.; Goldacker, T. *Macromol. Rapid Commun.* **2000**, *21*, 16-34.
8. Khandpur, A. K.; Foerster, S.; Bates, F. S.; Hamley, I. W.; Ryan, A. J.; Bras, W.; Almdal, K.; Mortensen, K. *Macromolecules* **1995**, *28*, 8796-8806.
9. Bates, F. S.; Fredrickson, G. H. *Phys. Today* **1999**, *52*, 32-38.
10. Hayashida, K.; Takano, A.; Arai, S.; Shinohara, Y.; Amemiya, Y.; Matsushita, Y. *Macromolecules* **2006**, *39*, 9402-9408.
11. Hückstädt, H.; Göpfert, A.; Abetz, V. *Macromol. Chem. Phys.* **2000**, *201*, 296-307.
12. Junnila, S.; Houbenov, N.; Hanski, S.; Iatrou, H.; Hirao, A.; Hadjichristidis, N.; Ikkala, O. *Macromolecules* **2010**, *43*, 9071-9076.
13. Matsen, M. W. *J. Chem. Phys.* **1998**, *108*, 785-796.
14. Tang, P.; Qiu, F.; Zhang, H.; Yang, Y. *Phys. Rev. E* **2004**, *69*, 031803.
15. Phan, S.; Fredrickson, G. H. *Macromolecules* **1998**, *31*, 59-63.
16. Breiner, U.; Krappe, U.; Stadler, R. *Macromol. Rapid Commun.* **1996**, *17*, 567-575.
17. Breiner, U.; Krappe, U.; Thomas, E. L.; Stadler, R. *Macromolecules* **1998**, *31*, 135-141.
18. Krappe, U.; Stadler, R.; Voigt-Martin, I. *Macromolecules* **1995**, *28*, 4558-4561.
19. Breiner, U.; Krappe, U.; Abetz, V.; Stadler, R. *Macromol. Chem. Phys.* **1997**, *198*, 1051-1083.
20. Breiner, U.; Krappe, U.; Jakob, T.; Abetz, V.; Stadler, R. *Polym. Bull.* **1998**, *40*, 219-226.
21. Brinkmann, S.; Stadler, R.; Thomas, E. L. *Macromolecules* **1998**, *31*, 6566-6572.
22. Fustin, C. A.; Abetz, V.; Gohy, J. F. *Eur. Phys. J. E* **2005**, *16*, 291-302.
23. Wyman, I. W.; Liu, G. *Polymer* **2013**, *54*, 1950-1978.
24. Abetz, V.; Boschetti-de-Fierro, A.; Gohy, J.-F., In *Controlled and Living Polymerizations*, Müller, A. H. E.; Matjaszewski, K., Eds. Wiley-VCH Verlag GmbH & Co. KGaA: 2010; pp 493-554.

25. Kriz, J.; Masar, B.; Plestil, J.; Tuzar, Z.; Pospisil, H.; Duskocilova, D. *Macromolecules* **1998**, *31*, 41-51.
26. Yu, G.-e.; Eisenberg, A. *Macromolecules* **1998**, *31*, 5546-5549.
27. Ishizone, T.; Sugiyama, K.; Sakano, Y.; Mori, H.; Hirao, A.; Nakahama, S. *Polym. J.* **1999**, *31*, 983-988.
28. Liu, F.; Liu, G. *Macromolecules* **2001**, *34*, 1302-1307.
29. Wang, X. S.; Winnik, M. A.; Manners, I. *Macromolecules* **2002**, *35*, 9146-9150.
30. Kubowicz, S.; Baussard, J.-F.; Lutz, J.-F.; Thünemann, A. F.; von Berlepsch, H.; Laschewsky, A. *Angew. Chem., Int. Ed.* **2005**, *44*, 5262-5265.
31. Berlepsch, H. v.; Böttcher, C.; Skrabania, K.; Laschewsky, A. *Chem. Commun.* **2009**, *0*, 2290-2292.
32. Skrabania, K.; Berlepsch, H. v.; Böttcher, C.; Laschewsky, A. *Macromolecules* **2009**, *43*, 271-281.
33. Schacher, F.; Walther, A.; Ruppel, M.; Drechsler, M.; Müller, A. H. E. *Macromolecules* **2009**, *42*, 3540-3548.
34. Schacher, F.; Walther, A.; Müller, A. H. E. *Langmuir* **2009**, *25*, 10962-10969.
35. Betthausen, E.; Drechsler, M.; Förtsch, M.; Schacher, F. H.; Müller, A. H. E. *Soft Matter* **2011**, *7*, 8880-8891.
36. Synatschke, C. V.; Schacher, F. H.; Förtsch, M.; Drechsler, M.; Müller, A. H. E. *Soft Matter* **2011**, *7*, 1714-1725.
37. O'Reilly, R. K.; Hawker, C. J.; Wooley, K. L. *Chem. Soc. Rev.* **2006**, *35*, 1068-1083.
38. Stewart, S.; Liu, G. *Chem. Mater.* **1999**, *11*, 1048-1054.
39. Jiang, X.; Luo, S.; Armes, S. P.; Shi, W.; Liu, S. *Macromolecules* **2006**, *39*, 5987-5994.
40. Ma, Q. G.; Wooley, K. L. *J. Polym. Sci. Pol. Chem.* **2000**, *38*, 4805-4820.
41. de Paz Banez, M. V.; Robinson, K. L.; Bütün, V.; Armes, S. P. *Polymer* **2001**, *42*, 29-37.
42. Jiang, X.; Zhang, G.; Narain, R.; Liu, S. *Langmuir* **2009**, *25*, 2046-2054.
43. Xu, X.; Smith, A. E.; Kirkland, S. E.; McCormick, C. L. *Macromolecules* **2008**, *41*, 8429-8435.
44. Tang, Y.; Liu, S. Y.; Armes, S. P.; Billingham, N. C. *Biomacromolecules* **2003**, *4*, 1636-1645.
45. Giebeler, E.; Stadler, R. *Macromol. Chem. Phys.* **1997**, *198*, 3815-3825.
46. Tsitsilianis, C.; Roiter, Y.; Katsampas, I.; Minko, S. *Macromolecules* **2008**, *41*, 925-934.
47. Sugihara, S.; Kanaoka, S.; Aoshima, S. *J. Polym. Sci., Part A: Polym. Chem.* **2004**, *42*, 2601-2611.
48. Xie, D.; Ye, X.; Ding, Y.; Zhang, G.; Zhao, N.; Wu, K.; Cao, Y.; Zhu, X. X. *Macromolecules* **2009**, *42*, 2715-2720.
49. Weiss, J.; Laschewsky, A. *Langmuir* **2011**, *27*, 4465-4473.

-
50. Njikang, G.; Han, D.; Wang, J.; Liu, G. *Macromolecules* **2008**, *41*, 9727-9735.
 51. Hu, J.; Njikang, G.; Liu, G. *Macromolecules* **2008**, *41*, 7993-7999.
 52. Han, D.; Li, X.; Hong, S.; Jinnai, H.; Liu, G. *Soft Matter* **2012**, *8*, 2144-2151.
 53. Schmalz, H.; Schmelz, J.; Drechsler, M.; Yuan, J.; Walther, A.; Schweimer, K.; Mihut, A. M. *Macromolecules* **2008**, *41*, 3235-3242.
 54. Schmelz, J.; Schedl, A. E.; Steinlein, C.; Manners, I.; Schmalz, H. *J. Am. Chem. Soc.* **2012**, *134*, 14217-14225.
 55. Du, J.; Armes, S. P. *Soft Matter* **2010**, *6*, 4851-4857.
 56. Fang, B.; Walther, A.; Wolf, A.; Xu, Y.; Yuan, J.; Müller, A. H. E. *Angew. Chem., Int. Ed.* **2009**, *48*, 2877-2880.
 57. Walther, A.; Barner-Kowollik, C.; Müller, A. H. E. *Langmuir* **2010**, *26*, 12237-12246.
 58. Borisov, O. V.; Zhulina, E. B. *Polymer* **2013**, *54*, 2043-2048.
 59. Gröschel, A. H.; Schacher, F. H.; Schmalz, H.; Borisov, O. V.; Zhulina, E. B.; Walther, A.; Müller, A. H. E. *Nat. Commun.* **2012**, *3*, 710.
 60. Gröschel, A. H.; Walther, A.; Löbbling, T. I.; Schmelz, J.; Hanisch, A.; Schmalz, H.; Müller, A. H. E. *J. Am. Chem. Soc.* **2012**, *134*, 13850-13860.
 61. Marsh, A.; Nolen, E. G.; Gardinier, K. M.; Lehn, J. M. *Tetrahedron Lett.* **1994**, *35*, 397-400.
 62. Cristol, S. J.; Lewis, D. C. *J. Am. Chem. Soc.* **1967**, *89*, 1476-1483.
 63. Casagrande, C.; Fabre, P.; Raphael, E.; Veyssie, M. *Europhys. Lett.* **1989**, *9*, 251-255.
 64. de Gennes, P.-G. *Angew. Chem., Int. Ed.* **1992**, *31*, 842-845.
 65. Jiang, S.; Chen, Q.; Tripathy, M.; Luijten, E.; Schweizer, K. S.; Granick, S. *Adv. Mater.* **2010**, *22*, 1060-1071.
 66. Lattuada, M.; Hatton, T. A. *Nano Today* **2011**, *6*, 286-308.
 67. Hu, J.; Zhou, S.; Sun, Y.; Fang, X.; Wu, L. *Chem. Soc. Rev.* **2012**, *41*, 4356-4378.
 68. Jiang, S.; Granick, S.; Eds., *Janus Particle Synthesis, Self-Assembly and Applications*. The Royal Society of Chemistry: 2012.
 69. Walther, A.; Müller, A. H. E. *Chem. Rev.* **2013**, DOI: 10.1021/cr300089t.
 70. Perro, A.; Reculosa, S.; Ravaine, S.; Bourgeat-Lami, E. B.; Duguet, E. *J. Mater. Chem.* **2005**, *15*, 3745-3760.
 71. Loget, G.; Kuhn, A. *J. Mater. Chem.* **2012**, *22*, 15457-15474.
 72. Walther, A.; Müller, A. H. E. *Soft Matter* **2008**, *4*, 663-668.
 73. Walther, A.; Drechsler, M.; Müller, A. H. E. *Soft Matter* **2009**, *5*, 385-390.
 74. Rodríguez-Fernández, D.; Liz-Marzán, L. M. *Part. Part. Syst. Char.* **2013**, *30*, 46-60.
 75. Wurm, F.; Kilbinger, A. F. M. *Angew. Chem., Int. Ed.* **2009**, *48*, 8412-8421.
 76. Ling, X. Y.; Phang, I. Y.; Acikgoz, C.; Yilmaz, M. D.; Hempenius, M. A.; Vancso, G. J.; Huskens, J. *Angew. Chem., Int. Ed.* **2009**, *48*, 7677-7682.

77. Lattuada, M.; Hatton, T. A. *J. Am. Chem. Soc.* **2007**, *129*, 12878-12889.
78. Nie, L.; Liu, S.; Shen, W.; Chen, D.; Jiang, M. *Angew. Chem., Int. Ed.* **2007**, *46*, 6321-6324.
79. Hong, L.; Jiang, S.; Granick, S. *Langmuir* **2006**, *22*, 9495-9499.
80. Jiang, S.; Schultz, M. J.; Chen, Q.; Moore, J. S.; Granick, S. *Langmuir* **2008**, *24*, 10073-10077.
81. Perro, A.; Meunier, F.; Schmitt, V. r.; Ravaine, S. *Colloids Surf., A* **2009**, *332*, 57-62.
82. Carbone, L.; Cozzoli, P. D. *Nano Today* **2010**, *5*, 449-493.
83. Yu, H.; Chen, M.; Rice, P. M.; Wang, S. X.; White, R. L.; Sun, S. *Nano Lett.* **2005**, *5*, 379-382.
84. Buonsanti, R.; Grillo, V.; Carlino, E.; Giannini, C.; Gozzo, F.; Garcia-Hernandez, M.; Garcia, M. A.; Cingolani, R.; Cozzoli, P. D. *J. Am. Chem. Soc.* **2010**, *132*, 2437-2464.
85. Lu, W.; Chen, M.; Wu, L. *J. Colloid Interface Sci.* **2008**, *328*, 98-102.
86. Zhang, C.; Liu, B.; Tang, C.; Liu, J.; Qu, X.; Li, J.; Yang, Z. *Chem. Comm.* **2010**, *46*, 4610-4612.
87. Ohnuma, A.; Cho, E. C.; Camargo, P. H. C.; Au, L.; Ohtani, B.; Xia, Y. *J. Am. Chem. Soc.* **2009**, *131*, 1352-1353.
88. Roh, K.-H.; Martin, D. C.; Lahann, J. *Nat. Mater.* **2005**, *4*, 759-763.
89. Kietzke, T.; Neher, D.; Kumke, M.; Ghazy, O.; Ziener, U.; Landfester, K. *Small* **2007**, *3*, 1041-1048.
90. Higuchi, T.; Tajima, A.; Yabu, H.; Shimomura, M. *Soft Matter* **2008**, *4*, 1302-1305.
91. Yabu, H.; Motoyoshi, K.; Higuchi, T.; Shimomura, M. *Phys. Chem. Chem. Phys.* **2010**, *12*, 11944-11947.
92. Ma, R.; Wang, B.; Xu, Y.; An, Y.; Zhang, W.; Li, G.; Shi, L. *Macromol. Rapid Commun.* **2007**, *28*, 1062-1069.
93. Voets, I. K.; de Keizer, A.; de Waard, P.; Frederik, P. M.; Bomans, P. H. H.; Schmalz, H.; Walther, A.; King, S. M.; Leermakers, F. A. M.; Stuart, M. A. C. *Angew. Chem., Int. Ed.* **2006**, *45*, 6673-6676.
94. Voets, I. K.; Fokkink, R.; Hellweg, T.; King, S. M.; Waard, P. d.; Keizer, A. d.; Cohen Stuart, M. A. *Soft Matter* **2009**, *5*, 999-1005.
95. Sfika, V.; Tsitsilianis, C.; Kiriy, A.; Gorodyska, G.; Stamm, M. *Macromolecules* **2004**, *37*, 9551-9560.
96. Erhardt, R.; Böker, A.; Zettl, H.; Kaya, H.; Pyckhout-Hintzen, W.; Krausch, G.; Abetz, V.; Müller, A. H. E. *Macromolecules* **2001**, *34*, 1069-1075.
97. Walther, A.; Gödel, A.; Müller, A. H. E. *Polymer* **2008**, *49*, 3217-3227.
98. Zhang, K.; Gao, L.; Chen, Y. *Polymer* **2010**, *51*, 2809-2817.
99. Walther, A.; Müller, A. H. E., In *Janus Particle Synthesis, Self-Assembly and Applications*,

- Jiang, S.; Granick, S., Eds. The Royal Society of Chemistry: 2012; pp 1-28.
100. Saito, R.; Fujita, A.; Ichimura, A.; Ishizu, K. *J. Polym. Sci., Part A: Polym. Chem.* **2000**, *38*, 2091-2097.
 101. Liu; Abetz, V.; Müller, A. H. E. *Macromolecules* **2003**, *36*, 7894-7898.
 102. Walther, A.; Drechsler, M.; Rosenfeldt, S.; Harnau, L.; Ballauff, M.; Abetz, V.; Müller, A. H. E. *J. Am. Chem. Soc.* **2009**, *131*, 4720-4728.
 103. Walther, A.; André, X.; Drechsler, M.; Abetz, V.; Müller, A. H. E. *J. Am. Chem. Soc.* **2007**, *129*, 6187-6198.
 104. Yuet, K. P.; Hwang, D. K.; Haghgooie, R.; Doyle, P. S. *Langmuir* **2009**, *26*, 4281-4287.
 105. Glaser, N.; Adams, D. J.; Böker, A.; Krausch, G. *Langmuir* **2006**, *22*, 5227-5229.
 106. Ruhland, T. M.; Gröschel, A. H.; Walther, A.; Müller, A. H. E. *Langmuir* **2011**, *27*, 9807-9814.
 107. Walther, A.; Matussek, K.; Müller, A. H. E. *ACS Nano* **2008**, *2*, 1167-1178.
 108. Binks, B. P.; Fletcher, P. D. I. *Langmuir* **2001**, *17*, 4708-4710.
 109. Ruhland, T. M.; Gröschel, A. H.; Ballard, N.; Skelhon, T. S.; Walther, A.; Müller, A. H. E.; Bon, S. A. F. *Langmuir* **2013**, *29*, 1388-1394.
 110. Walther, A.; Hoffmann, M.; Müller, A. H. E. *Angew. Chem., Int. Ed.* **2008**, *47*, 711-714.
 111. Gröschel, A. H.; Löbbling, T. I.; Petrov, P. D.; Müllner, M.; Kuttner, C.; Wieberger, F.; Müller, A. H. E. *Angew. Chem., Int. Ed.* **2013**, *52*, 3602-3606.
 112. Jiang, S.; Granick, S., In *Janus Particle Synthesis, Self-Assembly and Applications*, Jiang, S.; Granick, S., Eds. The Royal Society of Chemistry: 2012; pp v-xiv.
 113. Molina, L. M.; Hammer, B. *Phys. Rev. Lett* **2003**, *90*, 206102.
 114. Hu, S.-H.; Gao, X. *J. Am. Chem. Soc.* **2010**, *132*, 7234-7237.
 115. Sotiriou, G. A.; Hirt, A. M.; Lozach, P.-Y.; Teleki, A.; Krumeich, F.; Pratsinis, S. E. *Chem. Mater.* **2011**, *23*, 1985-1992.
 116. Synytska, A.; Khanum, R.; Ionov, L.; Cherif, C.; Bellmann, C. *ACS Appl. Mater. Interfaces* **2011**, *3*, 1216-1220.
 117. Conlon, D. A.; Crivello, J. V.; Lee, J. L.; O'Brien, M. J. *Macromolecules* **1989**, *22*, 509-516.
 118. Lin, C.-L.; Chen, W.-C.; Liao, C.-S.; Su, Y.-C.; Huang, C.-F.; Kuo, S.-W.; Chang, F.-C. *Macromolecules* **2005**, *38*, 6435-6444.
 119. Gao, H.; Matyjaszewski, K. *J. Am. Chem. Soc.* **2007**, *129*, 6633-6639.
 120. Sato, T.; Shimooka, S.; Seno, M.; Tanaka, H. *Macromol. Chem. Phys.* **1994**, *195*, 833-843.
 121. Ohno, K.; Ejaz, M.; Fukuda, T.; Miyamoto, T.; Shimizu, Y. *Macromol. Chem. Phys.* **1998**, *199*, 291-297.
 122. Stillings, C. Supramolekulare Strukturbildung von Polymer- und Flüssigkristallsystemen im nanoskaligen Confinement. Philipps-Universität Marburg, Marburg a. d.

- Lahn, 2006.
123. Shohi, H.; Sawamoto, M.; Higashimura, T. *Die Makromolekulare Chemie* **1992**, *193*, 1783-1792.
124. Hadjichristidis, N.; Pispas, S.; Floudas, G., *Block Copolymers: Synthetic Strategies, Physical Properties, and Applications*. John Wiley & Sons, Inc.: 2003; p 32.
125. BouchéKif, H.; Som, A.; Sipos, L.; Faust, R. *J. Macromol. Sci., Part A: Pure Appl. Chem.* **2007**, *44*, 359-366.
126. Li, M. Q.; Douki, K.; Goto, K.; Li, X. F.; Coenjarts, C.; Smilgies, D. M.; Ober, C. K. *Chem. Mat.* **2004**, *16*, 3800-3808.
127. Kuo, S. W.; Tung, P. H.; Chang, F. C. *Macromolecules* **2006**, *39*, 9388-9395.
128. Berger, S.; Synytska, A.; Ionov, L.; Eichhorn, K.-J.; Stamm, M. *Macromolecules* **2008**, *41*, 9669-9676.
129. Lee, N. S.; Sun, G.; Neumann, W. L.; Freskos, J. N.; Shieh, J. J.; Dorshow, R. B.; Wooley, K. L. *Adv. Mater.* **2009**, *21*, 1344-1348.
130. Ober, C. K.; Li, M.; Douki, K.; Goto, K.; Li, X. *Photopolym. Sci. Technol.* **2003**, *16*, 347-350.
131. Mountrichas, G.; Mantzaridis, C.; Pispas, S. *Macromol. Rapid Commun.* **2006**, *27*, 289-294.
132. Hameed, N.; Liu, J.; Guo, Q. *Macromolecules* **2008**, *41*, 7596-7605.
133. Yoshida, E.; Kuwayama, S. *Colloid Polym. Sci.* **2008**, *286*, 1621-1627.
134. Ruiz de Luzuriaga, A.; García, I.; Mecerreyes, D.; Etxeberria, A.; Pomposo, J. A. *Polymer* **2010**, *51*, 1355-1362.
135. Stepanek, M.; Matejicek, P.; Prochazka, K.; Filippov, S. K.; Angelov, B.; Slouf, M.; Mountrichas, G.; Pispas, S. *Langmuir* **2011**, *27*, 5275-5281.
136. Pettau, R.; Müller, T.; Khazimullin, M.; Rehberg, I.; Schmidt, H.-W. *Z. Phys. Chem.* **2012**, *226*, 645-664.
137. Jung, M. E.; Lyster, M. A. *J. Am. Chem. Soc.* **1977**, *99*, 968-969.
138. Jung, M. E.; Lyster, M. A. *J. Org. Chem.* **1977**, *42*, 3761-3764.
139. Reagents for Silicon-Mediated Organic Synthesis. In *Handbook of Reagents for Organic Synthesis*, Fuchs, P. L., Ed. John Wiley & Sons Ltd: 2011; pp 325-336.
140. Chen, Z.; Cui, H.; Hales, K.; Li, Z.; Qi, K.; Pochan, D. J.; Wooley, K. L. *J. Am. Chem. Soc.* **2005**, *127*, 8592-8593.
141. Smith, C. K.; Liu, G. *Macromolecules* **1996**, *29*, 2060-2067.
142. Dimitrov, I.; Jankova, K.; Hvilsted, S. *J. Polym. Sci., Part A: Polym. Chem.* **2010**, *48*, 2044-2052.
143. Thomsen, A. D.; Malmström, E.; Hvilsted, S. *J. Polym. Sci., Part A: Polym. Chem.* **2006**, *44*, 6360-6377.

-
144. Kolb, H. C.; Finn, M. G.; Sharpless, K. B. *Angew. Chem., Int. Ed.* **2001**, *40*, 2004-2021.
145. Evans, R. A. *Aust. J. Chem.* **2007**, *60*, 384-395.
146. Neises, B.; Steglich, W. *Angew. Chem., Int. Ed.* **1978**, *17*, 522-524.
147. Se, K. *Polym. Adv. Technol.* **2003**, *14*, 177-183.
148. Lowe, A. B.; Wang, R.; Tiriveedhi, V.; Butko, P.; McCormick, C. L. *Macromol. Chem. Phys.* **2007**, *208*, 2339-2347.
149. Mitsukami, Y.; Hashidzume, A.; Yusa, S.-i.; Morishima, Y.; Lowe, A. B.; McCormick, C. L. *Polymer* **2006**, *47*, 4333-4340.
150. Sumerlin, B. S.; Lowe, A. B.; Thomas, D. B.; Convertine, A. J.; Donovan, M. S.; McCormick, C. L. *J. Polym. Sci., Part A: Polym. Chem.* **2004**, *42*, 1724-1734.
151. Higo, Y.; Chosi, H.; Fujimoto, T.; Nagasawa, M. *Polym. J. (Tokyo, Jpn.)* **1980**, *12*, 729-734.
152. Se, K.; Kijima, M.; Fujimoto, T. *Polym. J. (Tokyo, Jpn.)* **1988**, *20*, 791-799.
153. Auschra, C.; Stadler, R. *Polym. Bull. (Berlin)* **1993**, *30*, 257-264.
154. Rembaum, A.; Siao, S.-P.; Indictor, N. *J. Polym. Sci.* **1962**, *56*, S17-S19.
155. Yakimansky, A. V.; Van Beylen, M. *Polymer* **2002**, *43*, 5797-5805.
156. Petzhold, C.; Morschhaeuser, R.; Kolshorn, H.; Stadler, R. *Macromolecules* **1994**, *27*, 3707-3713.
157. Schmalz, A.; Hanisch, M.; Schmalz, H.; Müller, A. H. E. *Polymer* **2009**, *51*, 1213-1217.
158. Plamper, F. A.; Ruppel, M.; Schmalz, A.; Borisov, O.; Ballauff, M.; Müller, A. H. E. *Macromolecules* **2007**, *40*, 8361-8366.
159. Wolf, A.; Walther, A.; Müller, A. H. E. *Macromolecules* **2011**, *44*, 9221-9229.
160. Schacher, F. H.; Reinicke, S.; Walther, A.; Schmalz, H.; Müller, A. H. E., In *New Smart Materials via Metal Mediated Macromolecular Engineering*, Khosravi, E.; Yagci, Y.; Savelyev, Y., Eds. Springer: 2009; pp 167-186.
161. Hsieh, H. L.; Quirk, R. P., In *Anionic polymerization: principles and practical applications*, Marcel Dekker, Inc.: 1996; p 233.
162. D'Alelio, G. F.; Hoffend, T. R. *J. Polym. Sci., Part A: Polym. Chem.* **1967**, *5*, 323-337.
163. Wolf, A. *Diploma thesis*, Universität Bayreuth, Bayreuth, 2008.
164. Fernyhough, C.; Ryan, A. J.; Battaglia, G. *Soft Matter* **2009**, *5*, 1674-1682.
165. Rolls, W.; Svec, F.; Fréchet, J. M. J. *Polymer* **1990**, *31*, 165-174.
166. Plamper, F. A.; Becker, H.; Lanzendörfer, M.; Patel, M.; Wittemann, A.; Ballauff, M.; Müller, A. H. E. *Macromol. Chem. Phys.* **2005**, *206*, 1813-1825.
167. Campese, G. M.; Rodrigues, E. M. G.; Tambourgi, E. B.; Pessoa Jr, A. *Braz. J. Chem. Eng.* **2003**, *20*, 335-337.
168. Li, F.-M.; Chen, S.-J.; Du, F.-S.; Wu, Z.-Q.; Li, Z.-C., In *Field Responsive Polymers Electroresponsive, Photoresponsive, and Responsive Polymers in Chemistry and Biolo-*

- gy*, Khan, M. I.; Harrison, J. S., Eds. 1999; pp 266-276.
169. Borisov, O. V.; Zhulina, E. B.; Leermakers, F. A. M.; Müller, A. H. E., In *Self Organized Nanostructures of Amphiphilic Block Copolymers I*, Springer Berlin Heidelberg: 2011; Vol. 241, pp 57-129.

List of Publications

1. **Wolf, A.**; Döhler, S.; Hanisch, A.; Müller, A.H.E.: Synthesis via Anionic Polymerization and LCST-Behavior of Narrowly Distributed Poly(4-(dimethylaminomethyl)-styrene), **2013**, to be submitted.
2. Plamper, F.A.; Gelissen, A.P.; Timper, J.; **Wolf, A.**; Zezin, A.B.; Richtering, W.; Tenhu, H.; Simon, U.; Mayer, J., Borisov, O.V.; Pergushov, D.V.: Spontaneous Assembly of Miktoarm Stars into Vesicular Interpolyelectrolyte Complexes, *Macromol. Rapid Commun.* **2013**, *34*, 855-860.
3. Sigolaeva, L.V.; Pergushov, D.V.; Synatschke, C.V.; **Wolf, A.**; Kurochkin, I.N.; Fery, A.; Müller, A.H.E.: Co-assemblies of Micelle-Forming Diblock Copolymers and Enzymes on Graphite for an Improved Design of Biosensor Systems, *Soft Matter* **2013**, *9*, 2858-2868.
4. Das, P.; Heuser, T.; **Wolf, A.**; Zhu, B.; Demco, D.E.; Ifuku, S.; Walther, A.: Tough and Catalytically Active Hybrid Biofibers Wet-Spun from Nanochitin Hydrogels, *Biomacromolecules* **2012**, *13*, 4205-4212.
5. **Wolf, A.**; Walther, A.; Müller, A.H.E.: Janus Triad: Three Types of Nonspherical, Nanoscale Janus Particles from One Single Triblock Terpolymer, *Macromolecules* **2011**, *44*, 9221-9229.
6. Babin, I.A.; Pergushov, D.V.; **Wolf, A.**; Plamper, F.A.; Schmalz, H.; Müller, A.H.E.; Zezin, A.B.: Micellar Interpolyelectrolyte Complexes Formed by Star Shaped Poly(acrylic acid) with Double Hydrophilic Cationic Diblock Copolymer, *Doklady Phys. Chem.* **2011**, *441*, 219-223.
7. **Wolf, A.**; Walther, A.; Müller, A.H.E.: Preparation of a Variety of Janus Particles from a New Versatile Block Terpolymer, *Polym. Prepr. (Am. Chem. Soc., Div. Polym. Chem.)* **2010**, *51*, 616-617.
8. Müller, A.H.E.; Betthausen, E.; Müllner, M.; Schacher, F.H.; Synatschke, C.V.; Walther, A.; **Wolf, A.**: Self-Organized Nanostructures from New Block Co- and Terpolymers, *Polym. Prepr. (Am. Chem. Soc., Div. Polym. Chem.)* **2010**, *51*, 308-309.

9. Fang, B.; Walther, A.; **Wolf, A.**; Xu, Y.; Yuan, J.; Müller, A.H.E.: Undulated Multicompartment Cylinders by the Controlled and Directed Stacking of Polymer Micelles with a Compartmentalized Corona, *Angew. Chem. Int. Ed.* **2009**, *48*, 2877-2880.

Danksagung

Mein erster Dank geht an Prof. Dr. Axel H. E. Müller für die Möglichkeit diese Arbeit in seiner Arbeitsgruppe anzufertigen und für seine Betreuung. Prof. Müller vereinigt einen überaus kompetenten Wissenschaftler mit einem überaus menschlichen Chef. So war er stets ansprechbar für alle wissenschaftlichen Belange, egal ob unter der Woche, am Wochenende oder sogar während des Sabbaticals, auf eine E-Mail egal mit welchen Fragen kam fast sofort eine Antwort. Er hat es außerdem geschafft mit seiner Art eine Arbeitsgruppe zu leiten eine Arbeitsatmosphäre zu schaffen die von Zusammenhalt und Zusammenarbeit geprägt war. Dazu hat auch seine menschliche Seite, der Gruppenunternehmungen und die einzelnen Mitarbeiter auch abseits der Wissenschaft wichtig waren, beigetragen. Dafür, dass ich an solch einem Lehrstuhl mein Promotionsstudium verbringen konnte, bin ich sehr dankbar. Außerdem möchte ich mich bedanken für die Ermöglichung zahlreicher Reisen zu Konferenzen bei denen sowohl wissenschaftlicher, als auch interkultureller und persönlicher Austausch stattfand. So habe ich im In- und Ausland nicht nur meinen wissenschaftlichen sondern auch meinen persönlichen Horizont erweitern können.

Ich möchte mich bedanken bei meinen BayNAT-Mentoren Prof. Dr. Alexander Böker und besonders bei Dr. Andreas Walther. Danke letzterem für die vielen Hilfestellungen, von der Zeit meines letzten Vertiefungspraktikums bis zu meiner Doktorarbeit. Das ging von der Einarbeitung in neue praktische Tätigkeiten über wissenschaftliche Impulse, Ratschläge, das Korrigieren von Manuskripten bis zum Vertrautmachen mit meinem liebsten Gerät, dem Elektronenmikroskop. Dafür vielen, vielen Dank.

Danke an die MCII, an alle Mitarbeiter und Gäste, es war einmalig!

An dieser Stelle besonderen Dank an meine „MCII-Mädels“, Annika, Eva, Gaby, Marietta, Marina und Meli. Wir haben uns gegenseitig das Leben versüßt, im sprichwörtlichen, aber auch im sehr wörtlichen Sinn! Ihr seid mir sehr ans Herz gewachsen. Danke Gaby auch für die viele Hilfe bei allen bürokratischen Dingen und vielen Dank Eva für tSBD-3, viele Ratschläge in wissenschaftlichen Dingen und bei Microsoft Office und für unvergessliche gemeinsame Konferenzreisen.

Vielen Dank an meine Laborkollegen über die Jahre, Stefan, Frankie, Felix und Christopher für gute Zusammenarbeit und eine gute Atmosphäre.

Ein herzliches Dankeschön an alle anderen: Hülya Arslan, Girish Behera, Meirav Ben-Lulu, Dane Blasser, Alexander Daniel, Markus Drechsler (Dankeschön für die Einweisungen am TEM und die Hilfe, speziell bei Cryo-TEM), Annika Eckardt, Susanne Edinger, Bing Fang, Anja Goldmann, André Gröschel (Danke für deine Hilfe bei den MCMs), Andreas Hanisch (vielen Dank für die Hilfe bei der Anionik und anderen Kleinigkeiten!), Prof. Dr. Tomohiro Hirano, Matt Hunley, Shohei Ida, Jie Kong, Annette Krökel (vielen Dank für die Hilfe bei allen kleinen „Annette, sag mal wo ist denn...?“-Fragen), Kerstin Küspert, Jun Ling, Tina Löbbling, Alexander Majewski, Pierre-Eric Millard, μ , Ramón Novoa-Carballal, Lourdes Pastor-Pérez, Dima Pergushov, Prof. Dr. Petar Petrov, André Pfaff, Daniela Pirner, Felix Plamper, Jeannine Rockser, Tobias Rudolph, Thomas Ruhland, Alexander Schmalz, Dr. Holger Schmalz, Joe Schmelz, Manuela Schumacher, Larisa Sigolaeva, Sandrine Tea (Thank you for the trip to

Danksagung

Italy!), Hans-Joachim Voigtländer, Stephan Weiß, Michael Witt, Sabine Wunder, Youyong Xu, Alexander Yakimansky, Jiayin Yuan, Weian Zhang und Zhicheng Zheng.

Danke meinen Mit-Exilanten Andreas, Thomas und Alex, dafür, dass wir das Beste daraus gemacht haben. Und vielen Dank an Prof. Dr. Schmidt und Prof. Dr. Kümmel und ihre Sekretärinnen Petra Weiß und Monika Birkelbach, die uns ein angenehmes Arbeiten ermöglicht haben.

Vielen Dank auch an die Studenten, die bei mir Praktikum, Bachelor- oder Masterarbeit gemacht haben, allen voran Stefan Döhler sowie Eddie Hofmann, Jonas Schubert und Josef Lange. Danke für eure engagierte Arbeit.

Für finanzielle Unterstützung danke ich dem Freistaat Bayern, der DFG und dem Büro der Frauenbeauftragten der Universität Bayreuth.

Danke an Dr. Andreas Walther und Prof. Dr. Felix Schacher für die unkomplizierten SAXS-Messungen und die Hilfe bei der Auswertung.

Ein besonderer Dank gilt meinem Chemie-Lehrer Rolf Vitzthum; wer weiss, wo ich jetzt wäre, wenn er mich nicht von Anfang an für die Chemie begeistert hätte.

Ein ganz lieber Dank geht an meine Mädels außerhalb der MCII, Julia Gensel, Katja Gräf und Katja Trenkenschuh, ihr wisst ja, ihr seid die Besten!

Von ganzem Herzen möchte ich mich bei meiner ganzen großen Familie bedanken, auch bei den Mitgliedern, die uns schon verlassen haben, und speziell natürlich bei meiner Schwester Julia und bei meinen Eltern Helmut und Ingrid Wolf, danke für alles, was ihr für mich seid und was ihr für mich getan habt!

Ich danke meinem Mann Anouar, anta koulshi dyali!

Und ich danke Gott, der mir all diese wunderbaren Menschen in meinem Leben geschenkt hat.

Erklärung

Die vorliegende Arbeit wurde von mir selbständig verfasst und ich habe dabei keine anderen als die von mir angegebenen Quellen benutzt.

Ferner habe ich nicht versucht, anderweitig mit oder ohne Erfolg eine Dissertation einzureichen oder mich der Doktorprüfung zu unterziehen.

Bayreuth, den

Andrea Wolf